약학박사 학위논문

Chemical profiling of Farfarae Flos sesquiterpenoids and the target protein identification of an oplopane sesquiterpenoid in breast cancer cells

관동화 유래 세스퀴테르펜 화합물의 성분프로파일 및 유방암 세포주에서의 oplopane 세스퀴테르펜의 표적 단백질에 관한 연구

2019 년 8 월

서울대학교 대학원

약학과 천연물과학 전공

송 광 호

Chemical profiling of Farfarae Flos sesquiterpenoids and the target protein identification of an oplopane sesquiterpenoid in breast cancer cells

관동화 유래 세스퀴테르펜 화합물의 성분프로파일 및 유방암 세포주에서의 oplopane 세스퀴테르펜의 표적 단백질에 관한 연구

지도교수 김 영 식

이 논문을 약학박사 학위논문으로 제출함

2019 년 8 월

서울대학교 대학원

약학과 천연물과학 전공

송 광 호

송광호의 약학박사 학위논문을 인준함

2019 년 7 월

위 원 장: 박 성혁 (인)

부위원장: 이 상훈 (인)

위 원: 서 은정 (인)

위 원: 노 민수 (인)

위 원: 김 영식 (인)

ABSTRACT

Chemical profiling of Farfarae Flos sesquiterpenoids and the target protein identification of an oplopane sesquiterpenoid in breast cancer cells

Kwangho Song
Natural Products Science Major
College of Pharmacy
Doctorate Course in the Graduate School
Seoul National University

Farfarae Flos is the dried buds of *Tussilago farfara* L., a perennial plant of the family Asteraceae, and has been used to treat coughs, bronchitis, and asthmatic conditions in traditional herbal medicine. Among its bioactive compounds, sesquiterpenoids exhibit various biological activities such as anti-inflammative, anti-proliferative, and neuroprotective effects. In the present study, preparative separation, chemical profiling, and activity-based proteome profiling of sesquiterpenoids from Farfarae Flos were performed.

Firstly, a novel fractionation and purification method of counter-current chromatography (CCC), called direct and continuous injection (DCI) mode, was developed to fractionate and preparatively separate sesquiterpenoids from Farfarae Flos. Since the extraction solution was used as a mobile phase in this method, solvent

consumption was greatly reduced. 6.8 g of sesquiterpenoid-enriched (STE) fraction was obtained from the crude extract (315.9 g) of Farfarae Flos (1 kg) in a single CCC run with a separation time of 8.5 hrs. The sample injection capacity of CCC-DCI was greater than 300 grams which could not be handled in conventional CCC methods. Moreover, quantification study indicated that the fractionation efficiency of CCC-DCI was higher than those of conventional fractionations: solvent partitioning and open column chromatography. The developed method demonstrates that CCC is a useful technique for enriching target components from natural products.

Secondly, a liquid chromatography-electrospray ionization tandem mass spectrometry (LC-ESI-MS/MS)-based dereplicative method was developed to identify and quantify oplopane- and bisabolane-type sesquiterpenoids of Farfarae Flos. The MS-based nontargeted metabolomic approach for these chemical analogues, sesquiterpene esters, is challenging because of their in-source fragmentation and structural diversity. In order to profile these sesquiterpenoids, four diagnostic ions (*m/z* 215.143, 217.158, 229.123, and 231.138) were suggested in the positive ion mode and the developed method utilized two sequential MS/MS scan modes to characterize common skeletons and investigate the fragmentation patterns of their parent molecules. Under the optimized UHPLC-MS/MS method, 74 sesquiterpenoids were identified from the Farfarae Flos and 11 compounds were isolated for the method validation. Furthermore, the diagnostic ions and the MS/MS fragment behaviors were applied to accurate quantification of the 8 isolated sesquiterpenoids. Consequently, the developed LC-MS/MS-based dereplicative method highlighted the chemical composition of the Farfarae Flos and could be applied to quality control of the herbal medicine.

Finally, target proteins of ECN (7β-(3′-ethyl *cis*-crotonoyloxy)-1α-(2′-methyl butyryloxy)-3,14-dehydro-*Z*-notonipetranone) in human breast cancer cells were identified by chemical proteomics methodology. ECN showed potent anti-proliferation activity in MDA-MB-231 and MCF-7 human breast cancer cells based on its α,β-unsaturated carbonyl moiety. Therefore, the potential cellular target proteins of ECN were identified using ECN-based clickable probe and quantitative MS/MS analysis. Among more than 200 identified proteins, 17 proteins showed more than 3 enrichment ratio in both cell lines. Furthermore, recombinant 14-3-3 protein zeta and peroxiredoxin-1 were further verified by isothermic calorimetry and their alkylation sites. Taking the interaction between α,β-unsaturated carbonyl moiety of ECN and cysteine residues of proteins into account, peptides containing Cys25, Cys94 of 14-3-3 protein zeta and Cys83 of peroxiredoxin-1 were significantly reduced by ECN. Although these results could not confirm the role of ECN in the breast cancer cells, this suggestion of multiple target proteins contributed to understand the ECN-mediated anti-proliferative and anti-inflammatory effects, leading to further studies.

Keywords: Farfarae Flos, oplopane and bisabolane sesquiterpenoid, Counter-current chromatography, Direct and continuous injection mode, LC-MS/MS chemical profiling, Anti-proliferation, Activity based proteome profiling

Student Number: 2013-23461

CONTENTS

LIST OF FIGURES

LIST OF TABLES

I. INTRODUCTION

1. Farfarae Flos

1.1. Constituents and bioactivities

Farfarae Flos, buds of *Tussilago farfara* L. **(Fig. 1A)**, commonly known as coltsfoot, is a perennial medicinal plant of the family Asteraceae that is widely spread in East Asia, Siberia, North Africa, Europe, and sporadically in the United States. The dried flower buds of *T. farfara* (Farfarae Flos; **Fig. 1B**) have been used to treat respiratory problems, such as cough, bronchitis, and asthmatic conditions in traditional medicine [1, 2]. A series of phytochemical studies on *T. farfara* have revealed that the plant contains a diverse number of compounds, including polysaccharides, quinic acid derivatives, flavonoids, terpenoids, chromones, and pyrrolizidine alkaloids [3-9]. Among those classes of compounds, sesquiterpenoids and quinic acid derivatives were reported as the characteristic and major components of Farfarae Flos [10]. It was recently reported that sesquiterpenoids from the Farfarae Flos exhibit several pharmacological properties, such as anti-inflammatory, anti-proliferative, anti-oxidative, and neuroprotective effects [11-16].

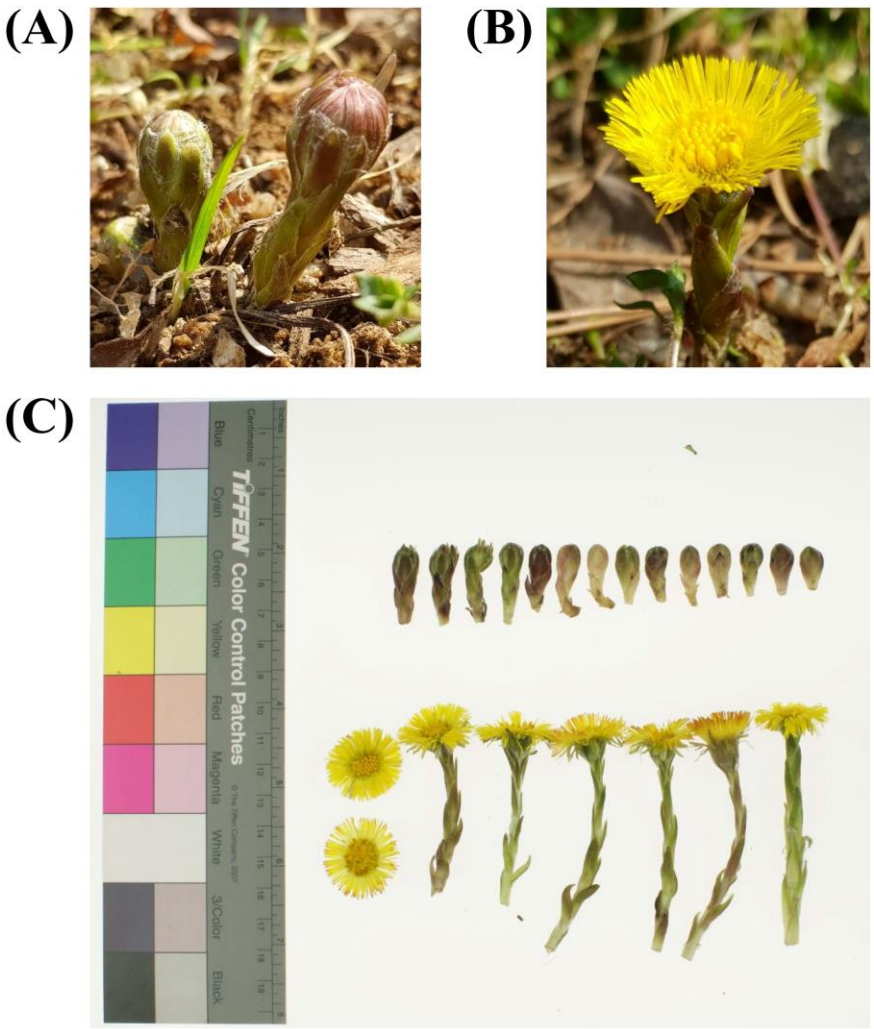

Figure 1. *Tussilago farfara* L.

Photographs of (A) buds and (B) flower of *Tussilago farfara* L. (C) Herbal materials of *T. farfara* from Medical Herb Garden, College of Pharmacy, Seoul National University.

1.2. Oplopane and bisabolane sesquiterpenoids

Farfarae Flos contains oplopane and bisabolane type sesquiterpenoids, whose skeletons are substituted with diverse ester derivatives and about 30 sesquiterpene esters have been reported up to date [17–25]. Considering the substituents in the R_1–R_3 positions, the sesquiterpene backbone could be decorated with various ester groups and six substituents were reported **(Fig. 2)**. Tussilagone, one of the oplopane sesquiterpenoids, is a chemical marker of the herbal medicine. Regulation of the Farfarae Flos in the Chinese Pharmacopoeia was implemented in 2010, which described that the tussilagone content of Farfarae Flos must be greater than 0.07% [26].

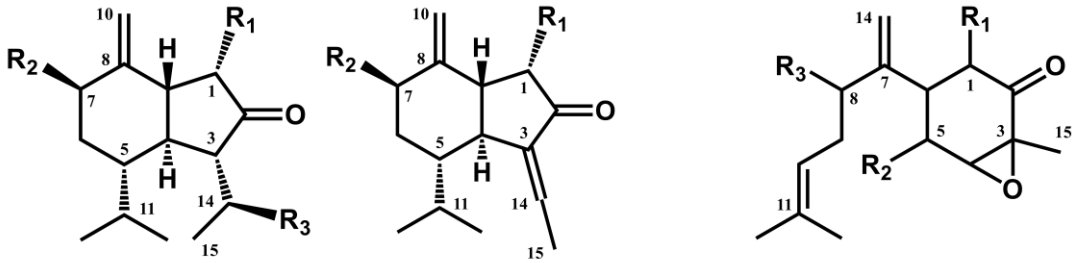

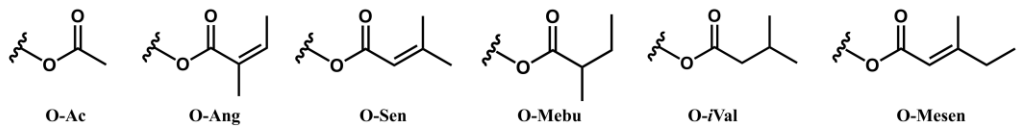

No.	R_1	R_2	R_3	MW	Ref.
1	H	O-Ang	OH	334.45	[23]
2	H	O-*i*Val	OH	336.47	[20]
3	H	O-Mesen	OH	348.48	[17]
4	H	O-Sen	O-Ac	376.49	[17]
5	H	O-Ang	O-Ac	376.49	[17]
6	H	O-*i*Val	O-Ac	378.50	[20]
7	H	O-Mesen	O-Ac	390.51	[17]
8	O-Mebu	O-Mesen	OH	448.59	[23]
9	O-Mebu	O-Mesen	$O\text{-}CH_3$	462.62	[24]
10	O-Mebu	O-Mesen	$O\text{-}C_2H_5$	476.65	[22]
11	O-Mebu	O-Mesen	O-Ac	490.63	[17]

No.	R_1	R_2	Δ3(14)	MW	Ref.
12	H	O-Sen	*Z*	316.43	[19]
13	H	O-Ang	*Z*	316.43	[19]
14	H	O-Mesen	*Z*	330.46	[21]
15	H	O-Mesen	*E*	330.46	[19]
16	O-Mebu	OH	*Z*	334.45	[25]
17	OH	O-Mesen	*Z*	346.46	[23]
18	O-Ang	O-Mesen	*Z*	428.56	[19]
19	O-Mebu	O-Mesen	*E*	430.58	[22]
20	O-Mebu	O-Mesen	*Z*	430.58	[19]
21	O-Mesen	O-Mesen	*Z*	442.59	[19]

No.	R_1	R_2	R_3	MW	Ref.
22	H	H	O-Ang	332.43	[21]
23	OH	OH	O-Ang	364.43	[25]
24	O-Ang	H	O-Ang	430.53	[23]
25	O-Ac	OH	O-Ang	406.47	[20]
26	O-Mesen	H	O-Ang	444.56	[23]
27	O-Ac	O-Ac	O-Ang	448.51	[18]

Figure 2. Chemical structures of reported oplopane and bisabolane type sesquiterpenoids from Farfarae Flos

2. Counter-current chromatography

2.1. Background

Counter-current distribution (CCD) was invented in 1940s as the original form of liquid chromatography using two immiscible solvent phases to separate natural products [27]. However, the advancement in the separation technique was yielded from counter current chromatography (CCC) developed by Ito in the 1970s overcoming the vulnerable points of CCD; time and solvent consuming and complex instrumental systems [28]. Planetary motion of the CCC instrumental systems **(Fig. 3)** provides two major functions for performing CCC separation: a rotary-seal-free elution system so that the mobile phase is continuously eluted through the rotating separation column. The second and more important function is that it produces a unique hydrodynamic motion of two solvent phases within the rotating multilayer coiled column mainly due to the *Archimedean screw effect*. When two immiscible solvent phases are introduced in the multilayer coiled column, the rotation separates the two phases completely along the length of the tube where the lighter phase occupies one end called the head and the heavier phase, the other end called the tail.

CCC is complementary to high performance liquid chromatography (HPLC) in isolation and purification of natural products with several advantages. CCC is cost-saving in maintenance of the column system compared to HPLC because the multifold tube wound around coils is generally made of

polytetrafluoroethylene (PTFE) and it does not critically depends on the optimal solvent grade. CCC also provides a wide range in the selection of solvent systems. HPLC has limitation in acidity, basicity or extreme polarity of mobile phases because they might be detrimental for the solid stationary phase in columns but CCC is less sensitive to the solvent properties. Due to the support-free liquid stationary phase, the biphasic solvents both can be the mobile phase and the gentle interaction between solutes and liquid stationary phase insignificantly affects the sample decomposition. In addition, no irreversible adsorption of the analytes to the solid stationary phase arises so that the sample can be recovered without loss [27]. With the advantages, CCC has been applied to preparative separation of natural products as a powerful tool [29, 30].

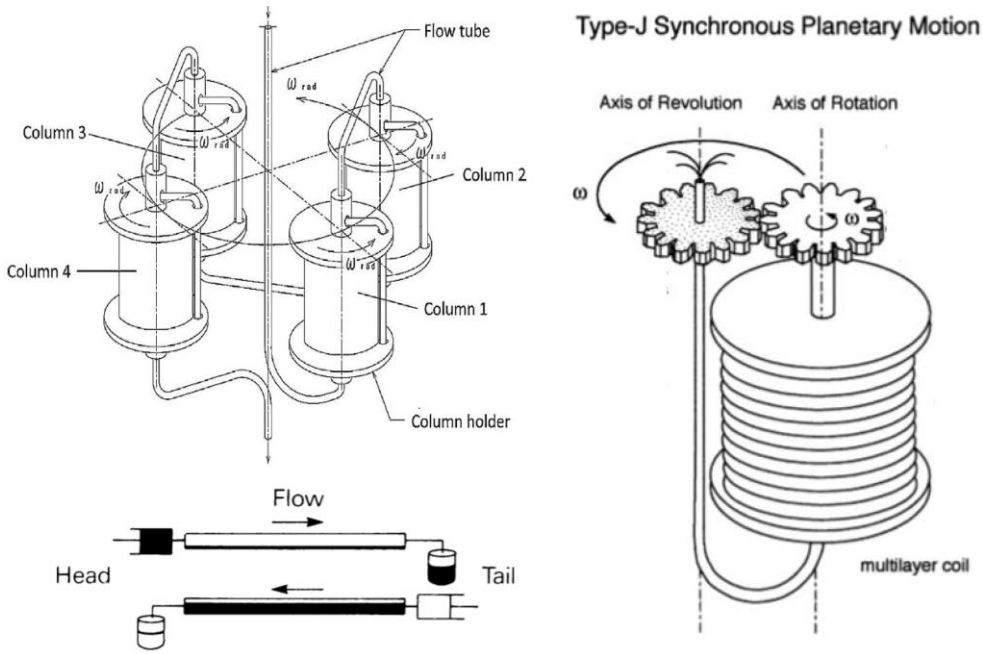

Figure 3. A schematic diagram of CCC system

The column holder rotates about its own axis and revolves around the centrifuge axis at the same angular velocity (ω) in the same direction. This type-J planetary motion of a multilayer coil separation column produces elution of both lighter and heavier phases through the coiled column where the lighter phase occupies one end called the head and the heavier phase, the other end called the tail. Reprinted with permission from [27]. Copyright 2005 by Elsevier (license number, 4621441102706).

2.2. Solvent selection and application

CCC solvent system consists of two immiscible phases and the target compounds relatively have different affinity or solubility toward the biphasic solvent system. Therefore, the analytes might be distributed with different ratio between the two phases **(Fig. 4)**. The distribution is evaluated by taking the upper phase concentration of the compound and then dividing it by the lower phase one. The ratio is a partition coefficient and symbolized by K_D [27]. Selecting effective solvent systems along with appropriate partition coefficients is most time-consuming but also most critical for the successful CCC separation. However, a little change in the one phase is able to change the other phase due to liquid-liquid equilibrium [31] so countless ways to create biphasic liquid systems which might confuse the researchers are possibly suggested. Most generally applied solvent systems are based on HEMWat (*n*-hexane / ethyl acetate / methanol / water, **Fig. 5**) [32] and ChMWat (chloroform / methanol / water) composition [33]. These solvent variations can be guidelines when selecting the proper solvent systems.

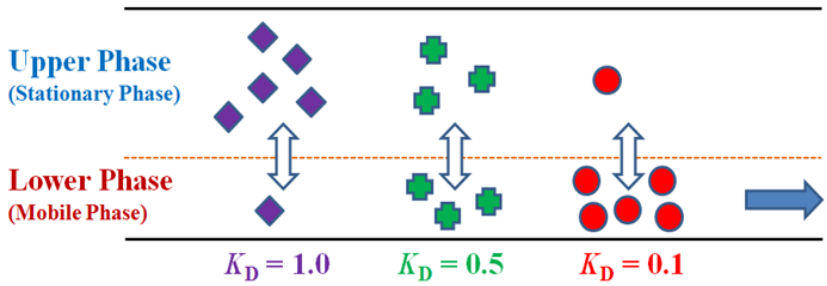

Figure 4. A schematic diagram of CCC separation based on K_D value

Target analytes are distributed and sequentially eluted in CCC system with different concentration ratio between the two phases (K_D). The K_D value is evaluated by dividing the upper phase concentration of the compound by the lower phase one.

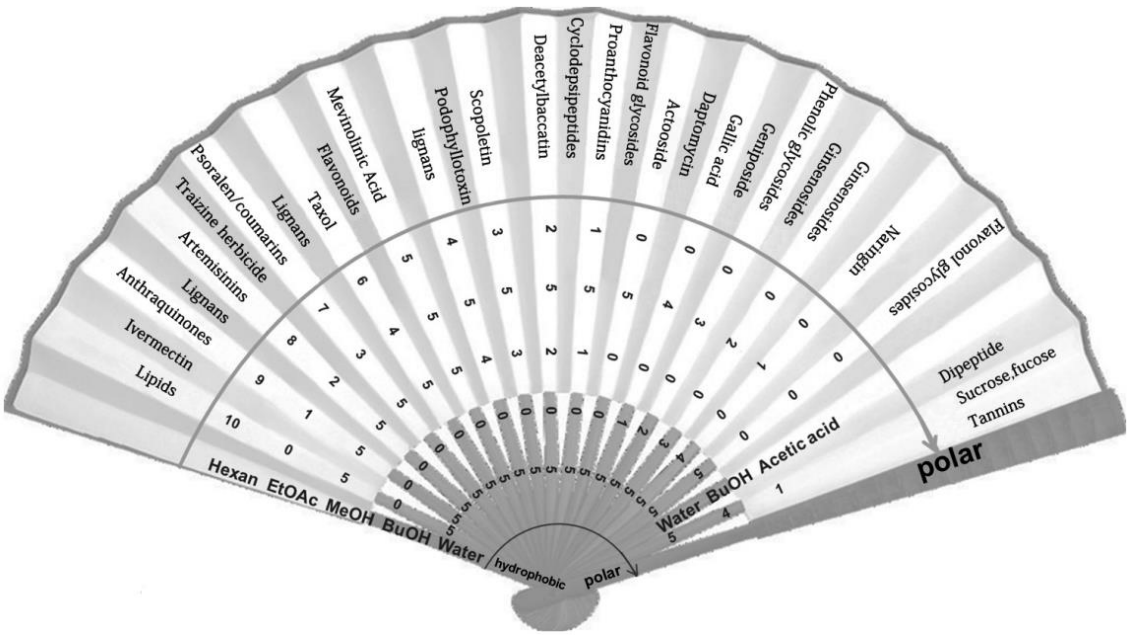

Figure 5. Polarity correlation between HEMWat systems and isolates

Reprinted with permission from [32]. Copyright 2014 by Elsevier (license number, 4621440973364).

3. Chemical profiling

3.1. Liquid chromatography and mass spectrometry (LC-MS)

Over the past few decades, advances in mass spectrometry (MS) have contributed to natural products research by providing qualitative and quantitative information [34]. MS can separate organic molecules according to their molecular weight and enable its detection with high sensitivity. It is not only regarded as having good selectivity, but also a very sensitive instrument. The mass spectrometer aim to boost the detection of low amounts of target compounds, while also to identify the species corresponding to each chromatographic peak through its unique mass spectrum [35]. Furthermore, the combination of liquid chromatography and MS (LC-MS) has become one of the powerful tools for the screening, identification, and quantification of complicated natural products **(Fig. 6)** [36].

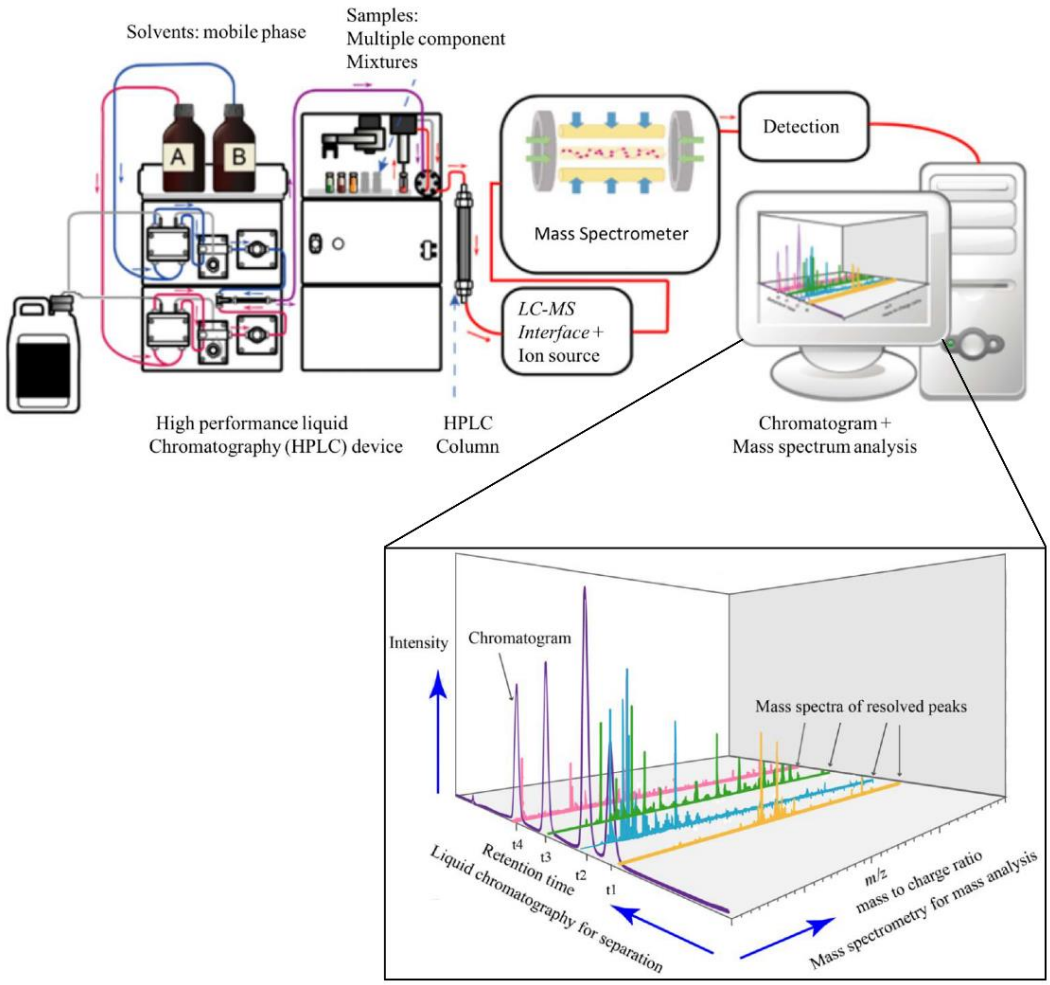

Figure 6. A schematic diagram of LC-MS system

3.2. Scan modes of tandem mass spectrometry (MS/MS)

Tandem mass spectrometry, called as MS/MS or MS2, allows for more informative mass analysis using a sequential scans in different regions of the instruments. [37]. A triple quadrupole mass spectrometer (QqQ-MS) is a kind of tandem mass spectrometer that is consisted of two quadrupole type mass analyzers (Q1 and Q3) and collision cell (Q2) between them [38]. The first and third quadrupoles can act as mass filters by detecting target ions, while the second quadrupole can fragment the precursor ion using collision gas. As shown in **Fig. 7**, the representative MS/MS technique is divided to four scan modes according to their experimental purpose: (A) In product ion scan, the first analyzer (Q1) is set to a value that selects one specific precursor ion at a time and the selected ion undergoes collision induced dissociation (CID) in Q2. The produced fragments are analyzed by the second analyzer (Q3). This method usually applied to screen known metabolites by matching their MS/MS fragmentation patterns. (B) In precursor ion scan, Q3 is set to transmit only one selected fragment ion to the detector, and Q1 scans all the precursor ions that generate this fragment. Typically, this scan mode is used to detect a subset of target molecules which contain common backbone or specific substituent groups. (C) Neutral loss scanning utilizes both analyzers in a synchronized manner, so that specific mass difference of ions was detected. The neutral loss scan is therefore used to detect those molecules that contain specific functional groups. (D) Selected reaction mornitoring (SRM) also use both analyzers, but select one precursor ion at Q1 and the other specific fragment at Q3, respectively. Therefore, the SRM method is usually used for

quantification of specific analytes in complex samples with known fragmentation properties. If multiple masses are selected for Q1 and Q3, this configuration is called multiple reaction monitoring (MRM) and the simultaneous quantification is possible in a single operation [39]. Although other MS/MS techniques such as Q-TOF MS and Orbitrap MS can utilize the scan modes, QqQ MS has gained their popularity for the precursor ion scan [40] and the MRM method [41] due to its fast scan speed and robustness, allowing the simultaneous detection of several hundreds of target analytes.

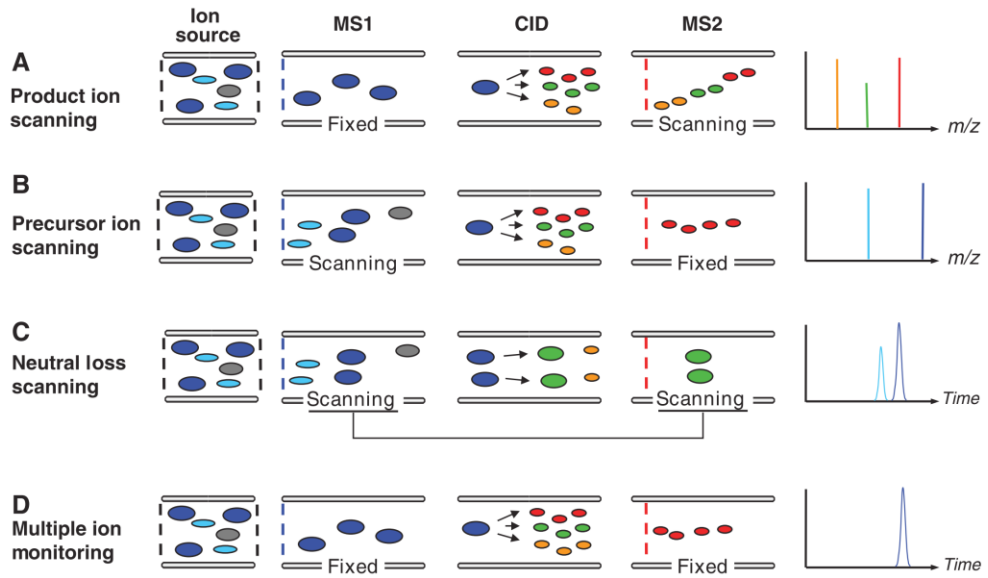

Figure 7. A schematic diagram of MS/MS scan modes

(A) Product ion scanning is the most common MS/MS experiment in metabolic analysis. The purpose is identification of fragment ion spectra of the target small molecules. (B) Precursor ion scanning is used to detect a subset of small molecules that contain specific skeletal backbone or substituent group. (C) Neutral loss scanning scans both analyzers in a synchronized manner, so that is used to detect those small molecules that contain specific substituent group. (D) Multiple reaction mornitoring is used for the detection of a specific analyte with known fragmentation properties in complex samples. Reprinted with permission from [38]. Copyright 2006 by American Association for the Advancement of Science.

3.3. LC-MS/MS-based dereplication methodology

Chemical profiling for secondary metabolites in natural products has been a laborious process, but underway for a few decades [42]. The main purpose of the profiling is to differentiate the whole constituents including bioactive or novel compounds. Extraction and elucidation of the chemical relationships within a given dataset are crucial to highlight the total number of detectable metabolites. However, deconvolution of each compound is challenging because natural products contain structurally diverse derivatives. In this perspective, dereplication strategy using LC-MS/MS techniques have gained more importance from both targeted and untargeted metabolomics [43]. The dereplication is rapid classification of complex mixtures in order to annotate the chemical structures and understand the significant variations. Investigation of the MS/MS information such as in-source fragmentation [44], accurate mass [45], adduct formation [46], neutral loss [47], and diagnostic ion [48] enabled us to dereplicate rapidly the secondary metabolites and sensitively quantify the interesting compounds, and the chemical composition of crude extracts could be established **(Fig. 8)**. Not only known compounds but also unknown and minor metabolites can be unveiled when the high-quality spectra are sophisticatedly interpreted. Moreover, MS and MS/MS spectral databases for the secondary metabolites have been established over the past few decades and offer a powerful tool to figure out complex natural products **(Fig. 9)** [49].

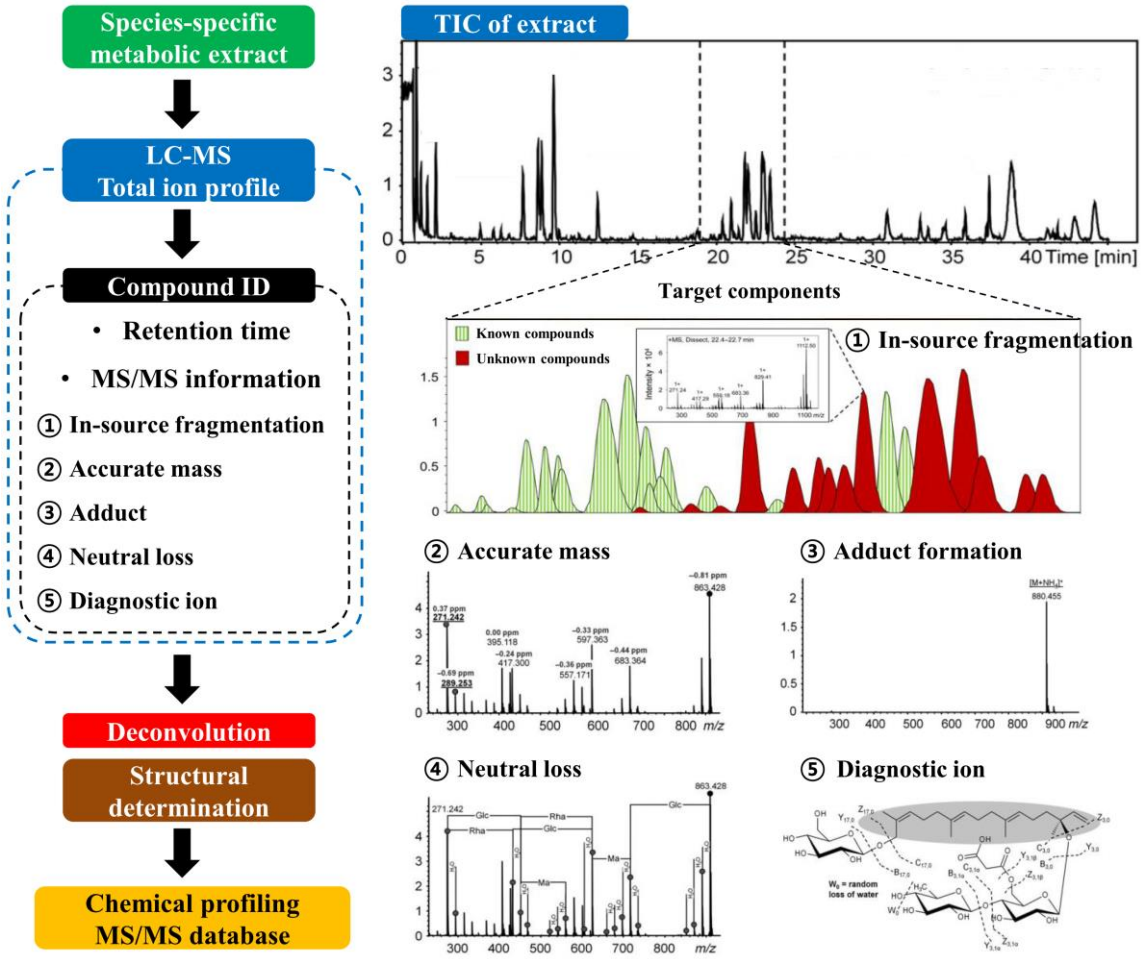

Figure 8. A schematic diagram of LC-MS/MS based dereplication

Reprinted with permission from [43]. Copyright 2016 by John Wiley and Sons (license number, 4621440434576).

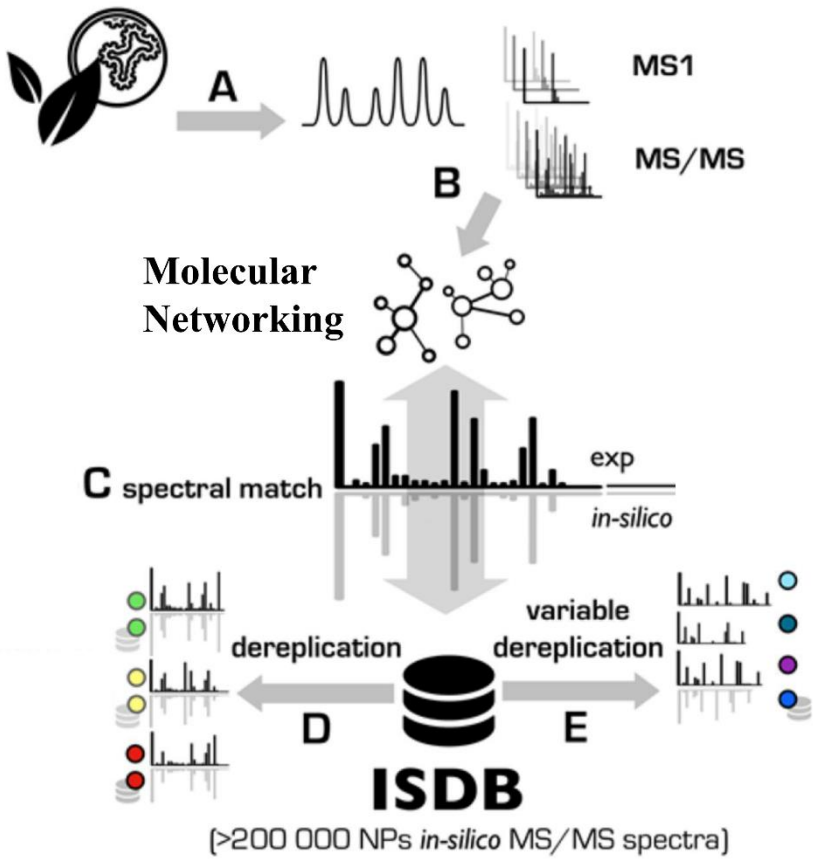

Figure 9. A schematic diagram of dereplication using MS/MS database

Molecular network (MN)-based dereplication using the *in-silico* MS/MS database (ISDB). (A) Crude extracts are profiled and untargeted MS/MS data are acquired. (B) Parent ions are organized as MN according to their MS/MS data. (C) The spectral library search can be made in two different modes. (D) Individual nodes are dereplicated against the ISDB using the parent ion mass as prefilter. Alternatively, (E) individual nodes can be dereplicated against the ISDB in a modification tolerant spectral library search called variable dereplication. Reprinted with permission from [49]. Copyright 2016 by American Chemical Society.

4. Activity-based proteome profiling

4.1. Background

Natural and traditional medicines, being a great source of drugs and drug leads, have regained wide interests due to the limited success of high-throughput screening of compound libraries in the past few decades and the recent technology advancement [50]. In many cases, bioactive compounds exert their functions through interaction with their multiple target proteins, thus target identification has an important role in drug discovery and biomedical research fields [51–53]. Identification of the specific target proteins not only unravels the mechanism of action (MOA) of the compound but also reveals its potential therapeutic applications and adverse side effects [54–56]. In this perspective, activity-based proteome profiling provides a direct and unbiased platform for comprehensive profiling of target proteins of a given bioactive compounds. This methodology is a multidisciplinary approach which integrates chemical modification with cell biology, resulting the enrichment of target proteins *in situ* **(Fig. 10)**. Using the bioactive compound-based probe as capture tag, reliable target proteins can be obtained under the physiological conditions and further identified by gel-based or MS-based approaches [57].

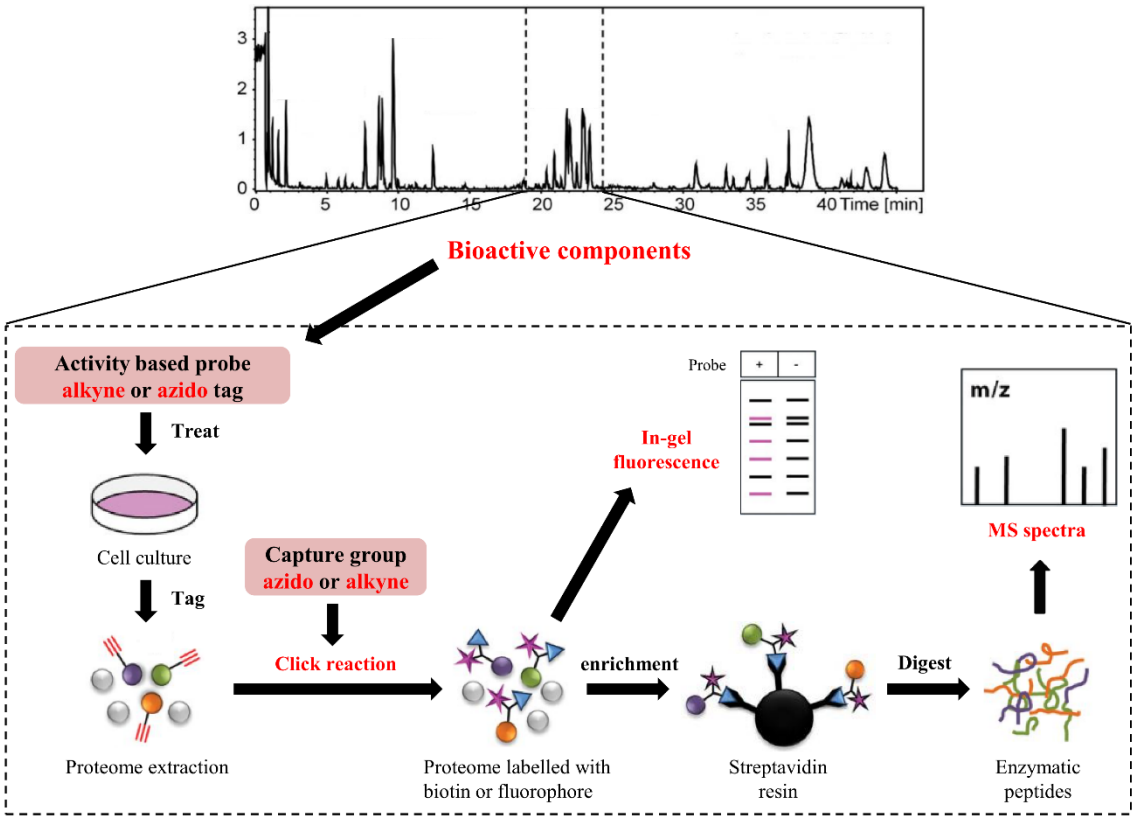

Figure 10. A schematic diagram of activity-based proteome profiling

4.2. Click chemistry

Although conventional affinity-based proteomics approaches have made great progress in the identification of cellular targets and elucidation of MOAs of many bioactive molecules, nonspecific binding remains a major issue which may reduce the accuracy of target identification and preclude the drug development process [51]. The *in vitro* target profiling may not accurately reflect the MOAs in the *in vivo* physiological environment. To overcome this limitation, bio-orthogonal methodologies have been developed to selectively enrich the target biomolecules in living systems (*in situ* or *in vivo*) [58–61]. One of these techniques, called click chemistry reaction, is copper-catalyzed azide-alkyne cycloaddition and enables the enrichment of target proteins *in situ* **(Fig. 11)** [62]. For the bio-orthogonal chemical reactions, the bioactive molecules must be modified to activity-based probes (ABPs) which contain either alkyne or azido group. The ABPs covalently react with target proteins through their reactive moieties, and the probe-labeled target proteins can be purified and identified by LC-MS/MS systems [63].

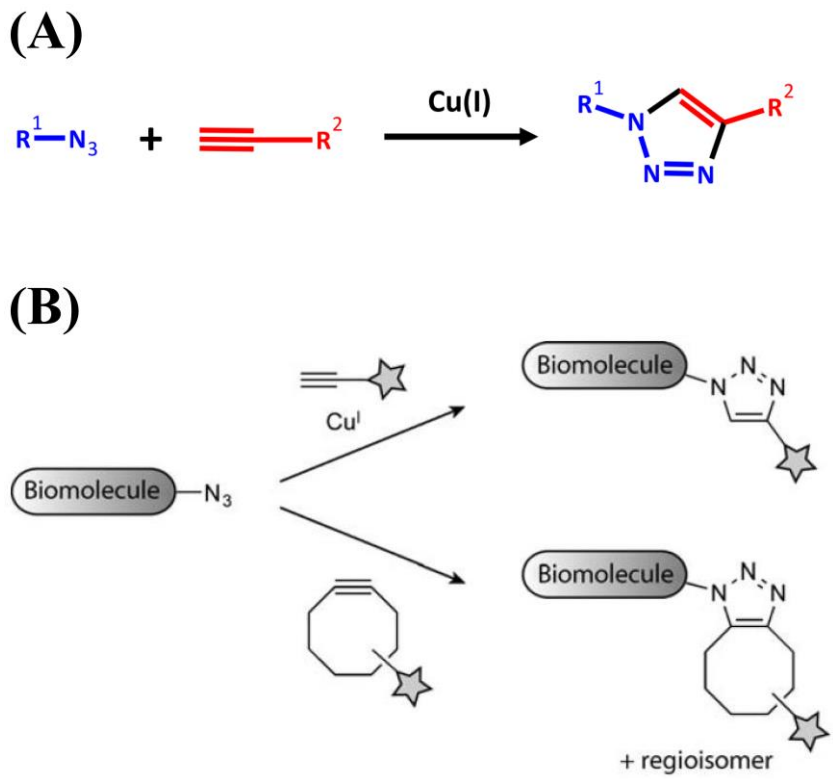

Figure 11. Click chemistry reaction

(A) Copper-catalyzed azide-alkyne cycloaddition to form triazole. (B) Terminal alkyne or cyclooctyne undergo cycloaddition with azide under physiological condition. Reprinted with permission from [62]. Copyright 2003 by American Chemical Society.

4.3. Quantitative proteome profiling based on mass spectrometry

Recently, chemical proteomics approaches have been a powerful tool in combination with modern high-resolution MS/MS analysis and bioinformatics for subsequent identification of binding proteins [64, 65]. In fact, several quantitative proteome profiling studies have been successfully performed using the MS/MS technique and characterized target proteins of traditional medicines [66–69]. Quantitative proteomics strategies could be divided in two groups, those that use some form of stable isotope labeling [66–70] and label-free quantification methods [71–73]. Stable isotope labeling-based methods are widely applied because they allowed the binary comparison experiments (control vs. treated, healthy vs. disease) **(Fig. 12)** [51]. In this strategy, two or more samples are modified with variants of a reagent that differ in their isotopic composition. Because the stable isotopes have virtually identical physicochemical properties as the natural isotopes, proteins incorporated with the stable isotope are almost identical to their natural counterparts [74]. Therefore, the difference in accurate mass of peptide and their fragments enables determination of the relative quantities of a peptide in different samples.

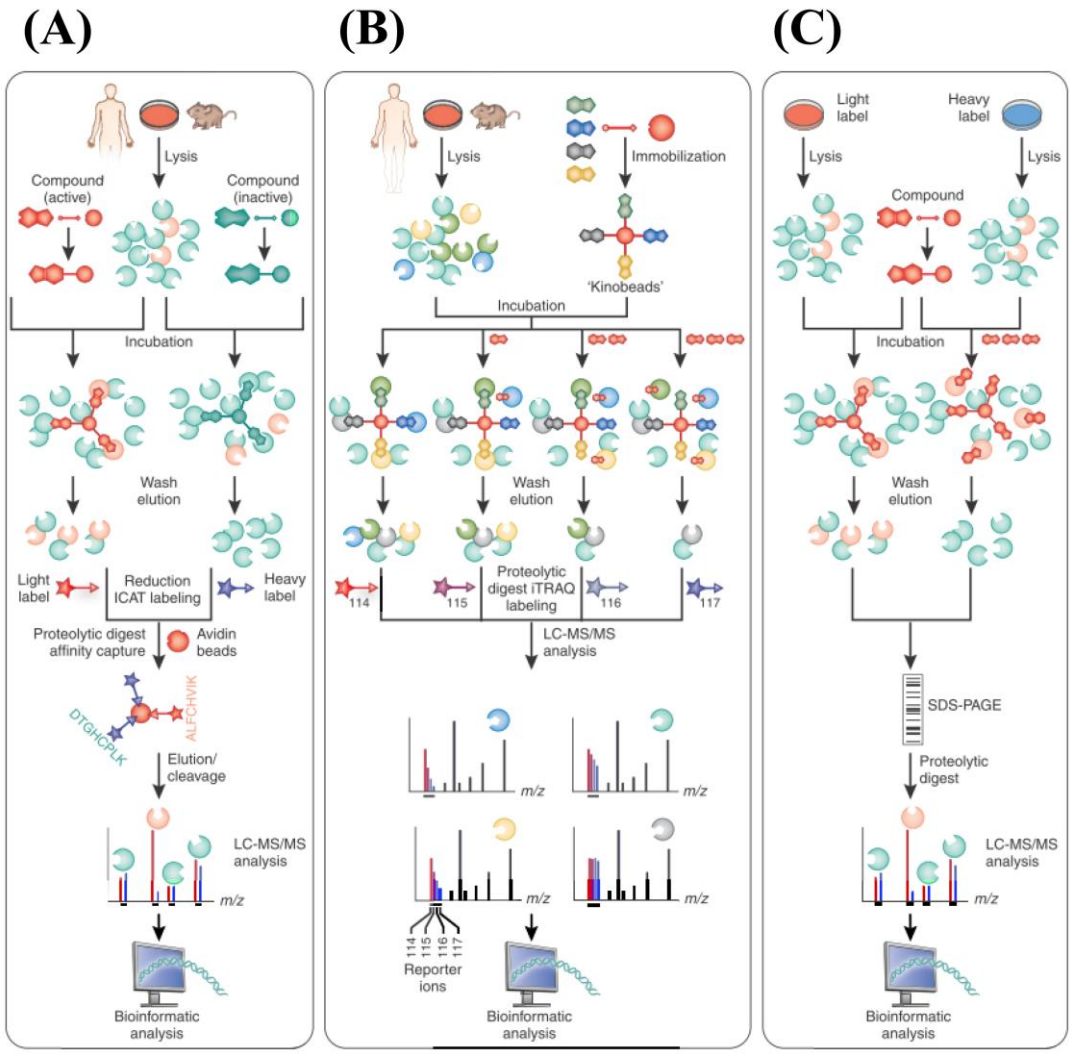

Figure 12. A schematic diagram of LC-MS based quantitative proteome profiling

Stable isotope labeling-based quantitative mass spectrometry approaches in chemical proteomics. (A) Comparison of two independent experiments with active and inactive molecules by isobaric labeling of eluted proteins. (B) Determination of specificity and affinity by isobaric labeling of obtained peptides. (C) Identification of specific protein targets by comparison of labeled eluates between compound-pretreated and -untreated group. Reprinted with permission from [51]. Copyright 2008 by Springer Nature (license number, 4621430351042).

II. STATE OF THE PROBLEM

Natural products, one of the key sources of biologically active metabolites, are commonly exploited for the development of drugs and dietary supplements [50]. However, the chemical analogues in one natural resource have similar structures sharing backbones and substituent groups, it is challenging to separate the complex mixture chromatographically and interpret the spectrometric information. Furthermore, the small molecule usually interact with multiple proteins, and their mechanism of action (MOA) and potential side effect are hard to recognize. In this perspective, the present study is focused on i) preparative separation, ii) chemical profiling, and iii) activity based proteome profiling of sesquiterpenoids from Farfarae Flos.

Firstly, it is essential to develop an efficient method for preparative enrichment and isolation of natural components for the structural determination and further pharmacological studies. Counter-current chromatography (CCC), one of liquid-liquid chromatographic technique, is suitable for the enrichment and preparative separation of target components because CCC theoretically generates 100% sample recovery [28]. However, the sample loading capacity of conventional CCC method does not exceed that of solvent partitioning and open column chromatography for a given separation column size [75–77]. Furthermore, scale-up of the CCC technique has focused on enlarging the size or improving the shape of the separation column [78–83]. Therefore, the aim of this study was to develop an efficient method for preparative enrichment and separation of target compounds from plant extracts using CCC.

The second objective of the present study was to develop LC-MS/MS dereplicative method for oplopane and bisabolane sesquiterpenoids from Farfarae Flos. The backbones of these compounds are substituted with diverse ester derivatives, and about 30 sesquiterpene esters have been reported up to date [17–25]. Although the sesquiterpenoids are hard to be fully separated and characterized because of their structural diversity, LC-MS-based analytical studies have not been reported except for tussilagone which is a chemical marker of the medicinal plant [84–86]. In addition, metabolomic profiling studies of the Farfarae Flos have focused on its phenolic compounds and pyrrolizidine alkaloids [87, 88]. Therefore, it is necessary to profile the sesquiterpenoids for quality control of the Farfarae Flos.

Finally, identification of target proteins of an oplopane sesquiterpenoid (7β-(3'-ethyl *cis*-crotonoyloxy)-1α-(2'-methylburyryloxy)-3, 14-dehydro-*Z*-notonipetranone, ECN) was conducted in human breast cancer cells. The Farfarae Flos have been reported to exhibit anti-proliferation activity in several cancer cell lines, and its oplopane type sesquiterpenoids were most potent [89–93]. However, the range of investigated molecular pathways were too narrow to specify the molecular targets of these compounds. Therefore, it is need to identify the direct target proteins of the oplopane sesquiterpenoid in order to understand its mechanism of action and potential therapeutic applications.

III. MATERIALS AND METHODS

1. Materials

1.1. Farfarae Flos

Korean Farfarae Flos was collected from Medical Herb Gargen of Seoul National University (Ilsan, Korea), and Chinese Farfarae Flos was purchased from Omniherb (Yeongchun, Korea).

1.2. Chemicals and reagents

Industrial grade *n*-hexane, methylene chloride, ethyl acetate, methanol, and acetonitrile (Daejung, Siheung, Korea); analytical grade water (NANO pure Diamond, Barnstead, NH, USA); analytical grade acetonitrile (J. T. Baker, NJ, USA); macroporous ion-exchange Diaion™ HP-20 resin (Mitsubishi Chemical Corporation, Tokyo, Japan); formic acid (Daejung, Siheung, Korea) were used for chromatographic and mass spectrometric experiments.

Dulbecco's phosphate buffered saline (PBS), dimethyl sulfoxide (DMSO), a protease inhibitor cocktail, 3-(4,5-dimethylthiazol-2-yl)-2,5 diphenyltetrazolium bromide (MTT), cerium (III) chloride heptahydrate ($CeCl_3$), tris-3-hydroxypropyl triazolyl methyl amine (THPTA), tris(2-carboxyethyl)phosphine hydrochloride (TCEP), triethyl ammonium bicarbonate (TEAB), and iodoacetamide (IAA) were obtained were purchased from Sigma Aldrich (St. Louis, MO). Penicillin, DMEM (high glucose), and fetal bovine serum (FBS) were obtained from GenDepot (Barker, TX). Cyanine3-alkyne (Cy3-alkyne) and dialkoxydiphenylsilane (DADPS)

biotin alkyne, were purchased form Click Chemistry Tools (Scottsdale, AZ, USA). 14-3-3 protein zeta and peroxiredoxin-1 were purchased from Fitzgerald (Cat # 80R-1064 and 80R-1854, respectively). All other chemicals were purchased from Sigma-aldrich unless otherwise specified.

1.3. Apparatus

The CCC instrument was a TBE-1000A (Tauto Biotech., Shanghai, China), including a six-port injection valve, a 60 mL sample loop, a Hitachi UV detector L-7400 (Hitachi, Tokyo, Japan), a Prep UV-10V detector (Yamazen, Osaka, Japan), a Waters fraction collector (Waters Corporation, MA, USA), and a Autochro data module with Autochro-2000 1.0 software (Younglin Instrument, Angyang, Korea). The TBE-1000A had three multilayer coil separation columns connected in series (tube I.D.: 3.0 mm, each volume of three coils: 330 mL, total volume: 1000 mL). The rotation speed of the apparatus ranged from 0 to 500 rpm. Samples were analyzed by high-performance liquid chromatography (HPLC) using a Hitachi L-6200 HPLC pump (Hitachi), a SIL-9A auto injector (Shimadzu, Kyoto, Japan), and a Spectra-100 UV detector (Spectra-Physics, Santa Clara, USA).

UHPLC separation of Farfarae Flos was performed on a Thermo Vanquish™ Flex UHPLC system (Thermo Scientific, Waltham, MA, USA) and a YMC Triart C_{18} column (2.0 mm × 50 mm, 1.9 μm particle size, YMC Co.). Precursor ion scan was performed using a 3200 QTrap system (AB Sciex, Foster

City, CA, USA), and product ion scan and high resolution multiple reaction monitoring (MRM^{HR}) were conducted using a Triple TOF 5600+ system (AB Sciex). The NMR spectra of isolated compounds were recorded by a Bruker Avance 500 MHz spectrometer and NMR solvents: DMSO-d_6, $CDCl_3$, and tetramethylsilane (TMS) were purchased from Cambridge Isotope Laboratories (Cambridge, MA).

Cell viability assessed by MTT assay was measured using a Molecular Devices Emax Microplate Reader (Sunnyvale, CA, USA). Mass spectrometric peptide analyses were performed using an Easy-nanoLC 1000 (Thermo Fisher Scientific, Waltham, MA) coupled to a Q-Exactive Hybrid Quadrupole-Orbitrap instrument mass spectrometer (Thermo Scientific).

1.4. Cell lines

MDA-MB-231 and MCF-7 human breast cancer cells were purchased from the Korea Cell Bank (Seoul, Korea). and maintained in DMEM supplemented with 10 % FBS and antibiotics (penicillin 100 U/mL and streptomycin 100 μg/mL). Cultures were maintained in a humidified atmosphere incubator at 37 °C with 5% CO_2.

2. Methods

2.1. An efficient fractionation method for the preparative separation of sesquiterpenoids from Farfarae Flos by CCC

2.1.1. Measurement of the partition coefficient (K_D)

The compositions of the extraction solvent and eluting solvent were selected based on the partition coefficient (K_D) of the three major sesquiterpenoids (**TG**: tussilagone, **AECN**: 14-acetoxy-7β-(3'-ethyl *cis*-crotonoyloxy)-1α-(2'-methylbutyryloxy)-notonipetranone, and **ECN**: 7β-(3'-ethyl *cis*-crotonoyloxy)-1α-(2'-methylbutyryloxy)-3,14-dehydro-*Z*-notonipetranone). An adequate amount (approximately 1 mg) of each compound was weighed into a test tube, to which 1 mL aliquots of a two-phase solvent were added (0.5 mL of *n*-hexane as the upper phase and aqueous acetonitrile as the lower phase: 35, 45, 55, 65, 75, 85, and 95% acetonitrile in a total volume of 0.5 mL). The tube was shaken vigorously to thoroughly equilibrate the compound between the two phases. Equal volume of each phase were separated and evaporated to dryness under N_2 gas. The residue was dissolved in methanol and was analyzed by HPLC. The K_D value was calculated from the peak area of the target compound in the upper phase divided by the peak area in the lower phase.

2.1.2 Preparation of the extract solution and solvent system

Dried Farfarae Flos (1 kg) were pulverized and extracted with 3 L of 45% acetonitrile by sonication for 1 h. The extraction process was repeated with 2 L of

45% acetonitrile two more times. The extract solution were passed through filter paper (Advantec, Tokyo, Japan), and all filtrates were combined. Total extract solution (5.4 L) was directly injected for CCC-DCI fractionation. Additional Farfarae Flos (1 kg) was extracted using the same method, and the extract solution was dried for conventional fractionation methods: solvent partitioning and open column chromatography.

2.1.3. CCC-DCI fractionation

Counter-current chromatography-direct and continuous injection (CCC-DCI) fractionation was conducted in four stages using the preparative CCC instrument (TBE-1000A). *n*-Hexane, acetonitrile, and water were used as the two-phase solvent system, and each solvent was prepared separately (only degassing) without time-consuming equilibration in a separatory funnel. Stage I: the multi-layered coiled column was filled with *n*-hexane to form the stationary phase. The apparatus was then rotated at 450 rpm, and the extraction solution of Farfarae Flos (5.4 L in total) was directly pumped into the head end of the column at a flow rate of 15 mL/min. Stage II: the extraction solution was continuously injected into the column. The eluent was continuously monitored by connecting the tail outlet of the coiled column to a UV detector. The UV system detection was performed at 235 nm and 2.5 (maximum) absorbance units. Stage III: after all the extraction solution was injected into the CCC instrument, pure 45% acetonitrile (same composition as the extraction solvent) was pumped into the head of the column at the same flow

rate. Stage IV: as the UV signal decreased, 100% acetonitrile (eluting solvent) was pumped into the CCC instrument. The sesquiterpenoid-enriched (STE) fraction was collected according to the elution profile and was analyzed by HPLC-UV. Stationary phase retention was measured after fractionation by forcing the contents through the column with pressurized N_2 gas and collecting the contents.

2.1.4. Solvent partitioning and open column chromatography

Another extract solution of Farfarae Flos (5.4 L) was evaporated with a rotary evaporator under reduced pressure, and the dried extract (513.9 g) was dissolved in 2.5 L of water and fractionated with 2.5 L of *n*-hexane (*n*-Hex) three times. The water residue was fractionated with 2.5 L of methylene chloride (MC) three times. Each solution (7.5 L, respectively) was evaporated to produce an *n*-Hex (5,816 mg) and MC (4,399 mg) fraction, and combined for subsequent open column chromatography. The combined fraction (10,215 mg) was dissolved in 1 L of 30% methanol (MeOH) and loaded onto a Diaion HP-20 open column (60 cm × 2.4 cm; the volume of the column was 270 mL and it was packed with 200 g of resin). Then, the fractions were sequentially eluted with a MeOH gradient beginning with 100% water and increasing to 30, 60, 90, and finally 100% MeOH. The volume of each elution solvent was 2 L. The STE fractions were eluted by 90% MeOH (2,033 mg) and 100% MeOH (4,055 mg).

2.1.5. Isolation of three major sesquiterpenoids

Three major sesquiterpenoids (**TG**, **AECN**, and **ECN**) were isolated from the STE fraction by CCC. *n*-Hexane was filled to the separation column of CCC as the stationary phase, and the apparatus was rotated at 450 rpm. Three grams of the STE fraction was dissolved in 60 mL of 65% acetonitrile and loaded into sample loop. The sample solution was injected through a six-port injection valve, and the mobile phase (65% acetonitrile) was directly pumped into the head of the column at a flow rate of 5 mL/min. The CCC separation condition was the following: water as eluent A; acetonitrile as eluent B; linear gradient: 0–300 min (65–100% B), 300–400 min (100% B). Then stationary phase retention was measured by forcing the contents through the column with pressurized N_2 gas and collecting the contents. The collected compounds were further refined by preparative HPLC to eliminate minor impurities. The purities of the sesquiterpenoids were assessed by HPLC-UV at 235 nm, and their chemical structures were determined by ^{1}H and ^{13}C NMR spectroscopy. The NMR spectra were recorded by a Bruker Avance 500 MHz spectrometer in $CDCl_3$ using TMS as the internal standard.

2.1.6. Preparation of sample solution

Accurately weighed samples: 10 mg of 45% ACN extract; 3 mg of CCC-DCI fraction; 5 mg of *n*-Hex fraction; 5 mg of MC fraction; 90% MeOH fraction (3 mg); 3 mg of 100%MeOH fraction; 1 mg of **TG**; 1 mg of **AECN**; 1 mg of **ECN**

were sonicated with 1 mL of methanol for 10 min and then filtered through a 0.45 μm syringe filter. The solutions of **TG**, **AECN**, and **ECN** were serially diluted with methanol to produce standard solutions at concentrations of 62.5, 125, 250, 500, and 1000 μg/mL.

2.1.7. HPLC analysis and calibration curve

A Phenomenex Luna C_{18} column (150 mm × 4.6 mm, 5 μm particle size) was used to analyze the extract, fractions (CCC-DCI, solvent partition, and open column chromatography), and three major sesquiterpenoids. The HPLC conditions were optimized by altering the elution gradient. The analysis used water as eluent A and acetonitrile as eluent B, and the elution program was as follows: 0–3 min (60–75% B); 3–28 min (75–100% B); 28–33 min (100% B); and equilibration with 60% B for 10 min at a flow rate of 0.9 mL/min. The column was at room temperature and the UV detection was performed at 235 nm. 5 μL of each sample solution was injected into the HPLC and analyzed in triplicate to ensure the reproducibility. Three standard solutions at concentrations of 62.5 – 1000 μg/mL were analyzed and their regression equations were calculated in the form of $y = ax + b$, where x and y correspond to the compound concentration and peak area of the UV response, respectively. The limits of detection (LODs) and limits of quantification (LOQs) were defined as the concentrations that produced signal-to-noise ratios of three and ten, respectively.

2.2. Chemical profiling of sesquiterpenoids from Farfarae Flos based on LC-MS/MS analysis

2.2.1. Sample preparation from Farfarae Flos

The dried parts (1 g each) of *T. farfara* were extracted with 10 mL of ethanol or *n*-hexane by sonication for 1h, triplicate. The STE fraction was isolated by CCC (TBE-1000A) and semi-preparative HPLC (YMC Triart C_{18}, 10 × 250 mm, 5 μm particle size, YMC Co.) to obtain 11 sesquiterpenoids (see Section 2.2.4). All the extracts, fractions, and compounds were accurately weighed, dissolved in LC-MS grade acetonitrile, and filtered through a 0.22 μm syringe filter before UHPLC-MS/MS analysis. The concentrations of the fraction (200 μg/mL) and the isolated compounds (10–20 μg/mL) were used for the qualitative analysis of the sesquiterpenoids. The concentrations of the extracts (50 and 500 μg/mL) and the compounds (2^{-5}, 2^{-4}, 2^{-3}, 2^{-2}, 2^{-1}, 2^{0}, 2^{1}, 2^{2}, and 2^{3} μg/mL) were used for the quantification of the sesquiterpenoids.

2.2.2 UHPLC separation

A YMC Triart C_{18} column (2.0 mm × 50 mm, 1.9 μm particle size, YMC Co.) was used for UHPLC separation. The UHPLC system used 0.1% formic acid in water as eluent A and 0.1% formic acid in acetonitrile as eluent B, and the optimized elution program was as follows: 0–3 min (45–60% B); 3–15 min (60–80% B); 15–16 min (80–100% B); 16–20 min (100% B) and equilibration with 45% B for 4 min at a flow rate of 0.4 mL/min. The column was at 30 °C and the auto-

sampler was maintained at 4 °C. The injection volume of each sample solution was 2 μL.

2.2.3 MS/MS analysis

The precursor ion scan was performed using a 3200 Q-Trap system (AB Sciex, Foster City, CA, USA). The product ion scan and high resolution multiple reaction monitoring (MRM^{HR}) were conducted using a Triple TOF 5600+ system (AB Sciex). Both systems were equipped with an electro spray ionization (ESI) source and operated in the positive ESI mode for detection. The MS/MS conditions were as follows: ion spray voltage, 5.5 kV; spray temperature, 500 °C; declustering potential (DP), 30 V; collision energy (CE) of QqQ MS/MS, 5, 15, 25 eV; CE of Q-TOF MS/MS, ramping from 5 to 25 eV for fragmentation pattern of diagnostic ions, 5, 15, 25 eV for fragmentation pattern of precursor ions, 15 eV for MRM^{HR} quantification; nitrogen gas for nebulizer gas, 50 L/min; heater gas, 50 L/min; curtain gas, 25 L/min. The scan range was set to *m/z* 250–550 with 2.0 s cycle time for the precursor ion scan, and *m/z* 50–550 with 1.4 s cycle time and 0.1 s accumulation time for the product ion scan. The MS/MS data for qualitative analysis were processed using Peakview and MasterView software (AB Sciex) to screen the probable metabolites based on accurate mass and isotope distribution. MultiQuant software (AB Sciex) was used to monitor the selected ions for the quantification study.

2.2.4. Separation of sesquiterpenoids and structural determination

Eleven sesquiterpenoids (No. **7**, **11**, **12**, **14**, **23**, **36**, **39**, **45**, **60**, **68**, and **72** in **Table 5**) were isolated from the STE fraction by CCC and semi-preparative HPLC. The CCC separation used *n*-hexane as the stationary phase and aqueous acetonitrile as the mobile phase. The multilayered coiled column was filled with 1 L of *n*-hexane and the apparatus was rotated at 450 rpm. The mobile phase was pumped into the head of the column at a flow rate of 6 mL/min and a linear gradient separation was performed: 0–250 min (55–95% aqueous acetonitrile) and 250–350 min (100% acetonitrile). In a single operation, three grams of the STE fraction were dissolved in 20 mL of acetonitrile and injected through a six-port injection valve. In addition, compounds **12** and **68** were further hydrolyzed to obtain **23**, **36**, and **7**. One gram of **12** was dissolved in 100 mL of 70% aqueous acetonitrile and sodium hydroxide (NaOH) was added to 100 mM NaOH solution. The reaction mixture was stirred at 25 ℃ for 1 h, followed by solvent extraction with chloroform and water to obtain **23** and **36**. Likewise, compound **68** was hydrolyzed (500 mM NaOH, 25 ℃, 2 h) to obtain **7**. Each chloroform layer was evaporated and further separated by semi-preparative HPLC. The HPLC system used water as eluent A and acetonitrile as eluent B, and the optimized elution program was as follows: 0–25 min (75–100% B) for **23** and **36**; 0–20 min (60–80% B) for **7** at a flow rate of 4 mL/min. All the separated compounds were structurally determined by ^{1}H, ^{13}C, and HSQC NMR spectroscopy. Compound **7**, **23**, and **45** were further analyzed using nuclear Overhauser effect spectroscopy (NOESY). The NMR spectra were recorded by a Bruker Avance 500 MHz spectrometer in DMSO-

d_6 using TMS as the internal standard.

2.2.5. Validation parameters for quantification

The sensitivity and repeatability of the UHPLC-MS/MS method was assessed by determining the selectivity, linearity, limit of detection (LOD), limit of quantification (LOQ), and precision. The selectivity of each sesquiterpenoid was established depending on the UHPLC-MS/MS parameters to distinguish unambiguous analytes of interest from the complex mixture: retention time, *m/z* of precursor ion, and *m/z* of diagnostic ion. The calibration curve of each isolated sesquiterpenoid was assessed using a serial dilution of the mixed stock solution (8 sesquiterpenoids at 200 μg/mL, respectively). Each peak area was measured by analyzing the solutions at 9 concentration (2^{-5}, 2^{-4}, 2^{-3}, 2^{-2}, 2^{-1}, 2^{0}, 2^{1}, 2^{2}, and 2^{3} μg/mL) three times. Regression equations were calculated in the form of $y = ax + b$, where x and y correspond to the compound concentration (ng/mL) and peak area of the MS response, respectively. The LODs and LOQs for the 8 sesquiterpenoids were determined by analyzing the mixed standard solutions at the lowest concentrations (2^{-7}, 2^{-6}, and 2^{-5} μg/mL) and measuring their signal-to-noise ratio (S/N) of three and ten, respectively. The S/N was determined by comparing the heights of the analyte peaks in the standard solutions with background noise of blank sample (the regions equivalent to 20 times the width of the analyte peaks at the half-height). The intra-day and inter-day precision were evaluated by measuring the peak area repeatability of three standard solution (2^{-3}, 2^{0}, and 2^{3} μg/mL) five

times within one day and three different days, respectively. The precision was measured by calculating the relative standard deviation (RSD) of variations in the retention time and peak area.

2.3. Activity based proteome profiling: Identification of target proteins of an oplopane sesquiterpenoid in breast cancer cells

2.3.1. Fractionation of Farfarae Flos extract

Korean and Chinese Farfarae Flos (10 g) were extracted with ethanol (10 mL) by sonication for 1h, triplicate. Each ethanol extract was concentrated using a rotary vacuum evaporator, and further isolated by semi-preparative HPLC (YMC Triart C_{18}, 10 × 250 mm, 5 μm particle size, YMC Co.) to obtain 11 fractions. The HPLC system used water as eluent A and acetonitrile as eluent B, and the optimized elution program was as follows: 0–35 min (20–100% B) at a flow rate of 4 mL/min. Fractions were collected according to the elution profile of UV detector (220 nm). Each fraction was concentrated, accurately weighed, and dissolved in DMSO for further anti-proliferation test.

2.3.2. Cell viability assay

The anti-proliferation activities of test samples on MDA-MB-231 and MCF-7 human breast cancer cells were evaluated by MTT assay. Cells were seeded at a density of 1×10^5 and 1×10^4 cells per well into 24-well and 96-well plates, respectively, and incubated at 37 ºC for 24 h. The cells were treated with vehicle (medium with 0.1% DMSO) or increasing concentrations of test samples for 24 h. The 500 μL of MTT solution (0.5 mg/mL) was added to each well, followed by incubation for 3 h. The MTT formazan crystals were dissolved in DMSO and the

absorbance at a wavelength of 540 nm was measured by using a microplate reader. The above experiments were conducted in biological triplicated for each sample and cell line (n = 3). IC_{50} values and 95% confidence intervals (CI) were estimated using GraphPad Prism 6.01 (GraphPad Software).

2.3.3. Synthesis of ECN-based clickable probe

ECN (861.0 mg, 2.0 mmol) and m-CPBA (1035.3 mg, 3.0 mmol) were dissolved in CH_2Cl_2 (10 mL), respectively. The solution was mixed and stirred at 4 ℃ for 12 h. The reaction mixture was filtered through 0.45 μm filter paper (Advantec.) and dried with a rotary evaporator under reduced pressure. The sample was then dissolved in 10 mL of methanol, and separated by CCC. The CCC condition as follows: *n*-hexane as stationary phase; water (eluent A) and acetonitrile (eluent B) as mobile phase; linear gradient, 0–100 min (75–95% B) and 100–150 min (95% B) at a flow rate of 8 mL/min. Eluate from 110–125 min was collected and dried (187.6 mg), followed by structural determination. **ECN-E** (178.6 mg, 0.4 mmol) was dissolved in 10 mL of water/acetonitrile (2:8, v/v) and NaN_3 (78.0 mg, 1.2 mmol) and $CeCl_3 \cdot 7H_2O$ (74.4 mg, 0.2 mmol) was added, followed by incubated (50 ºC, agitation at 200 rpm, 24 h). The reaction mixture was filtered and diluted with 10 mL of H_2O and CH_2Cl_2, respectively. The organic phase was collected and evaporated. The sample dissolved in acetonitrile and separated by semi-preparative HPLC to obtain **ECN-N_3** (26.1 mg, 0.052 mmol, 2.6% yield in total).

2.3.4. Gel-based ABPP of MDA-MB-231 and MCF-7 cell lines *in situ*

MDA-MB-231 and MCF-7 cells were grown in 25 cm^2 cell culture plate (SPL) until 90% confluence. The medium was removed and replenished with 2.0 mL of fresh media containing DMSO (negative control), ECN-N_3 (1.0, 3.0, 9.0, and 27.0 μM), ECN-N_3 (27.0 μM) with excess ECN (54.0 and 90.0 μM). Following incubation at 37.5 °C for 3 h, cells were washed with cold PBS twice and harvested. After centrifugation (14,000 × g, 3 min, 4 ºC), cell pellet was lysed with 100 μL of cold lysis buffer (20 mM HEPES of pH 7.9, 20% glycerol, 350 mM NaCl, 1.0 mM $MgCl_2$, 0.5 mM EDTA, 0.1 mM EGTA, 1% NP-40, 0.1 mM DTT, 0.1 mM PMSF, and protease inhibitor cocktail) for 30 min on ice. The cell lysate was centrifuged (14,000 × g, 10 min, 4ºC) and the supernatant was collected as whole cellular proteome sample. The protein concentration was determined by Bradford reagent according to the manufacturer's protocol (Bio-Rad). The proteomes from cell lysis were diluted to 2.0 mg/mL (cold lysis buffer and 1% final SDS concentration) and either directly processed or stored at –80 ºC until use. Click reaction was performed as below: 20 μL of proteome samples were added with freshly prepared Cy3-alkyne (1 μL of 2.0 mM stock in DMSO), $CuSO_4$ (1 μL of 30 mM stock in water), THPTA (1 μL of 10 mM stock in water) and sodium ascorbate (1 μL of 30 mM stock in water). The mixture were incubated in dark to click reaction (25 ºC, agitation at 200 rpm, 1 h). For gel-based experiment, 12 μL of the click labeled proteome was added with 6 μL of 3X SDS loading buffer and applied to SDS-PAGE (20 μg total protein loaded per gel lane) and imaged by Biomolecular imager FLA7000IP (GE Healthcare).

2.3.5. Preparation of probe-labeled proteome for MS-based analysis

MDA-MB-231 and MCF-7 cells were grown in 75 cm^2 cell culture plate (SPL) until 90% confluence. The medium was removed and replenished with 6.0 mL of fresh media containing DMSO (negative control) and ECN-N_3 (10.0 μM). Following incubation at 37 °C for 3 h, cells were washed with cold PBS twice and harvested. After centrifugation (14,000 × g, 3 min, 4 ºC), cell pellet was lysed with 300 μL of the cold lysis buffer (see Section 2.3.4) for 30 min on ice. The cell lysate was centrifuged (14,000 × g, 10 min, 4 ºC) and the supernatant was collected as whole cellular proteome sample. The protein concentration was determined by Bradford reagent according to the manufacturer's protocol (Bio-Rad). The proteome sample was diluted to 2.0 mg/mL (cold lysis buffer and 1% final SDS concentration) and either directly processed or stored at –80 ºC until use. Each 100 μL of proteome sample was transferred to a new 2 mL tube and added with 20 μL of PBS containing DADPS biotin-alkyne (0.5 mM), $CuSO_4$ (7.5 mM), THPTA (2.5 mM), and sodium ascorbate (7.5 mM) to click reaction (25 ºC, agitation at 200 rpm, 1 h). The reaction mixture was added with cold methanol (600 μL), chloroform (150 μL), and water (530 μL) sequentially and briefly vortexed. The cloudy sample was centrifuged (1,500 × g, 10 min, 4 ºC), and upper and lower solvent layer were removed without disturbing protein disk. After resuspension with 1.0 mL of cold methanol and centrifugation (14,000 × g, 10 min, 4 ºC), the supernatant was removed carefully. The each protein pellet was dissolved in 160 μL of urea buffer (6 M urea and 0.2% SDS in PBS) by sonication. The proteins were reduced by adding 20 μL of PBS containing TCEP (200 mM) and TEAB (200 mM) and the

reaction mixture was incubated (50 ºC, 1 h). After cooling the sample to room temperature, the reduced protein was alkylated by adding 20 µL of freshly prepared IAA solution (400 mM IAA and 100 mM TEAB in PBS) and incubated (25 ºC, in dark, 30 min). To each sample, 50 µL of SDS solution (10% w/v in PBS) and 100 µL of 50% aqueous slurry containing streptavidin agarose resin was sequentially added, followed by incubation (25 ºC, agitation at 200 rpm, 1 h). The reaction mixture was transferred to 15 mL tube and the streptavidin beads were sequentially washed a total of nine times: 0.2% SDS in PBS (3 × 5 mL), 6 M urea in PBS (3 × 5 mL), and PBS (3 × 5 mL). Each wash was performed by agitation (25 ºC, 200 rpm, 15 min), followed by centrifugation (2,500 × g, 3 min, 25 ºC) and supernatant suction. The beads were resuspended with 200 µL of PBS (2 M urea, 1 mM $CaCl_2$, and 10% formic acid), agitated (25 ºC, 200 rpm, 15 min), centrifuged (2,500 × g, 3 min, 25 ºC), and the supernatant was collected. This procedure was repeated in triplicate and all the supernatant were combined. The proteins were then digested with 1.0 µg of sequencing grade modified trypsin (Promega), (37 ºC, agitation at 300 rpm, 16 h). The peptides were labeled with TMT-duplex™ isobaric label reagent kit (Thermo Scientific) according to the manufacturer's protocol. The labeled peptides were desalted by Pierce™ spin column (Thermo Scientific) and collected to 1.5 mL protein low-binding tube (Thermo Scientific). The solvent was evaporated in a Speed-Vac and the dried peptides were dissolved in 50 µL of LC-MS grade solvent consisted of water/acetonitrile (98:2, v/v) with 0.1% formic acid. The above experiment was performed in biological duplicates.

2.3.6. LC-MS/MS analysis and data processing

The fractionated peptide samples were analyzed by LC-MS/MS system. Peptides were separated on the 2-column setup with a Acclaim PepMap 100 trap column (100 µm x 2 cm, nanoViper C_{18}, 5 µm, 100 Å, Thermo Scientific) and an Acclaim PepMap 100 capillary column (75 µm x 50 cm, nanoViper C_{18}, 2µm, spherical fully porous ultrapure, Thermo Scientific). Solvent A consisted of water with 0.1% formic acid and solvent B consisted of acetonitrile with 0.1% formic acid were used to establish the 180 minutes gradient from 10% to 40% solvent B at a flow rate of 300 nL/min. The spray voltage was 2.2 kV in positive ion mode, and the temperature of the heated capillary was set to 300 ℃. Mass spectra were acquired in a data-dependent manner using a top 10 method on a Q-Exactive. The Orbitrap analyzer scanned precursor ions with a mass range of 350-1800 *m/z* with 70,000 resolution at *m/z* 200. The automatic gain control (AGC) target value for MS/MS was 3 x 10^6 and the isolation window for MS/MS was 2.0 *m/z*. HCD scans were acquired at a resolution of 17,500 and 27 normalized collision energy (NCE). The maximum ion injection time for survey scan and MS/MS scan was 100 ms. Dynamic exclusion was enabled with an exclusion period of 15 s. Mass data are acquired automatically using Xcaliber software version 3.1 and converted to mzml format. Protein identification and TMT quantification were performed using Maxquant 1.6 software. All spectra were searched against protein database (Uniprot) using a target false discovery rate (FDR) of 1%. The precursor mass tolerance was set to 10 ppm and fragment ion mass tolerance to 0.02 Da. One missed cleavage site of trypsin was allowed. Carbamidomethyl (C) and TMT-

duplex (K and N-terminal) were used as a fixed modification. Oxidation (M) was used as variable modifications. The proteins identified in positive group (ECN-treated samples) were additionally filtered by at least two spectral counts and one unique peptides in each experimental replicate. Protein ratios from were calculated as the median of two high-score peptides belonging to a protein.

2.3.7. Modification sites of identified proteins by ECN

The modification of recombinant proteins (14-3-3 protein zeta and peroxiredoxin-1) by ECN was carried out at different molar ratios as follow. The recombinant proteins were dissolved in 100 µL of Tris buffer (25 mM, pH 7.8) at a concentration of 2 µM, and incubated with ECN at molar ratios [ECN]/ [protein] = 0, 1, and 5 (25 ºC, agitation at 200 rpm, 2 h). The proteins were reduced by adding 2 µL of PBS containing TCEP (200 mM) and TEAB (200 mM) and the reaction mixture was incubated (50 ºC, 1 h). After cooling the sample to room temperature, the reduced protein was alkylated by adding 2 µL of freshly prepared IAA solution (400 mM IAA and 100 mM TEAB in PBS) and incubated (25 ºC, in dark, 30 min). Next, 1 mL of acetone was added to precipitate proteins (–20 ºC and 4 h), followed by centrifugation (14,000 × g, 5 min, 4 ºC) and supernatant suction. The protein pellet was resuspended with 200 µL of TEAB (200 mM) and digested with 0.1 µg of sequencing grade modified trypsin (37 ºC, agitation at 300 rpm, 16 h). The tryptic peptides were desalted by Pierce™ spin column and collected to protein low-binding tube. Solvent was evaporated in a Speed-Vac and the dried peptides

were reconstituted in 50 µL of LC-MS grade solvent consisted of water/acetonitrile (98:2, v/v) with 0.1% formic acid, and were analyzed by LC-MS/MS system. Solvent A consisted of 2% aqueous acetonitrile with 0.1% formic acid and solvent B consisted of 98% aqueous acetonitrile with 0.1% formic acid were used. Peptides were first trapped on a Acclaim PepMap 100 trap column (100 µm × 2 cm, nanoViper C_{18}, 5 µm, 100Å, Thermo Scientific) and washed for 6 min with 98% solvent A at a flow rate of 4 µL/min, and then separated on a Acclaim PepMap 100 capillary column (75 µm × 15 cm, nanoViper C_{18}, 3 µm, 100Å, Thermo Scientific) at a flow rate of 300 nL/min. The LC gradient was run at 2% to 35% solvent B over 30 min, then from 35% to 90% over 10 min, followed by 90% solvent B for 5 min. The Orbitrap analyzer scanned precursor ions with a mass range of 350-1800 *m/z* with 70,000 resolution at *m/z* 200. The mass data are acquired automatically by Xcaliber software version 3.1 and converted to mzml format for further data processing.

2.3.8. Isothermal titration calorimeter

Isothermal titration calorimeter (ITC) analysis was conducted on an MicroCal iTC200 (Malvern, Northampton, MA, USA). For ITC analysis, solutions of 0.3 mM ECN and 0.03 mM 14-3-3 protein zeta were dissolved in 25 mM Tris buffer at pH 7.8 containg 5% DMSO. ECN solution was loaded into the syringe and titrated into the sample cell, which contained the protein solution in a sequence of 20 x 1.5 µL injections. The titration was conducted at 25 °C. Data analysis was

conducted using MicroCal analysis software (Malvern). The stoichiometry (*n*), enthalpy (ΔH) and association constant (*K*a) for ECN was estimated by fitting each data set to a single sites binding model provided. Control injections of ECN sample and blank buffer into sample cell showed negligible ΔH. Errors shown are based on the accuracy of the curve fit to the data.

IV. RESULTS AND DISCUSSION

1. An efficient fractionation method for the preparative separation of sesquiterpenoids from Farfarae Flos by CCC

1.1. Principle of CCC-DCI fractionation

The crucial point for the successful fractionation by CCC-DCI is what the target components should not be eluted with the extraction solvent until all the polar components are completely removed, and eventually, the target components should be easily eluted with the elution solvent. That is to say, the target compounds are retained in the stationary phase when the extraction solution is used as the mobile phase, and then they migrate to the lower phase when the elution solvent is used as the mobile phase. As shown in **Fig. 13**, the CCC-DCI fractionation is composed of four stages. Stage I (direct injection): the extraction solution was directly injected into the CCC instrument without achieving two-phase solvent equilibrium. Stage II (continuous injection): the extraction solution was continuously injected into the CCC column, and the target components and less polar components were concentrated in the stationary phase, whereas the polar impurities were passing through the column. Stage III (washing polar components): the polar impurities were completely washed from the column with pure extraction solvent. Stage IV (eluting target components): the target components were eluted with the elution solvent.

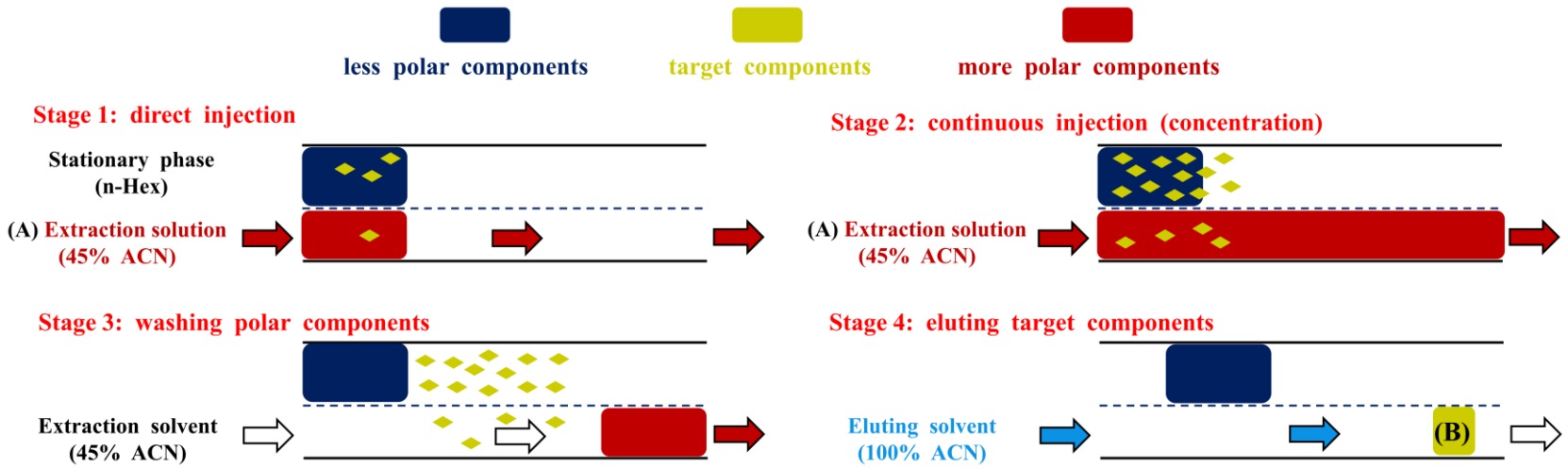

Figure 13. A schematic diagram of CCC-DCI mode

Direct and continuous injection mode of countercurrent chromatography (CCC-DCI) was developed to enrich target components from natural extract: An *n*-hexane-acetonitrile-water solvent system was pumped through the column, and the extraction solution was directly and continuously injected into the CCC column. (B) The sesquiterpenoid-enriched (STE) fraction was obtained from the (A) extract solution.

1.2. Selection of the extraction and elution solvents based on K_D values

Successful fractionation by CCC-DCI is dependent on the selection of suitable extraction and elution solvents that provide an optimum range of K_D values for the target components. As sesquiterpenoids in *T. farfara* are hydrophobic, they are difficult to be dissolved in water but can be easily solubilized in acetonitrile. Therefore, a solvent system composed of *n*-hexane-acetonitrile-water (HAcW) was selected for its range of polarities; this solvent system is commonly applied to enrich and isolate terpenoids from plant extracts [29–32]. In this study, the K_D values of the three major sesquiterpenoids in seven compositions of HAcW at volume ratios of 10:3.5:6.5, 10:4.5:5.5, 10:5.5:4.5, 10:6.5:3.5, 10:7.5:2.5, 10:8.5:1.5, and 10:9.5:0.5 were analyzed by HPLC-UV, and the results are shown in **Table 1**. Considering the K_D values of **TG** (most polar target compound), I could determine the maximum volume of the extraction solvent, calculated based on the equation [95]:

$$V_R = V_M + K_D V_S$$

where V_M and V_S are the volumes of the mobile and stationary phases, respectively, and V_R is the retention volume of the target compound. K_D is the partition coefficient of the target compound.

The K_D value of **TG** in solvent system 3 was 2.77 and the HAcW solvent systems showed 60-70% of stationary phase retention (operated by TBE-1000A at a flow rate 15 mL/min). Therefore, the maximum volume of extraction was less

than 2 L. However, large amount of raw material (1 kg of Farfarae Flos in this study) could not be dipped in the volume of extraction solvent. On the other hand, extraction volume of solvent system 2 was up to 6 L, calculated by the above equation. Although solvent systems 1 and 2 possessed suitable K_D values, solvent system 2 was selected to extract the target sesquiterpenoids due to its better polarity.

The contents of the three major sesquiterpenoids in the 45% acetonitrile extract were not greatly different from those of the methanol extract. Woo *et al.* reported the optimum extraction conditions of Farfarae Flos, and methanol showed better extraction efficiency than those of other solvents [10]. As shown in **Table 2**, the total contents of **TG**, **AECN**, and **ECN** were 119.8, 250.7, and 60.2 mg in the 45% acetonitrile extract (33,087 mg), and the contents in the methanol extract (15,717 mg) were 118.3, 226.8, and 74.5 mg, respectively. Thus, 45% acetonitrile was selected as both the mobile phase and extraction solvent for CCC-DCI.

Table 1. The partition coefficients (K_D) of three major sesquiterpenoids in different solvent composition

No.	solvent systems *n*-hexane:acetonitrile:water	K_D values		
		TG	**AECN**	**ECN**
1	10:3.5:6.5	13.21	> 20	> 20
2	10:4.5:5.5	9.67	17.47	> 20
3	10:5.5:4.5	2.77	7.29	> 20
4	10:6.5:3.5	0.93	2.80	10.71
5	10:7.5:2.5	0.38	0.71	4.46
6	10:8.5:1.5	0.17	0.48	1.86
7	10:9.5:0.5	0.06	0.14	0.55

Table 2. Comparison of the extraction efficiency of 45% acetonitrile and methanol

Extraction solvent	45% ACN	MeOH
Yield (mg)	33,087	15,717
TG (mg/g), (total contents (mg))	3.62 (119.81)	7.53 (118.28)
AECN (mg/g), (total contents (mg))	7.58 (250.70)	14.43 (226.76)
ECN (mg/g), (total contents (mg))	1.82 (60.21)	4.74 (74.49)

1.3. CCC-DCI fractionation

1.3.1. Four stages of CCC-DCI

Stage I (direct injection): the extraction solution was directly injected into the CCC instrument without achieving two-phase solvent equilibrium. This method eliminated several laborious steps, including evaporation of the extraction solution, preparation of the solvent system, and dissolution of the sample in the solvent system. Thus, the process time and the solvent consumption were greatly reduced by using the extraction solution as the mobile phase. The flow rate and composition of the extraction solvent were selected based on the K_D values of the three major sesquiterpenoids (especially the most polar compound, **TG**). When two-phase equilibrium was reached, a dark brown solution was eluted from the separation column. As shown in **Fig. 14**, CCC chromatogram showed a broad rectangular peak during stage I and II, which indicated that the polar components were being washed out. Stage II (continuous injection): the extraction solution was continuously injected into the CCC column, and the target components and less polar components were concentrated in the stationary phase, whereas the polar impurities were passing through the column. During this stage, no bleeding of the stationary phase was observed. Because the amount of polar components in the extraction solution was much greater than the amounts of the target components and less polar components, the inflow and outflow of total components was almost identical. Therefore, the equilibrium of the two-phase system was maintained while concentrating the target components. Stage I and II took approximately 360 min to

inject all the extraction solution. Stage III (washing polar components): the polar impurities were completely washed from the column with pure extraction solvent (45% acetonitrile). The UV signal started to decrease, and dilute solution was eluted 40 min after the pumping of the pure solvent was initiated. Because the calculated retention volumes of **TG**, **AECN**, and **ECN** were more than 6.4 L based on the K_D value, target compounds were not eluted during stage III. In fact, the target compounds were not detected from the eluted solution of Stage III (data not shown). Stage IV (eluting target components): the target components were eluted with the eluting solvent. The composition of the eluting solvent was selected based on the K_D values of the three major sesquiterpenoids (especially the least polar compound, **ECN**). Finally, sesquiterpenoid-enriched (STE) fraction was obtained (collected during 430-490 min) from 315.9 g of the extract. The total CCC-DCI operation time was approximately 500 minutes, and the CCC-DCI fractionation of Farfarae Flos was performed in triplicate to ensure reproducibility of the method.

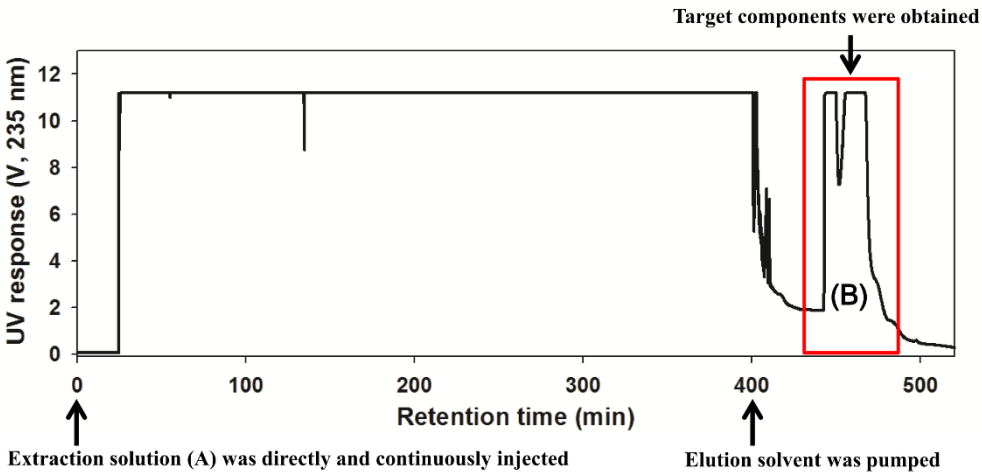

Figure 14. CCC-DCI chromatogram of Farfarae Flos extract

The *n*-hexane-acetonitrile-water solvent system was separately pumped into the CCC column; stationary phase: *n*-hexane; mobile phase: water and acetonitrile. The flow rate was 15 mL/min, the rotation speed was 450 rpm, and the UV detection wavelength was 235 nm. The retention of the stationary phase was 63%, and no bleeding of the stationary phase was observed. (B) The sesquiterpenoid-enriched (STE) fraction was obtained (collected during 430-490 min) from 315.9 g of (A) 45% acetonitrile extract.

1.3.2. Preparative separation of three major sesquiterpenoids

Three grams of the STE fraction was successfully isolated by CCC **(Fig. 15A)**. Three major sesquiterpenoids: **TG** (collected during 110-130 min, 320 mg); **AECN** (collected during 150-175 min, 1350 mg); **ECN** (collected during 330-350 min, 290 mg) were obtained from the STE fraction from a single purification. The retention of the stationary phase (S_f) was 80%, and no bleeding of the stationary phase was observed. The collected sesquiterpenoids were further refined by preparative HPLC to eliminate minor impurities. The purity of all isolated sesquiterpenoids was greater than 97%, as assessed by HPLC-UV **(Fig. 15B–D)**. The chemical structure of the compounds was determined by ^{1}H and ^{13}C NMR analysis **(Fig. 16–18)** and comparison with reported data [17, 19].

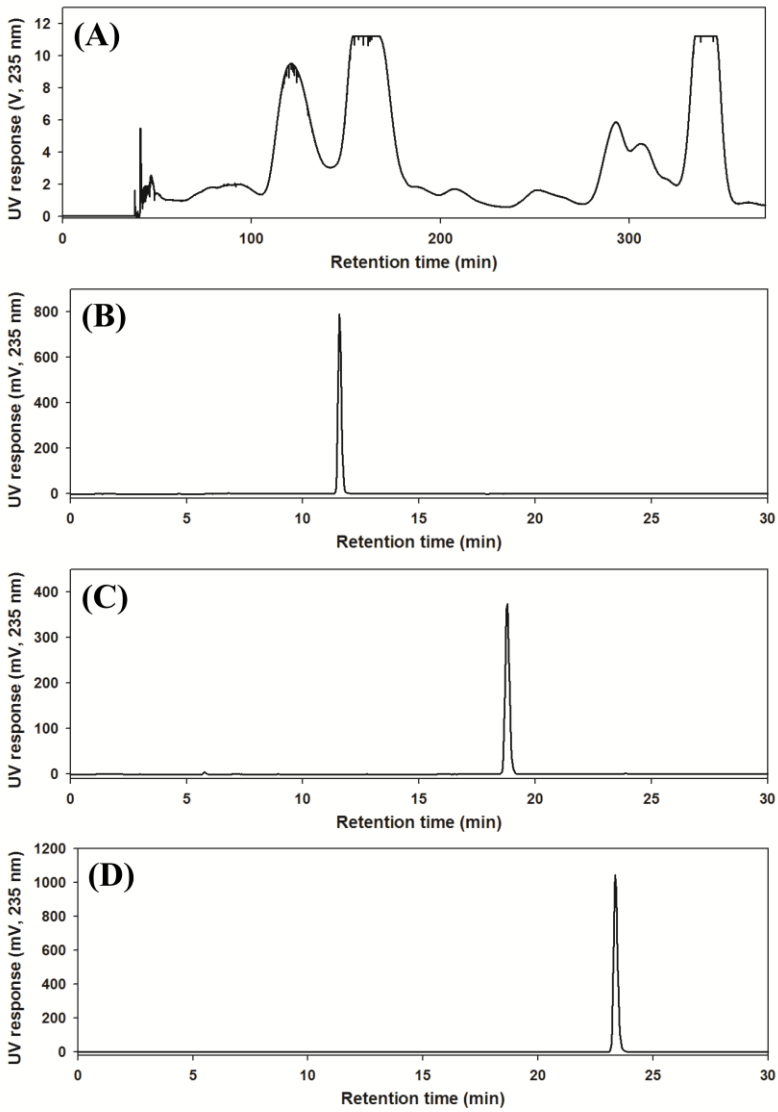

Figure 15. Preparative separation of three major sesquiterpenoids

(A) CCC chromatogram of the sesquiterpenoid-enriched fraction. (B) **TG** (collected during 110-120 min, 320 mg); (C) **AECN** (collected during 150-170 min, 1350 mg); (D) **ECN** (collected during 330-350 min, 290 mg).

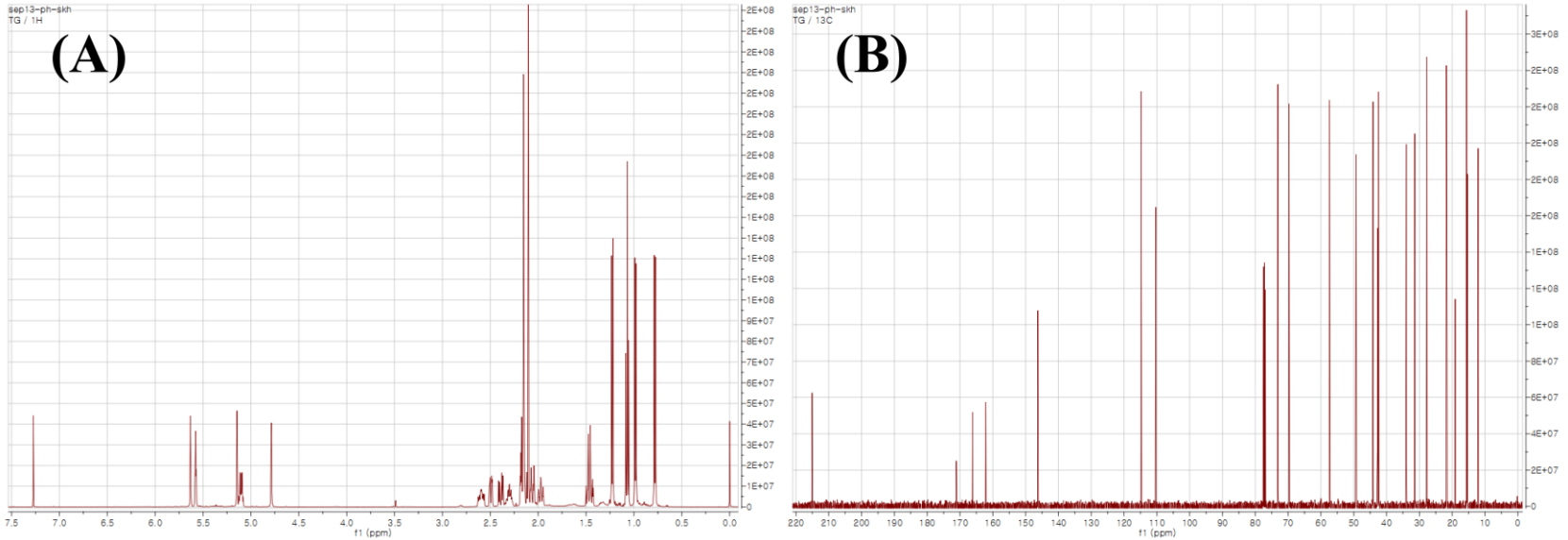

Figure 16. (A) ^{1}H and (B) ^{13}C spectrum of TG

(in $CDCl_3$, 500 and 125 MHz, respectively)

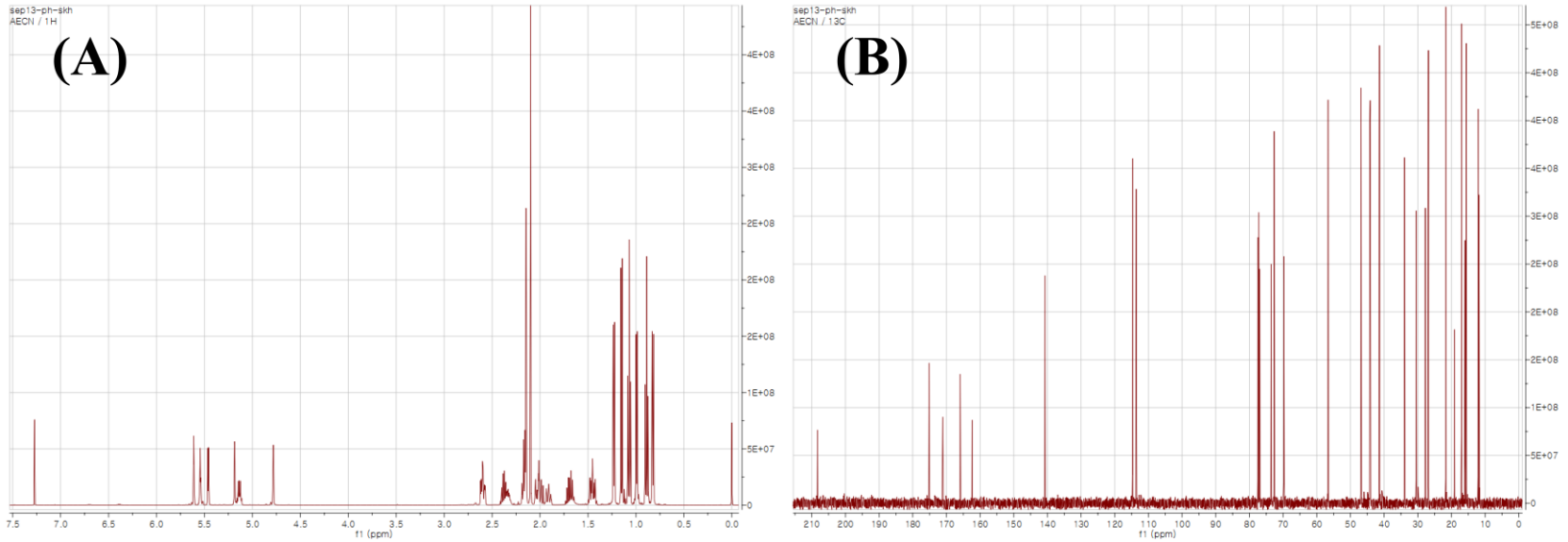

Figure 17. (A) ^{1}H and (B) ^{13}C spectrum of AECN

(in $CDCl_3$, 500 and 125 MHz, respectively)

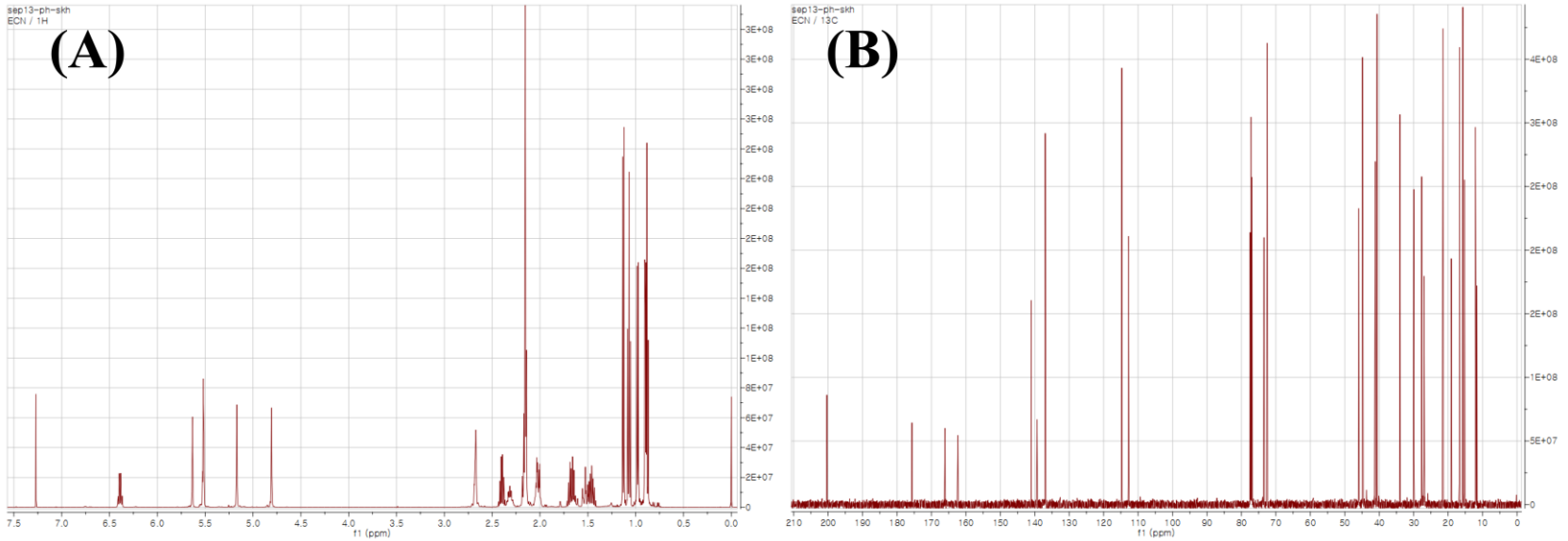

Figure 18. (A) ^{1}H and (B) ^{13}C spectrum of ECN

(in $CDCl_3$, 500 and 125 MHz, respectively)

1.4. Quantification study

Using CCC-DCI fractionation, the entire extract of *T. farfara* (315.9 g/5.4 L) was injected in a single CCC operation, and 6.8 g of the STE fraction was obtained from the crude extract within 8.5 hrs. For evaluating the fractionation efficiency of CCC-DCI, another extraction solution was dried and enriched by conventional multi-step fractionation in series, including solvent partitioning and open column chromatography. To compare these samples, quantification of the three major sesquiterpenoids (**TG**, **AECN**, and **ECN**) in each extract and fraction sample was conducted by HPLC-UV analysis.

1.4.1. Validation parameters

As shown in **Table 3**, calibration curves of **TG**, **AECN**, and **ECN** were calculated and all the least squares coefficients of correlation (R^2) were higher than 0.999 with broad linear range (62.5–1000 μg/mL), suggesting a strong linear relation between the compound concentrations and the UV peak area. In addition, the limits of detection (LODs) and the limits of quantitation (LOQs) were determined. The LODs and LOQs were defined at signal-to-noise (S/N) ratios of 3 and 10, respectively. The LOQs were experimentally verified by analyzing three sesquiterpenoids at each concentration (data not shown), and were sufficiently low to detect trace amount in the samples.

Table 3. The linear range, linearity, LOD, and LOQ of the three major sesquiterpenoids

Analytes	Linear range (μg/mL)	Calibration curve	Correlation coefficient (R^2)	LOD (μg/mL)	LOQ (μg/mL)
TG	62.5-1000	y = 4.191x – 16.815	0.9999	4.39	14.63
AECN	62.5-1000	y = 4.518x + 0.5125	0.9998	5.02	16.73
ECN	62.5-1000	y = 7.106x + 11.108	0.9995	3.54	11.81

1.4.2. Comparison of CCC-DCI with conventional methods

The quantification of the **TG**, **AECN**, and **ECN** in each sample was conducted by HPLC-UV based on the corresponding calibration curves **(Fig. 19)**. As shown in **Table 4**, the average contents of **TG** (155.3 mg/g), **AECN** (333.1 mg/g), and **ECN** (70.9 mg/g) in CCC-DCI fraction were much higher than other fraction samples. The average recoveries **TG**, **AECN**, and **ECN** were 96.1%, 96.9%, and 94.6% by CCC-DCI; 87.6%, 87.0%, and 94.6% by solvent partitioning (sum of *n*-Hex and MC fraction); 77.7%, 66.5%, and 58.4% by open column chromatography (sum of 90% and 100% MeOH fraction). These data indicate that solvent partitioning cannot completely eliminate all the polar impurities, and considerable amount of the target components was adsorbed onto the solid support. Furthermore, CCC-DCI method utilized the extraction solution as both the sample and mobile phase, greatly reducing the solvent consumption. Only 4.1 L of water, 4.6 L of acetonitrile, and 1.2 L of *n*-hexane were required to enrich 315 g of extract, and the solvent consumption of CCC-DCI was less than half of other fractionation methods. Therefore, the developed CCC-DCI fractionation is a powerful and applicable method with high time- and cost-efficiency.

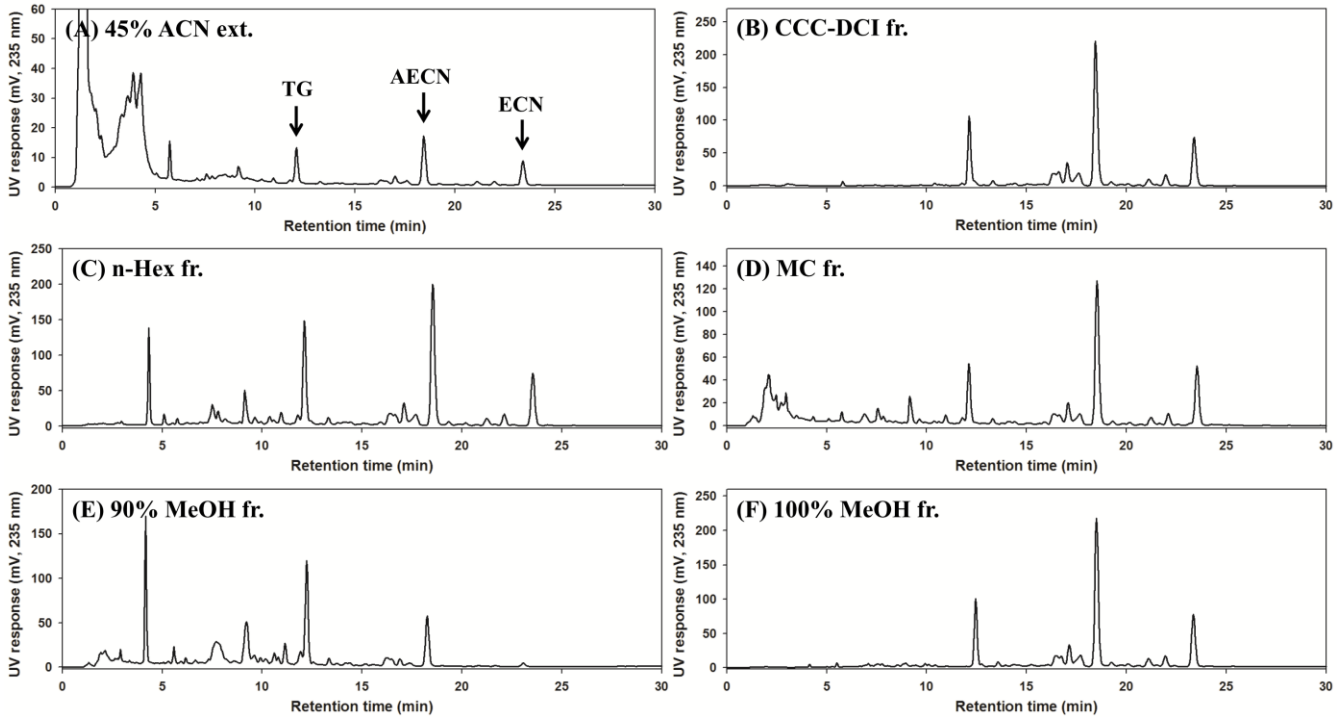

Figure 19. HPLC-UV chromatograms of extract and fraction

(A) Extract of Farfarae Flos with 45% acetonitrile; Fractions obtained from (B) CCC-DCI; solvent partitioning with (C) *n*-hexane and (D) methylene chloride; Diaion HP-20 open column chromatography with (E) 90% methanol and (F) 100% methanol.

Table 4. The comparison of the fractionation efficiency of CCC-DCI, solvent partitioning, and open column chromatography

Fractionation Method		Extract	CCC	Solvent partitioning		Open column (Diaion HP-20)	
		(A) 45% ACN	(B) CCC-DCI	(C) *n*-Hex	(D) MC	(E) 90% MeOH	(F) 100% MeOH
Yield (mg)		315875	6806	5816	4399	2033	4055
TG (mg/g), (% recovery)		3.5 (100.0)	155.3 (96.1)	132.4 (70.0)	44.1 (17.6)	156.3 (28.9)	129.2 (48.8)
AECN (mg/g), (% recovery)		7.4 (100.0)	333.1 (96.9)	214.0 (53.2)	179.8 (33.8)	74.1 (6.4)	338.8 (60.1)
ECN (mg/g), (% recovery)		1.6 (100.0)	70.9 (94.6)	46.9 (53.5)	47.6 (41.1)	3.2 (1.3)	70.1 (57.1)
Solvent consumption (mL) (including extraction)	Water	3850	4180	6680	6680	9430	9430
	ACN	3150	4620	3150	3150	3150	3150
	n-Hex	-	1200	7500	7500	7500	7500
	MC	-	-	-	7500	7500	7500
	MeOH	-	-	-	-	3750	5750

1.5. Discussion

This study was designed to develop an efficient fractionation and separation method to enrich target compounds from plant extract. Taking Farfarae Flos as a case study, CCC-DCI mode was established and validated. There are several advantages of this method:

i) For CCC-DCI, the *n*-hexane–acetonitrile–water solvent system (HAcWat) was prepared and pumped separately, as in the HPLC solvent system. Therefore, CCC-DCI avoided the time-consuming solvent equilibrium for liquid-liquid chromatography. In addition, this solvent system showed high stationary phase retention and enabled a high mobile phase flow rate (63% S_f at a flow rate of 15 mL/min) even at 450 rpm. Although a higher revolution speed shows a better stationary phase retention and separation profile, 450 rpm (not 500 rpm) was selected not to stress the device.

ii) CCC-DCI utilized extract solution as both sample and mobile phase, greatly reducing the solvent consumption. Only 4.1 L of water, 4.6 L of acetonitrile, and 1.2 L of *n*-hexane were required to enrich 315 g of extract. The solvent consumption of CCC-DCI was less than half of the consumption of other fractionation methods **(Table 4)**. Futhermore, direct and continuous injection of extract solution enables industrial-scale fractionation, avoiding the solubility problems that arise with large sample quantities. The sample injection capacity of CCC-DCI is greater than 300 grams, which is difficult to be injected in conventional CCC. For the TBE-1000A used in this study, it is impossible to

dissolve and inject more than 300 grams of extract through a 60 mL sample loop. In fact, 10 grams of 45% acetonitrile extract of *T. farfara* was difficult to be re-dissolved in 60 mL of the solvent, and equilibrium of the HAcWat system was not achieved even at a mobile phase flow rate of 5 mL/min.

iii) CCC-DCI efficiently enriched target components by eliminating polar and non-polar impurities compared to conventional multi-step fractionation methods, solvent partitioning and open column chromatography. The STE fraction from CCC-DCI was easily dissolved in methanol, and it made the sample analysis and further purification more efficient. It also showed high contents and recoveries of the target components because CCC, as a liquid-only technique, avoids adsorptive loss of the sample onto the solid stationary phase. The contents of the three major sesquiterpenoids (**TG**, **AECN**, and **ECN**) in CCC-DCI fraction were the highest among the fractionated samples in this study, and their recoveries were greater than 94% **(Table 4)**. Considering its lab-scale CCC instrument, solvent consumption, and processing time, CCC-DCI enables powerful product recovery with high-quality enrichment of target components.

2. Chemical profiling of sesquiterpenoids from Farfarae Flos based on LC-MS/MS analysis

2.1. Characterization of diagnostic ions

When the STE fraction and isolated compounds (**TG**, **AECN**, and **ECN**) were analyzed by LC-ESI-MS system, these sesquiterpenoids could be easily in-source fragmented and detection of the parent molecular ions was disturbed. In addition, the in-source fragmentation of their multiple labile ester linkages makes the identification of the similar derivatives more difficult. As shown in **Fig. 20**, full MS scan (ESI positive, *m/z* 50–1000) of the STE fraction showed consistent in-source fragmentations regardless of the ionization energy (DP: 10, 30, 50, 70, and 90 V), and several characteristic fragment ions were commonly observed over the chromatographic retention time. Taking their ester linkage into account, I supposed that the oplopane and bisabolane sesquiterpenoids would be fragmented to four diagnostic ions under the LC-ESI-MS condition **(Fig. 21)**.

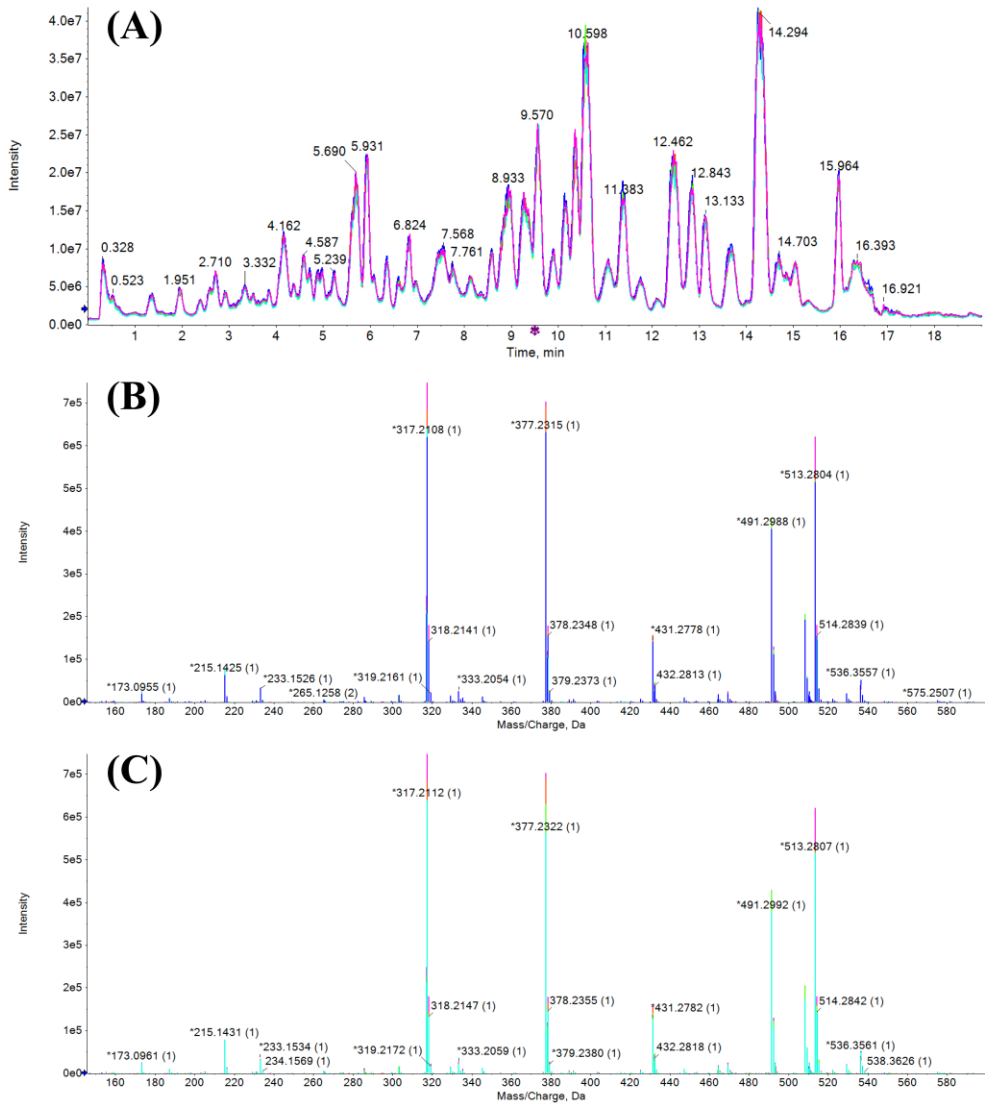

Figure 20. In-source fragmentation of sesquiterpenoids

(A) Total ion chromatogram of STE fraction under DP 10, 30, 50, 70, and 90 V (overlapped). Full MS scan at Rt 10.6 min under (B) DP 10 V and (C) DP 90 V.

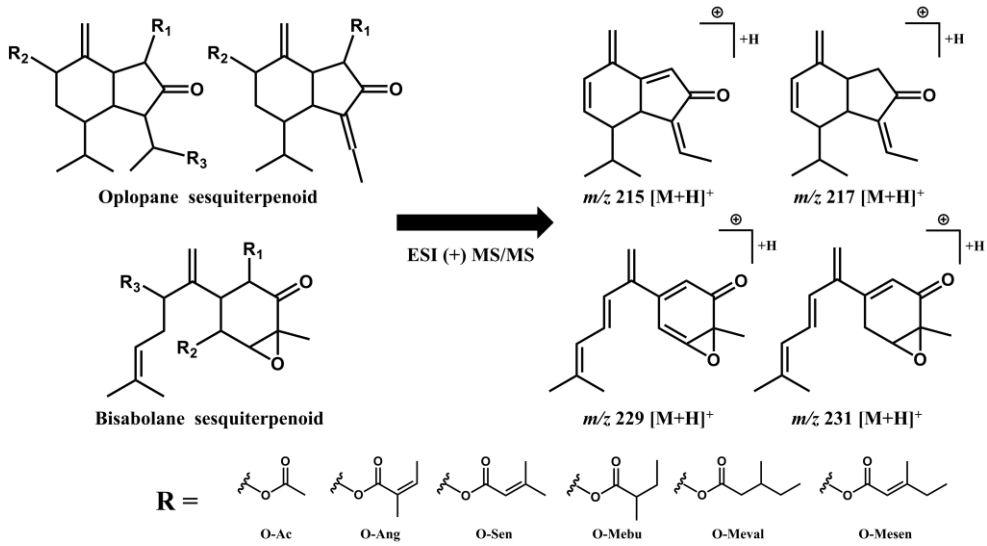

Figure 21. Proposed diagnostic ions under LC-ESI-MS analysis

Four diagnostic ions were proposed based on chemical structures of the oplopane and bisabolane sesquiterpenoids and their ester cleavage.

2.1.1. Diagnostic filtering

The diagnostic cations with *m/z* 215.143 and 217.158 were of oplopane sesquiterpenoids, and *m/z* 229.123 and 231.138 were those of bisabolane sesquiterpenoids. The difference in the two cations (*m/z* 215.143 versus 217.158 or *m/z* 229.123 versus 231.138) is the number of the ester linkages. Because the cleavage of ester linkage dominantly undergoes a double bond reduction [47], the cations of *m/z* 217.158 (oplopane) and 231.138 (bisabolane) were caused from two cleavages of ester bond and the cations of *m/z* 215.143 (oplopane) and 229.123 (bisabolane) were derived from three cleavages. As shown in **Fig. 22**, the extracted ion chromatogram with the diagnostic ions provided a more concise chromatographic profile rather than the total ion chromatogram and the overlapped peaks could be easily distinguishable by the diagnostic filtering.

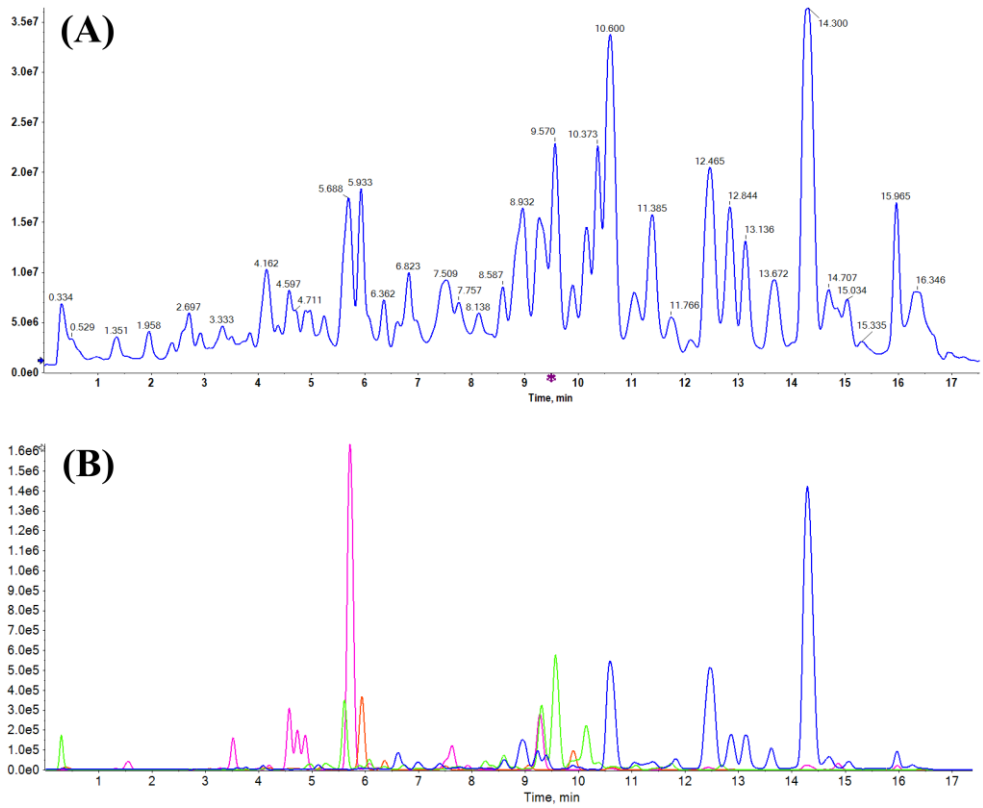

Figure 22. Ion chromatogram of STE fraction and diagnostic filtering

(A) Total ion chromatogram of STE fraction in ESI(+) mode using UHPLC-QTOF-MS. (B) Extracted ion chromatogram with four diagnostic ions (blue line for *m/z* 215.143; pink line for *m/z* 217.158; orange line for *m/z* 229.123; green line for *m/z* 231.138).

2.1.2. Fragmentation patterns of the diagnostic ions

Product ion scans for the proposed diagnostic ions at *m/z* 215.143, 217.158, 229.123, and 231.138 were performed and their fragmentation behaviors were investigated. As shown in **Fig. 23**, their MS/MS spectra (sum of the retention time from 1 to 17 min) showed characteristic fragmentation behavior indicating the same chemical structure, respectively. Moreover, the cations with *m/z* 215.143 and 217.158 (also 229.123 and 231.138) were fragmented by maintaining the *m/z* difference of 2 Da.

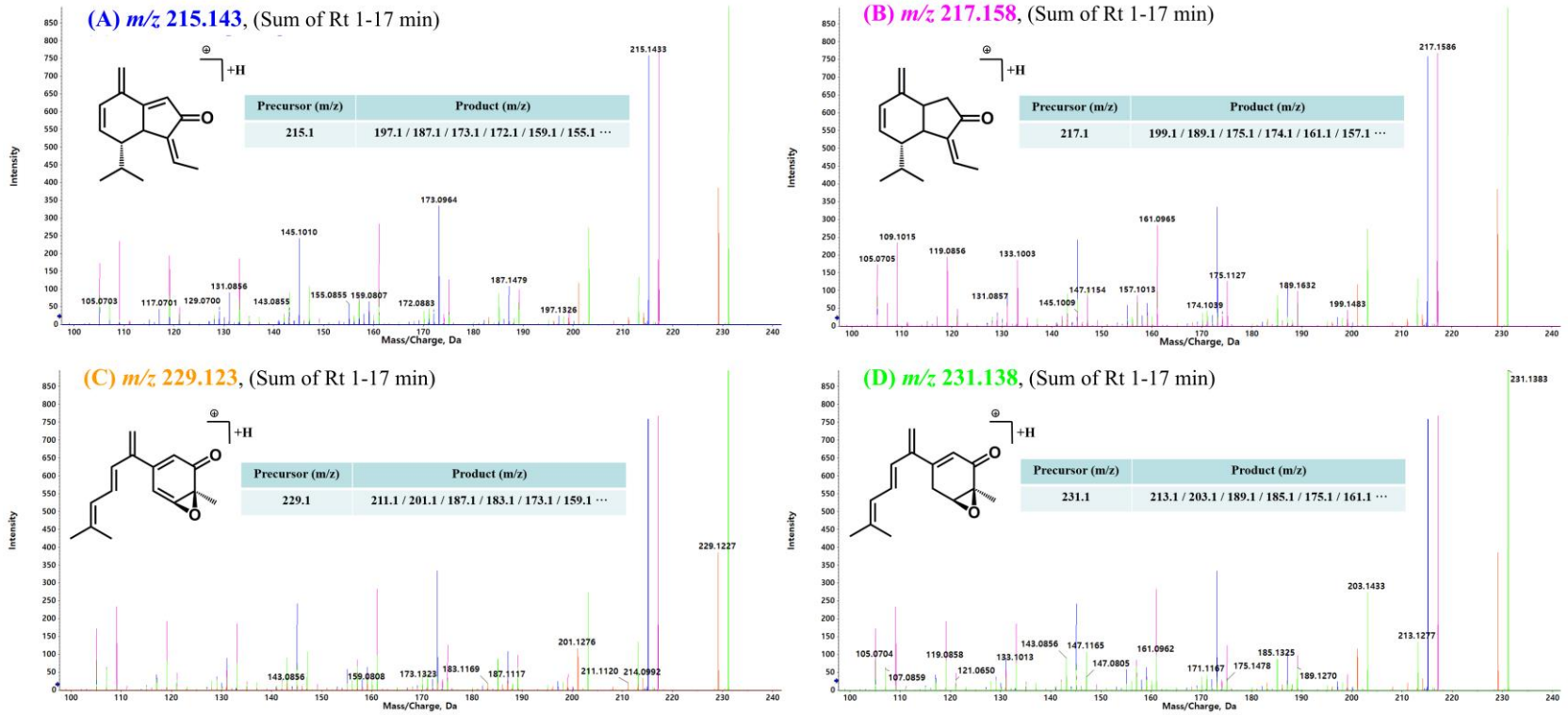

Figure 23. Fragmentation patterns of diagnostic ions

Fragmentation pattern of each diagnostic ion was investigated by UHPLC-QTOF-MS/MS. The MS/MS spectra (sum of the retention time range 1–17 min) of $[M+H]^+$ at *m/z* (B) 215, blue; (C) 217, pink; (D) 229, orange; (E) 231, green.

2.2. Precursor ion scan for the diagnostic ions

As shown in **Fig. 2**, about 30 sesquiterpenoids of Farfarae Flos have been reported [17–25] and these compounds can be divided into four types according to the proposed diagnostic ions, oplopane (*m/z* 215.143 and 217.158) and bisabolane (*m/z* 229.123 and 231.138) sesquiterpenoid. To characterize more diverse oplopane and bisabolane sesquiterpenoids, especially their parent molecular ions, precursor ion scans (*m/z* 250–550) for the diagnostic ions were performed using a QqQ-MS/MS system **(Fig. 24)**. The DP was fixed at 30 V and three CEs (5, 15, 25 eV) were selected to screen all the intermediate and parent molecular ions. The total ion chromatograms of the precursor ion scans showed similar profiles to those of the extracted ion chromatograms for each diagnostic ion **(Fig. 22B)**, and the parent molecular ions were identified based on the MS/MS spectra over the retention time. Although several intermediate molecular ions were also detected because of the in-source fragmentation under the ESI ionization, this information also provided the structural annotation in terms of their ester cleavage. As a result, 74 sesquiterpenoids were identified and thier retention times, diagnostic ions, relative peak area (%), observed intermediate and parent molecular ions, formulas, and annotated substituent groups are given in **Table 5**.

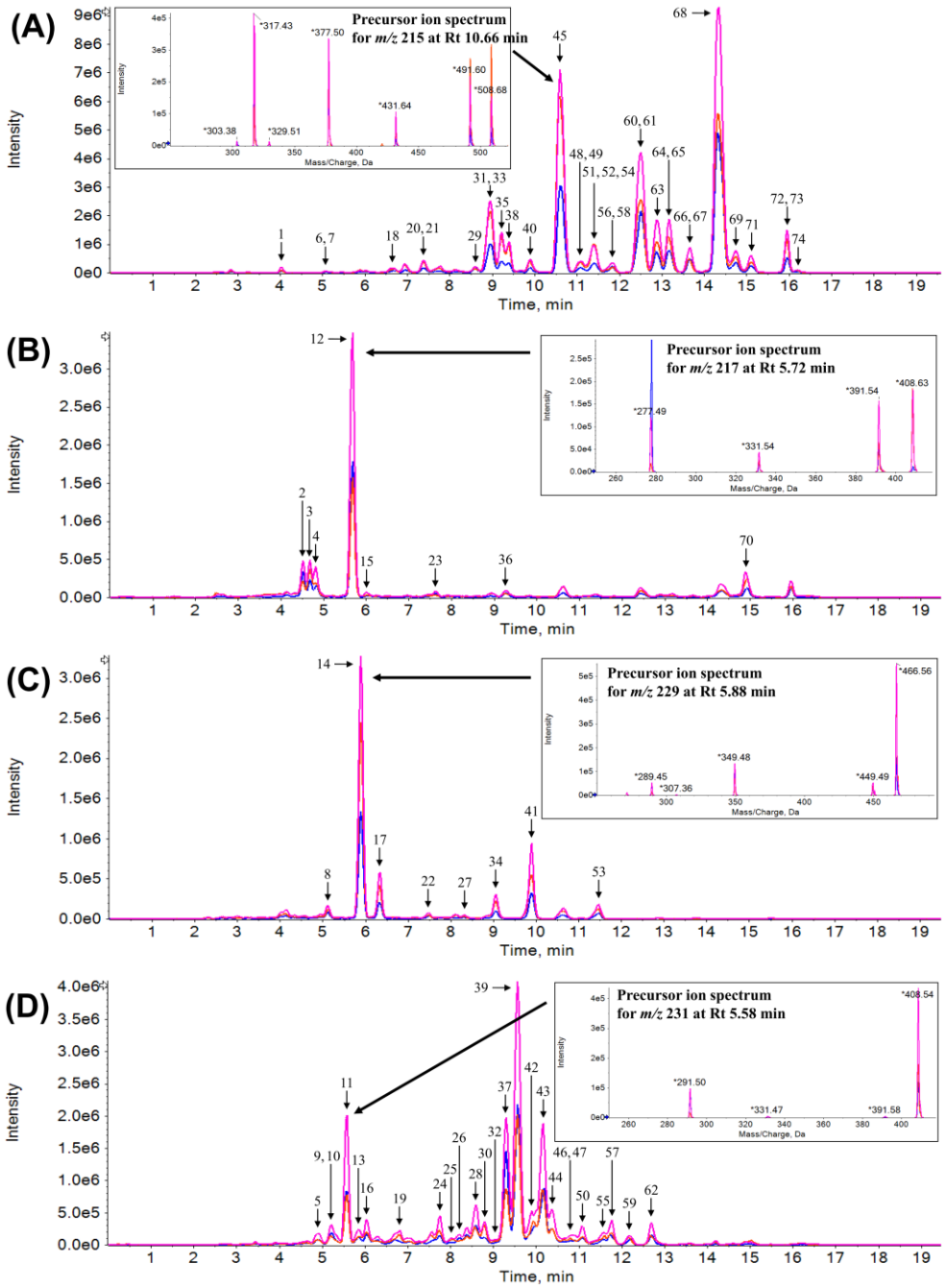

Figure 24. Total ion chromatograms of precursor ion scan

Peaks are numbered to indicate dereplicated sesquiterpenoids based on retention time and diagnostic ions of *m/z* (A) 215, (B) 217, (C) 229, (D) 231. Three collision energies shown in blue for 5 eV, pink for 15 eV, and orange for 25 eV were selected to investigate all the intermediate and parent molecular ions.

Table 5. Identified sesquiterpenoids of Farfarae Flos by precursor ion scan of UHPLC-QqQ-MS/MS

No.	Rt (min)	Diagnostic *m/z*	Relative Area (%)	Precursor *m/z*	M.W.	Formula	R group*	Ref.
1	4.11	215	0.22	317, 335, 352	334	$C_{20}H_{30}O_4$	c, f	[25]
2	4.57	217	3.48	277, 317, 377, 394	376	$C_{22}H_{32}O_5$	a, b	[17]
3	4.73	217	2.46	277, 317, 377, 394	376	$C_{22}H_{32}O_5$	a, b	[17]
4	4.87	217	1.99	277, 319, 379, 396	378	$C_{22}H_{34}O_5$	a, c	[20]
5	4.90	231	0.33	291, 396	378	$C_{21}H_{30}O_6$	a, i	
6	5.07	215	0.09	317, 377, 394	376	$C_{22}H_{32}O_5$	a, c	
7	5.11	215	0.13	311, 329, 347, 364	346	$C_{21}H_{30}O_4$	e, f	[23]
8	5.17	229	0.19	289, 349, 377, 437, 454	438	$C_{23}H_{32}O_8$	a, a, i	
9	5.25	231	0.24	331, 431, 448	430	$C_{25}H_{34}O_6$	b, b	
10	5.35	231	0.12	291, 331, 391, 408	390	$C_{22}H_{30}O_6$	a, b	
11	5.60	231	3.97	291, 331, 391, 408	390	$C_{22}H_{30}O_6$	a, b	
12	5.70	217	17.87	277, 331, 391, 408	390	$C_{23}H_{34}O_5$	a, e	[17]
13	5.88	231	0.22	345, 445, 462	444	$C_{26}H_{36}O_6$	b, e	[23]
14	5.93	229	3.85	289, 349, 449, 466	448	$C_{24}H_{32}O_8$	a, a, b	[18]
15	6.02	217	0.35	333, 393, 410	392	$C_{23}H_{36}O_5$	a, d	
16	6.08	231	0.60	291, 393, 410	392	$C_{22}H_{32}O_6$	a, c	
17	6.34	229	0.60	289, 349, 451, 468	450	$C_{24}H_{34}O_8$	a, a, c	
18	6.63	215	0.87	317, 335, 419, 437, 454	436	$C_{26}H_{44}O_5$	c, c, f	
19	6.78	231	0.24	331, 431, 448	430	$C_{25}H_{34}O_6$	b, b	
20	7.36	215	0.08	275, 317, 377, 394	376	$C_{22}H_{32}O_5$	a, c	
21	7.41	215	0.23	303, 363, 403, 463, 480	462	$C_{27}H_{42}O_6$	a, b, i	
22	7.49	229	0.23	329, 347, 447, 464	446	$C_{24}H_{30}O_8$	b, b, f	
23	7.60	217	1.39	331, 348	330	$C_{21}H_{30}O_3$	e	[19]
24	7.76	231	0.19	333, 393, 507, 524	506	$C_{28}H_{42}O_8$	a, c, e	
25	8.03	231	0.08	291, 333, 345, 493, 510	492	$C_{27}H_{40}O_8$	a, b, c	
26	8.26	231	0.52	319, 331, 419, 436	418	$C_{24}H_{34}O_6$	b, i	
27	8.34	229	0.12	289, 349, 449, 466	448	$C_{24}H_{32}O_8$	a, a, b	[18]
28	8.60	231	0.81	319, 331, 419, 436	418	$C_{24}H_{34}O_6$	b, i	
29	8.61	215	0.56	275, 389, 406	388	$C_{23}H_{32}O_5$	a, e	
30	8.80	231	0.24	333, 393, 507, 524	506	$C_{28}H_{42}O_8$	a, c, e	
31	8.83	215	0.34	303, 363, 417, 477, 494	478	$C_{27}H_{40}O_7$	a, e, i	
32	9.02	231	0.10	331, 333, 433, 450	432	$C_{25}H_{36}O_6$	b, c	
33	9.04	215	1.35	317, 377, 417, 477, 494	478	$C_{27}H_{40}O_7$	a, b, c	
34	9.10	229	0.26	289, 317, 377, 477, 494	478	$C_{26}H_{36}O_8$	a, b, i	
35	9.16	215	1.19	317, 445, 462	444	$C_{27}H_{40}O_5$	c, j	
36	9.27	217	2.62	331, 348	330	$C_{21}H_{30}O_3$	e	[21]
37	9.29	231	3.26	331, 431, 448	430	$C_{25}H_{34}O_6$	b, b	[23]
38	9.38	215	0.71	317, 377, 419, 479, 496	478	$C_{27}H_{42}O_7$	a, c, c	
39	9.56	231	6.16	331, 431, 448	430	$C_{25}H_{34}O_6$	b, b	[23]
40	9.89	215	0.23	315, 375, 429, 489, 506	488	$C_{28}H_{40}O_7$	a, b, e	

* R groups, a: O-Ac, b: O-Ang or O-Sen, c: O-Mebu or O-*i*Val, d: O-Meval, e: O-Mesen, f: OH, g: OMe, h: OEt, i: unknown (88 Da), j: unknown (128 Da)

(Data continued)

(Data continued)

No.	Rt (min)	Diagnostic *m/z*	Relative Area (%)	Precursor *m/z*	M.W.	Formula	R group*	Ref.
41	9.89	229	1.01	289, 329, 389, 489, 506	488	$C_{27}H_{36}O_8$	a, b, b	
42	10.00	231	0.60	333, 433, 450	432	$C_{25}H_{36}O_6$	b, c	
43	10.14	231	1.79	345, 445, 462	444	$C_{26}H_{36}O_6$	b, e	[23]
44	10.36	231	0.56	331, 433, 450	432	$C_{25}H_{36}O_6$	b, c	
45	10.60	215	5.96	317, 377, 431, 491, 508	490	$C_{28}H_{42}O_7$	a, c, e	[17]
46	10.76	231	0.25	333, 345, 447, 464	446	$C_{26}H_{38}O_6$	c, e	
47	10.89	231	0.11	333, 435, 452	434	$C_{25}H_{38}O_6$	c, c	
48	11.03	215	0.28	317, 377, 433, 493, 510	492	$C_{28}H_{44}O_7$	a, c, d	
49	11.08	215	0.10	303, 317, 405, 422	404	$C_{24}H_{36}O_5$	c, i	
50	11.08	231	0.28	345, 447, 464	446	$C_{26}H_{38}O_6$	c, e	
51	11.24	215	0.08	317, 417, 434	416	$C_{25}H_{36}O_5$	b, c	
52	11.37	215	0.46	329, 389, 443, 503, 520	502	$C_{29}H_{42}O_7$	a, e, e	
53	11.45	229	0.16	289, 331, 391, 493, 510	492	$C_{27}H_{40}O_8$	a, c, c	
54	11.47	215	0.06	317, 419, 436	418	$C_{25}H_{38}O_5$	c, c	
55	11.56	231	0.17	347, 447, 464	446	$C_{26}H_{38}O_6$	b, e	
56	11.68	215	0.18	317, 419, 436	418	$C_{25}H_{38}O_5$	c, c	
57	11.76	231	0.35	347, 447, 464	446	$C_{26}H_{38}O_6$	b, d	
58	11.83	215	0.58	317, 377, 491, 508	490	$C_{28}H_{42}O_7$	a, c, e	
59	12.15	231	0.10	347, 449, 466	448	$C_{26}H_{40}O_6$	c, d	
60	12.45	215	0.71	331, 391, 445, 505, 522	504	$C_{29}H_{44}O_7$	a, d, e	
61	12.47	215	4.25	317, 417, 434	416	$C_{25}H_{36}O_5$	b, c	
62	12.70	231	0.26	347, 449, 466	448	$C_{26}H_{40}O_6$	c, d	
63	12.86	215	2.10	317, 419, 436	418	$C_{25}H_{38}O_5$	c, c	
64	13.14	215	0.71	317, 431, 448	430	$C_{26}H_{38}O_5$	c, e	[22]
65	13.16	215	1.03	261, 317, 363, 477, 494	476	$C_{28}H_{44}O_6$	c, e, h	[22]
66	13.62	215	0.95	315, 429, 446	428	$C_{26}H_{36}O_5$	b, e	[19]
67	13.76	215	0.24	247, 291, 317, 349, 463, 480	462	$C_{27}H_{42}O_6$	c, e, g	[24]
68	14.30	215	15.49	317, 431, 448	430	$C_{26}H_{38}O_5$	c, e	[19]
69	14.67	215	0.64	317, 331, 433, 450	432	$C_{26}H_{40}O_5$	c, d	
70	14.90	217	0.32	319, 433, 450	432	$C_{26}H_{40}O_5$	c, e	
71	15.11	215	0.46	329, 443, 460	442	$C_{27}H_{38}O_5$	e, e	[19]
72	15.91	215	0.04	331, 445, 462	444	$C_{27}H_{40}O_5$	d, e	
73	15.94	215	0.99	261, 317, 363, 477, 494	476	$C_{28}H_{44}O_6$	c, e, h	
74	16.25	215	0.26	317, 329, 419, 431, 533, 550	532	$C_{31}H_{48}O_7$	c, c, e	

* R groups, a: O-Ac, b: O-Ang or O-Sen, c: O-Mebu or O-*i*Val, d: O-Meval, e: O-Mesen, f: OH, g: OMe, h: OEt, i: unknown (88 Da), j: unknown (128 Da)

2.3. Method validation

2.3.1. Separation of 11 sesquiterpenoids

In order to validate the dereplicative method, 11 sesquiterpenoids were isolated from the STE fraction. As shown in **Fig. 25**, compounds **14**, **11**, **12**, **39**, **45**, **60**, **68**, and **72** were sequentially eluted by the CCC separation and further refined by preparative HPLC. Compounds **11**, **12**, and **14** were easily separated by CCC rather than C_{18} reverse-phase column chromatography. In addition, compounds **23** and **36**, low-abundant and highly overlapped compounds, were obtained by NaOH hydrolysis of **12**. The aldol intermediate (a C14-hydroxyl derivative) was rapidly dehydrated to form an α, β-unsaturated carbonyl group in this condition. Likewise, compound **68** was hydrolyzed by NaOH to obtain **7** (a C1-hydroxyl derivative).

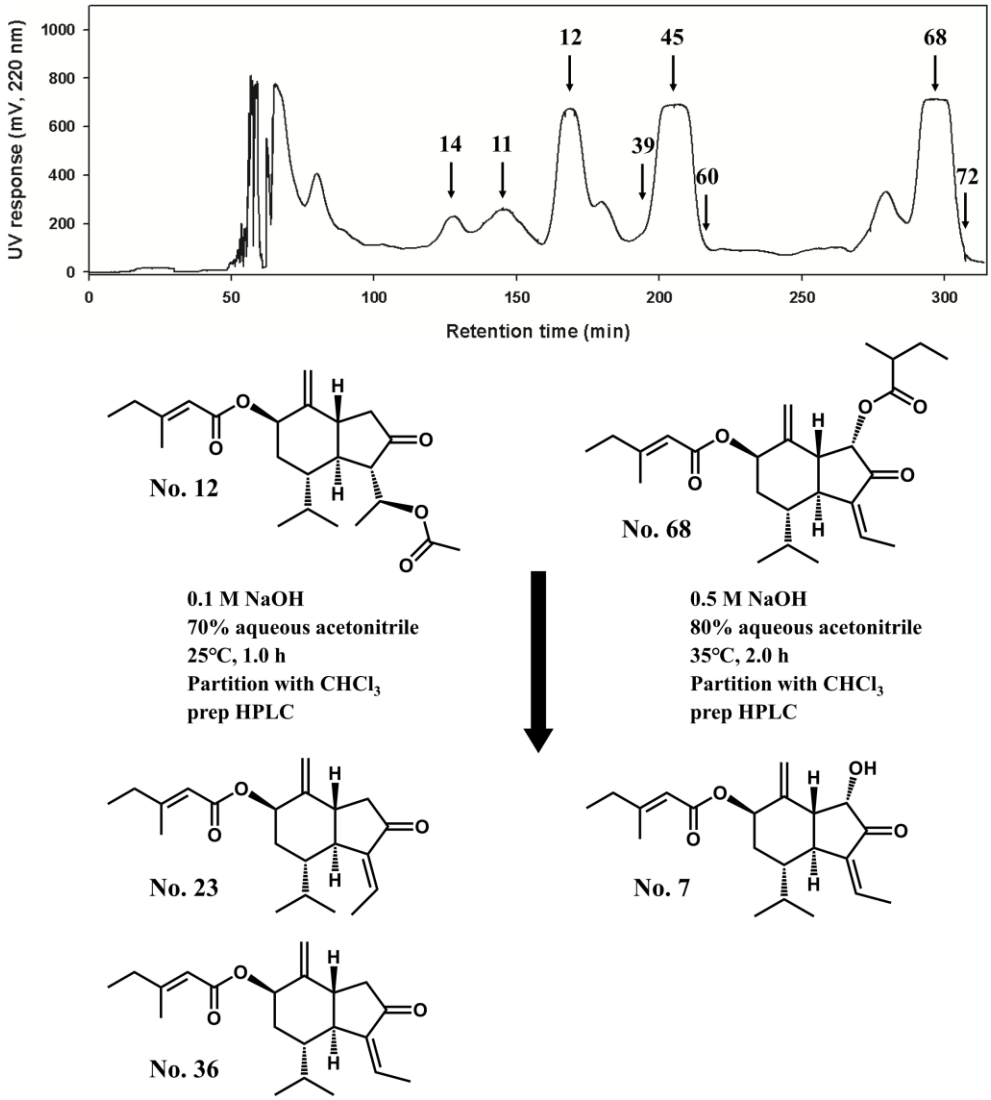

Figure 25. Preparation of 11 sesquiterpenoids from STE fraction

Eight sesquiterpenoids (**11**, **12**, **14**, **39**, **45**, **60**, **68**, and **72**) were separated from the STE fraction by CCC separation, and three sesquiterpenoids (**7**, **23**, **36**) were obtained from NaOH hydrolysis of **12** and **68**.

2.3.2. Structural elucidation

All the isolated compounds were analyzed by precursor ion scan **(Fig. 26)** and structurally elucidated by NMR spectroscopy **(Fig. 27–40)**. Among these compounds, **11**, **60**, and **72** were newly isolated from Farfarae Flos. Compound **11**, altaicalarin C, was first reported from *Ligularia altaica* [95], but compounds **60** and **72** have not been reported previously. As shown in **Fig. 26I** and **Fig. 26K**, both compounds showed the loss of 116 Da (*m/z* 215 → 331) indicating an unreported substituent and the comparison of the NMR spectrum between **45** and **60** (likewise **68** and **72**) represented that the C1 positions of **60** and **72** were substituted with 3-methylvaleric acid by an ester linkage. In addition, the peak at *m/z* 329 was rarely observed in the MS/MS spectra of **45**, **60**, **68**, and **72**, indicating that the ester linkage at the C1 position of the oplopane sesquiterpenoids was hard to be dissociated in the ESI-MS/MS condition rather than those at positions C7 and C14. Compounds **23** and **36** were isomeric forms (Δ3(14)-*E* and -*Z*) and the C14-proton of the *E* isomer was downfield relative to the proton of the *Z* isomer [19, 21]. Furthermore, the C14-proton (δ_H 6.35) of the *E* isomer did not interact with the C4-proton (δ_H 2.26) in the NOESY correlations **(Fig. 39)**. Comparing the retention time of **23** with **36**, the *E* isomer was eluted earlier than the *Z* isomer in the UHPLC separation. Therefore, compounds **51**, **56**, and **64** were annotated to the *E* isomers of **61**, **63**, and **68** (the *Z* isomeric counterparts), respectively. To determine the stereochemistry of the hydroxyl group of **7**, NOESY correlations were investigated **(Fig. 38)**. The hydroxyl proton interacted with the protons of C1 (δ_H 3.95), C4 (δ_H 2.64), and C10 (δ_H 5.19) position. Considering the reported stereochemistry of the

oplopane backbone (4*S* and 9*R*) from the Farfarae Flos [17–25], the hydroxyl group was α-oriented (1S) because the NOESY correlation with the axial proton (δ_H 2.32) of the C9 position was not detected. Furthermore, the NOESY correlations of compounds **7**, **23**, and **45** showed the stereochemistries 1*S*, 4*S*, 5*S*, 7*R*, 9*R* **(Fig. 38–40)**.

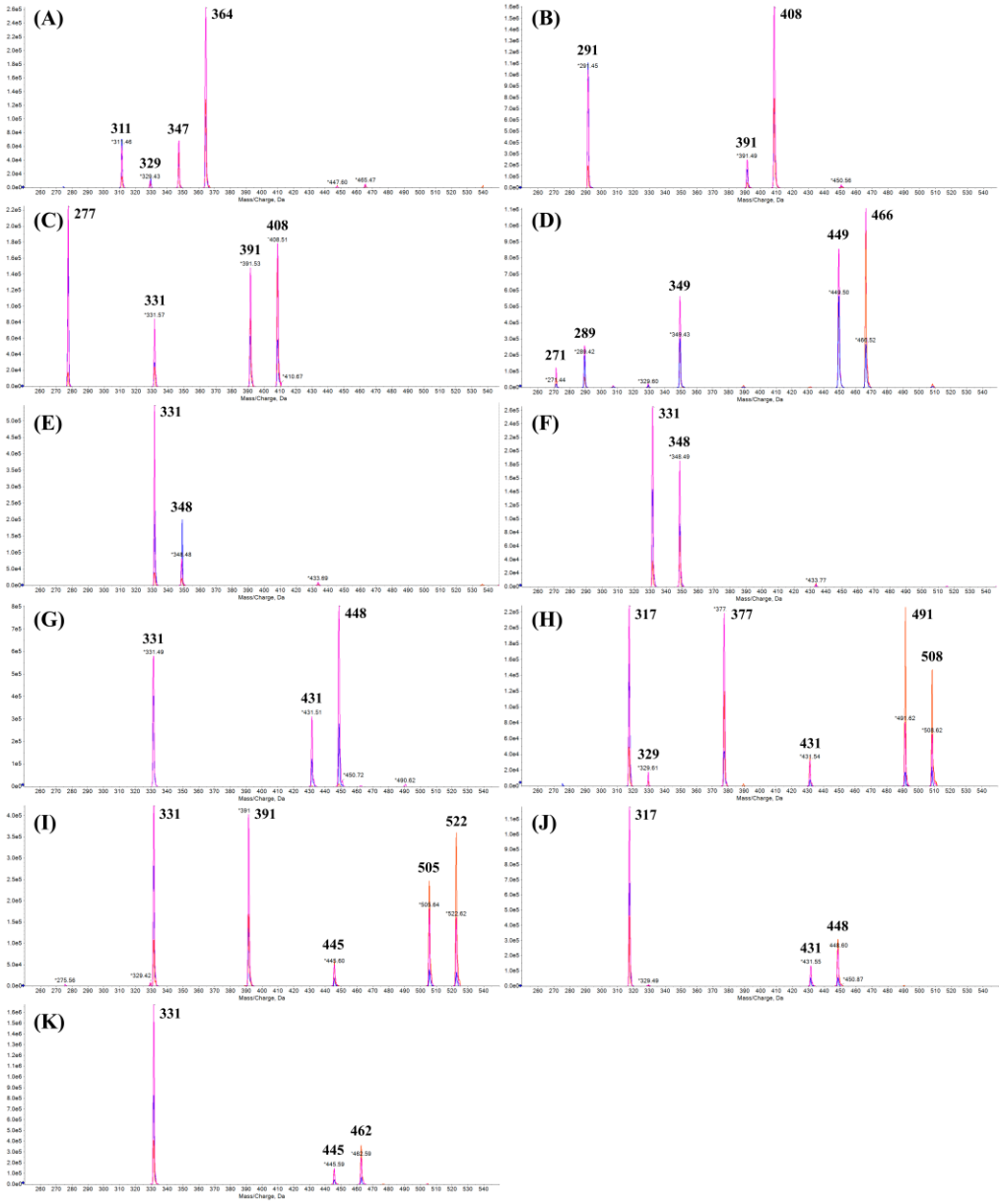

Figure 26. Precursor ion scans for isolated sesquiterpenoids

Precursor ion scans for oplopane and bisabolane sesquiterpenoids isolated from Farfarae Flos: (A) **7**, (B) **11**, (C) **12** (D) **14**, (E) **23**, (F) **36**, (G) **39**, (H) **45**, (I) **60**, (J) **68**, (K) **72**. Three collision energies (blue line for 5 eV; pink line for 15 eV; orange line for 25 eV) were selected in all the QqQ-MS/MS analysis to investigate all the intermediate and parent molecular ions.

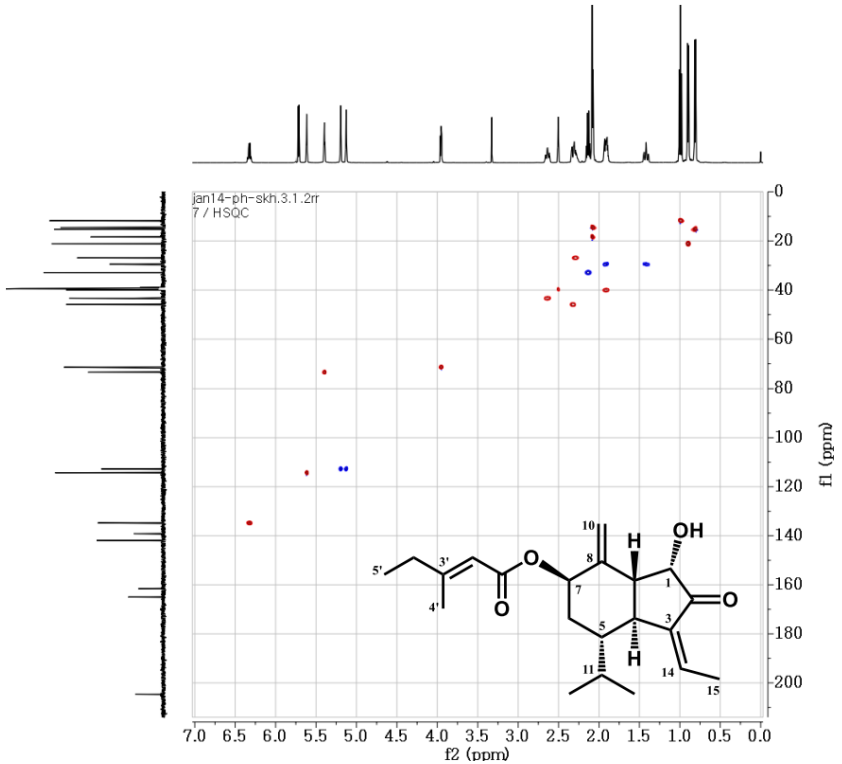

	^{13}C	^{1}H
1	71.4	3.95 (1H, dd, 5.5, 5.0)
C1-OH		5.72 (1H, d, 5.0)
2	204.7	
3	139.1	
4	43.4	2.64 (1H, m)
5	40.0	1.91 (1H, m)
6	29.5	1.42 (1H, m) 1.91 (1H, m)
7	73.5	5.40 (1H, dd, *J* = 4.0, 2.2)
8	141.9	
9	45.9	2.32 (1H, m)
10	112.7	5.13 (1H, br s) 5.19 (1H, br s)
11	26.9	2.29 (1H, m)
12	21.1	0.90 (3H, d, *J* = 7.0)
13	15.2	0.81 (3H, d, *J* = 7.0)
14	134.7	6.32 (1H, qd, *J* = 7.0, 2.0)
15	14.5	2.08 (3H, dd, *J* = 7.0, 2.5)
C7-OMesen		
1′	165.0	
2′	114.3	5.62 (1H, br s)
3′	161.5	
4′	32.9	2.13 (2H, br q, 7.0)
5′	11.8	0.99 (3H, t, *J* = 7.5)
6′	18.4	2.08 (3H, d, *J* = 0.8)

Figure 27. HSQC spectrum of compound No. 7

(in DMSO-d_6, 500 MHz)

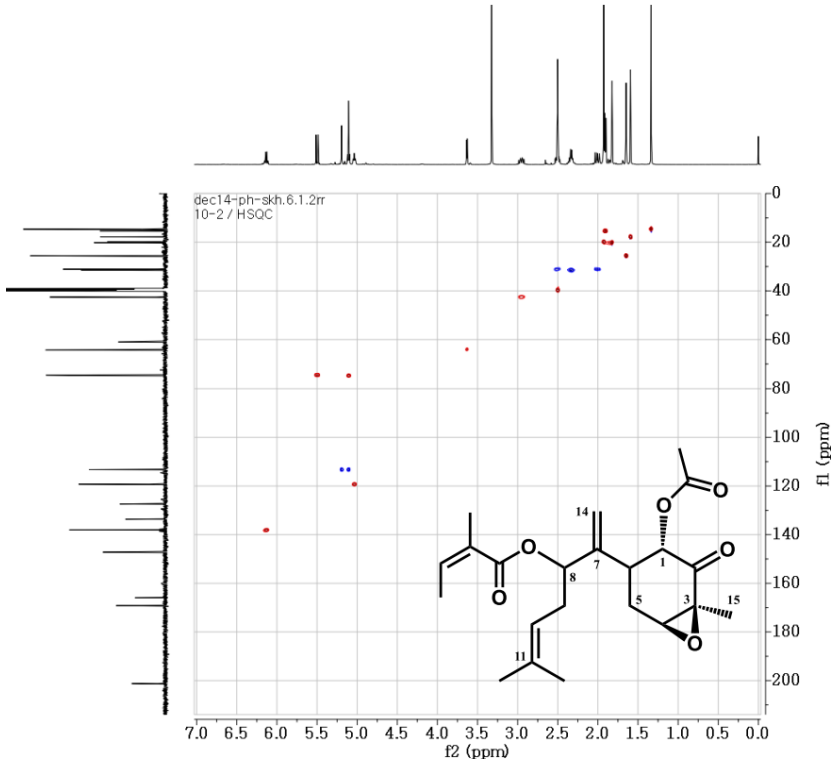

	^{13}C	^{1}H
1	74.6	5.50 (1H, d, J = 13.0)
2	201.2	
3	61.0	
4	64.3	3.63 (1H, d, J = 4.5)
5	31.1	2.01 (1H, dd, J = 15.5, 11.0) 2.50 (1H, m)
6	42.5	2.95 (1H, ddd, J = 14.0, 12.0, 7.5)
7	147.2	
8	74.8	5.11 (1H, dd, J = 8.0, 5.5)
9	31.5	2.33 (2H, m)
10	119.2	5.04 (1H, m)
11	133.6	
12	25.6	1.65 (3H, s)
13	17.8	1.59 (3H, s)
14	113.2	5.11 (1H, br s) 5.20 (1H, br s)
15	14.6	1.34 (3H, s)
C1-OAc		
1′	169.2	
2′	19.9	1.93 (3H, s)
C8-OAng		
1″	165.9	
2″	127.4	
3″	138.0	6.13 (1H, qq, J = 7.0, 1.5)
4″	15.4	1.91 (3H, qd, 7.0, 1.5)
5″	20.2	1.82 (3H, qd, 1.5, 1.0)

Figure 28. HSQC spectrum of compound No. 11

(in DMSO-d_6, 500 MHz)

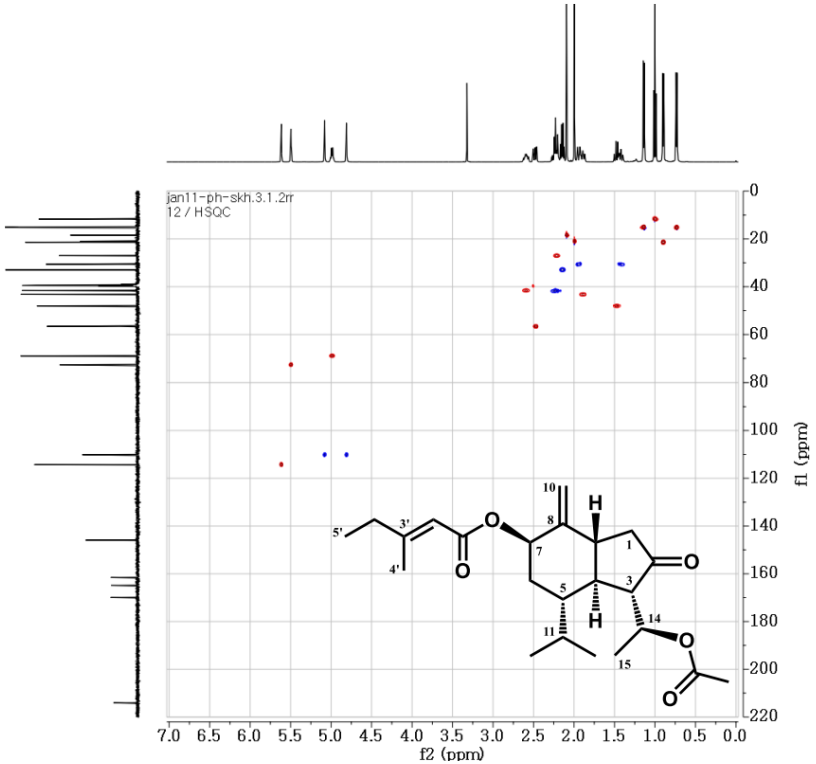

	^{13}C	^{1}H
1	41.7	2.22 (2H, m)
2	214.0	
3	56.6	2.47 (1H, dd, *J* = 11.0, 2.5)
4	48.0	1.47 (1H, m)
5	43.2	1.89 (1H, m)
6	30.6	1.42 (1H, m) 1.94 (1H, m)
7	72.7	5.50 (1H, dd, *J* = 3.0, 1.8)
8	145.9	
9	41.5	2.59 (1H, m)
10	110.1	4.81 (1H, br s) 5.08 (1H, br s)
11	27.0	2.21 (1H, m)
12	21.0	0.90 (3H, d, *J* = 7.0)
13	15.2	0.73 (3H, d, *J* = 7.0)
14	68.9	4.99 (1H, qd, *J* = 6.5, 3.0)
15	15.1	1.14 (3H, d, *J* = 6.6)
C7-OMesen		
1′	164.9	
2′	114.3	5.62 (1H, br s)
3′	161.5	
4′	32.9	2.14 (2H, br q, 7.0)
5′	11.7	1.00 (3H, t, *J* = 7.5)
6′	18.4	2.09 (3H, d, *J* = 0.8)
C14-OAc		
1″	169.9	
2″	21.4	2.00 (3H, s)

Figure 29. HSQC spectrum of compound No. 12

(in DMSO-d_6, 500 MHz)

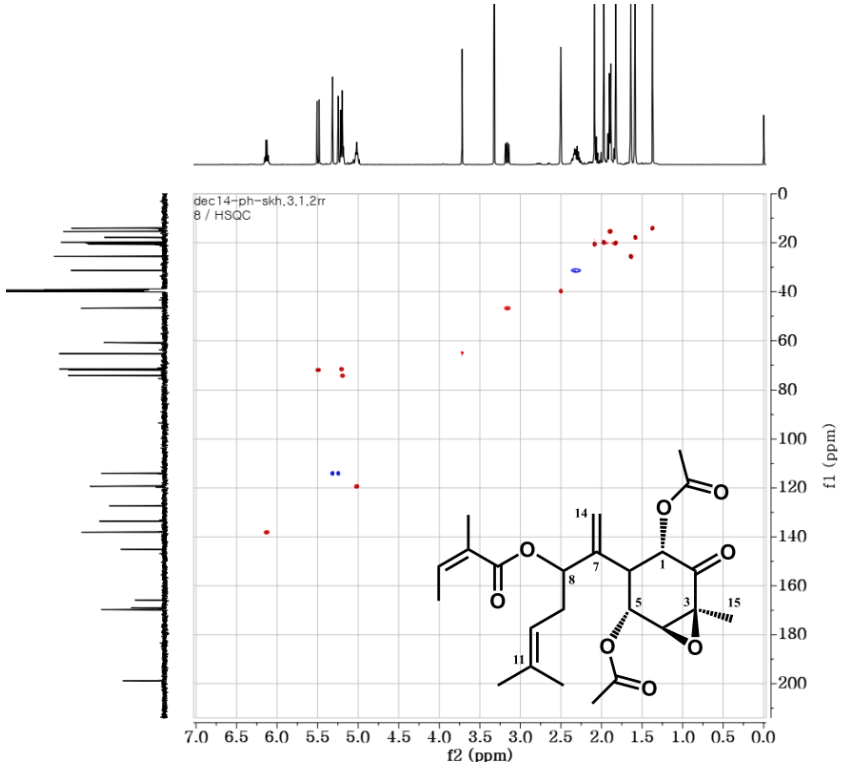

	^{13}C	^{1}H
1	71.9	5.49 (1H, d, *J* = 13.0)
2	198.8	
3	60.8	
4	65.3	3.72 (1H, s)
5	71.6	5.21 (1H, d, *J* = 9.5)
6	46.7	3.16 (1H, dd, *J* = 13.0, 9.5)
7	145.0	
8	74.3	5.19 (1H, dd, *J* = 8.0, 4.5)
9	31.3	2.32 (1H, m)
10	119.3	5.02 (1H, br t, *J* = 7.5)
11	133.6	
12	25.5	1.64 (3H, s)
13	17.8	1.59 (3H, s)
14	114.0	5.25 (1H, s) 5.32 (1H, s)
15	14.1	1.37 (3H, s)
C1, 5-OAc		
1′, 1″	169.0 169.7	
2′, 2″	19.9 20.6	1.97 (3H, s) 2.09 (3H, s)
C8-OAng		
1‴	165.8	
2‴	127.3	
3‴	138.0	6.13 (1H, qq, *J* = 7.0, 1.5)
4‴	15.4	1.90 (3H, qd, 7.0, 1.5)
5‴	20.1	1.82 (3H, qd, 1.5, 1.0)

Figure 30. HSQC spectrum of compound No. 14

(in DMSO-d_6, 500 MHz)

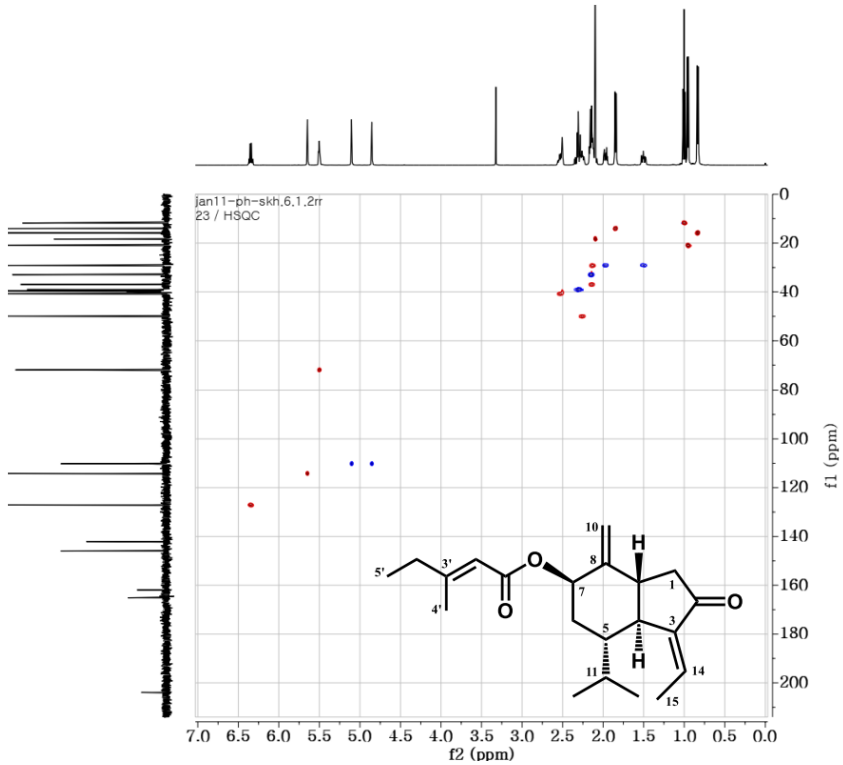

	^{13}C	^{1}H
1	39.0	2.31 (2H, m)
2	203.9	
3	142.1	
4	49.9	2.26 (1H, m)
5	36.9	2.14 (1H, m)
6	29.1	1.50 (1H, m) 1.96 (1H, m)
7	71.9	5.50 (1H, dd, J = 3.0, 1.8)
8	145.9	
9	40.7	2.53 (1H, m)
10	110.2	4.85 (1H, br s) 5.10 (1H, br s)
11	29.2	2.13 (1H, m)
12	21.0	0.95 (3H, d, J = 7.0)
13	15.8	0.83 (3H, d, J = 6.5)
14	127.1	6.35 (1H, qd, J = 8.0, 2.5)
15	14.1	1.85 (3H, dd, J = 8.0, 2.5)
C7-OMesen		
1′	165.1	
2′	114.2	5.65 (1H, br s)
3′	161.9	
4′	32.9	2.15 (2H, br q, 7.0)
5′	11.8	1.00 (3H, t, J = 7.0)
6′	18.4	2.10 (3H, d, J = 0.8)

Figure 31. HSQC spectrum of compound No. 23

(in DMSO-d_6, 500 MHz)

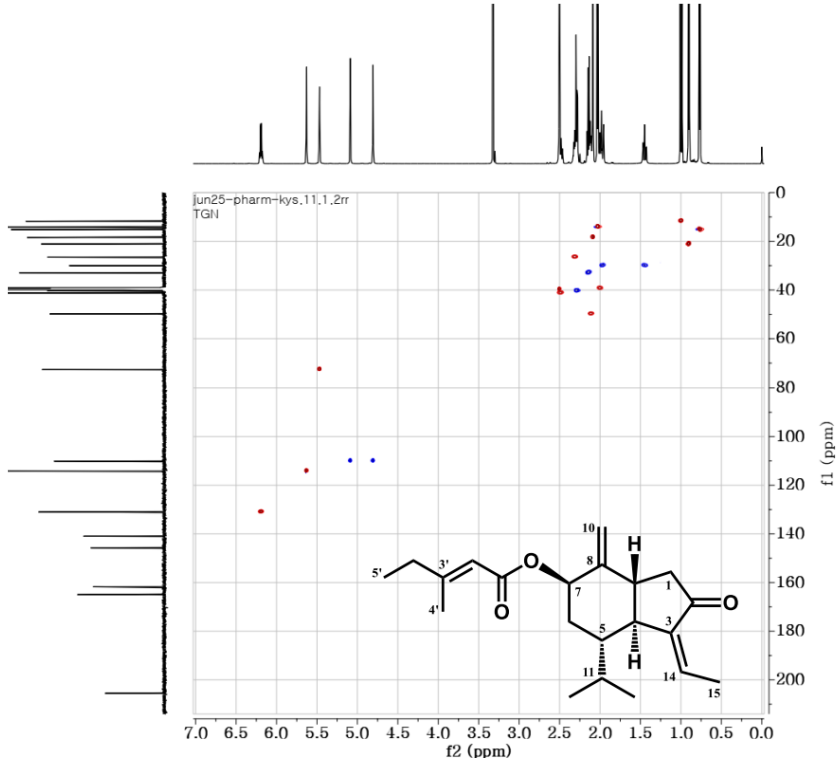

	^{13}C	^{1}H
1	40.3	2.28 (2H, m)
2	205.5	
3	140.9	
4	49.8	2.12 (1H, m)
5	39.3	2.00 (1H, m)
6	30.0	1.45 (1H, m) 1.97 (1H, m)
7	72.7	5.47 (1H, dd, J = 3.0, 1.8)
8	145.7	
9	41.2	2.49 (1H, m)
10	110.1	4.81 (1H, br s) 5.09 (1H, br s)
11	26.5	2.31 (1H, m)
12	21.2	0.90 (3H, d, J = 7.0)
13	15.2	0.77 (3H, d, J = 6.6)
14	131.0	6.19 (1H, qd, J = 7.2, 2.5)
15	14.1	2.03 (3H, dd, J = 7.2, 2.5)
C7-OMesen		
1′	165.0	
2′	114.2	5.63 (1H, br s)
3′	161.7	
4′	32.9	2.14 (2H, br q, 7.0)
5′	11.8	1.00 (3H, t, J = 7.2)
6′	18.4	2.09 (3H, d, J = 0.8)

Figure 32. HSQC spectrum of compound No. 36

(in DMSO-d_6, 500 MHz)

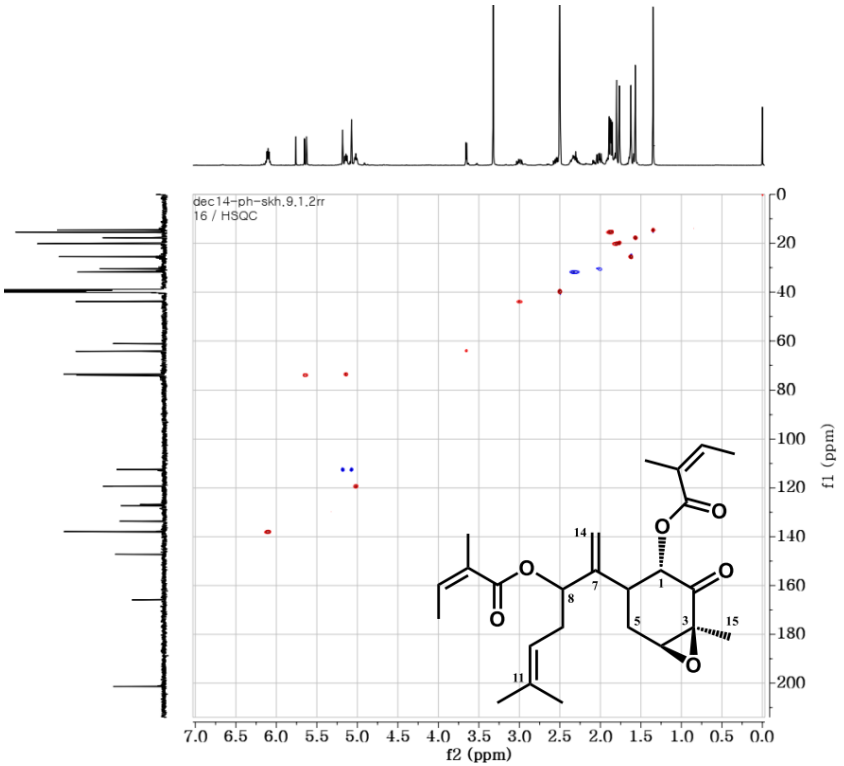

	^{13}C	^{1}H
1	74.0	5.64 (1H, d, J = 13.0)
2	201.3	
3	61.1	
4	64.2	3.66 (1H, d, J = 4.0)
5	30.5	2.01 (1H, dd, J = 15.0, 10.5) 2.55 (1H, m)
6	43.9	3.00 (1H, ddd, J = 14.0, 12.0, 7.5)
7	147.2	
8	73.6	5.14 (1H, dd, J = 5.0, 2.5)
9	31.8	2.32 (2H, m)
10	119.3	5.02 (1H, m)
11	133.6	
12	25.5	1.62 (3H, s)
13	17.7	1.57 (3H, s)
14	112.5	5.07 (1H, br s) 5.18 (1H, br s)
15	14.7	1.35 (3H, s)
C1, C8-OAng		
1′, 1″	165.9 166.0	
2′, 2″	126.7 127.3	
3′, 3″	137.9 138.0	6.10 (1H, m) 6.10 (1H, m)
4′, 4″	15.4 15.4	1.86 (3H, qd, 7.0, 1.5) 1.89 (3H, qd, 7.0, 1.5)
5′, 5″	19.9 20.2	1.77 (3H, qd, 1.5, 1.0) 1.80 (3H, qd, 1.5, 1.0)

Figure 33. HSQC spectrum of compound No. 39

(in DMSO-d_6, 500 MHz)

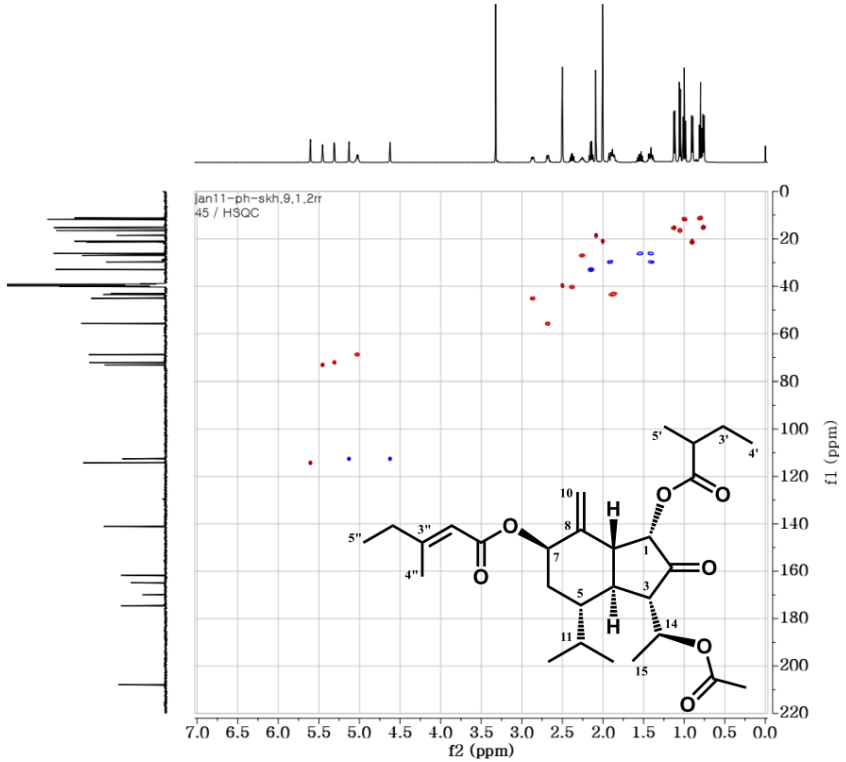

	^{13}C	^{1}H
1	72.1	5.31 (1H, d, J = 3.0)
2	207.9	
3	55.7	2.68 (1H, dd, J = 9.5, 3.0)
4	43.5	1.89 (1H, m)
5	43.1	1.87 (1H, m)
6	29.7	1.41 (1H, m) 1.91 (1H, m)
7	73.1	5.46 (1H, dd, J = 3.0, 1.8)
8	141.1	
9	45.1	2.87 (1H, m)
10	112.5	4.62 (1H, br s) 5.13 (1H, br s)
11	27.0	2.26 (1H, m)
12	21.0	0.90 (3H, d, J = 7.0)
13	15.1	0.76 (3H, d, J = 7.0)
14	68.8	5.03 (1H, m)
15	15.3	1.12 (3H, d, J = 6.6)
C1-OMebu		
1′	174.5	
2′	40.3	2.38 (1H, m)
3′	26.2	1.41 (1H, m) 1.55 (1H, m)
4′	11.2	0.80 (3H, t, J = 7.2)
5′	16.5	1.05 (3H, d, 6.6)
C7-OMesen		
1″	164.8	
2″	114.2	5.60 (1H, br s)
3″	161.6	
4″	32.9	2.15 (2H, m)
5″	11.7	1.00 (3H, t, J = 7.2)
6″	18.5	2.09 (3H, d, J = 0.8)
C14-OAc		
1‴	169.9	
2‴	21.3	2.00 (3H, s)

Figure 34. HSQC spectrum of compound No. 45

(in DMSO-d_6, 500 MHz)

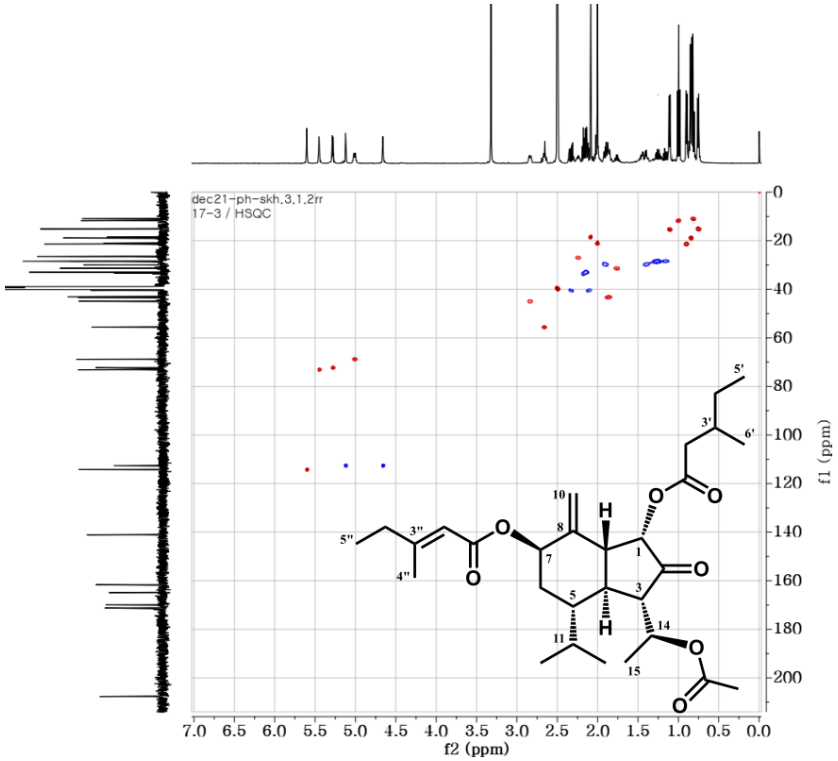

	^{13}C	^{1}H
1	72.3	5.28 (1H, d, J = 3.6)
2	207.6	
3	55.6	2.66 (1H, dd, J = 9.5, 3.0)
4	43.4	1.88 (1H, m)
5	43.1	1.84 (1H, m)
6	29.7	1.40 (1H, m) 1.90 (1H, m)
7	73.1	5.45 (1H, dd, J = 3.0, 1.8)
8	141.1	
9	44.9	2.84 (1H, m)
10	112.6	4.66 (1H, br s) 5.12 (1H, br s)
11	27.0	2.24 (1H, m)
12	21.3	0.90 (3H, d, J = 7.0)
13	15.1	0.76 (3H, d, J = 7.0)
14	68.8	5.01 (1H, m)
15	15.3	1.11 (3H, d, J = 6.6)
C1-OMeval		
1′	171.2	
2′	40.4	2.11 (1H, m) 2.33 (1H, m)
3′	31.4	1.76 (1H, m)
4′	28.4	1.16 (1H, m) 1.29 (1H, m)
5′	11.0	0.82 (3H, t, J = 7.2)
6′	18.9	0.84 (3H, d, 7.2)
C7-OMesen		
1″	164.8	
2″	114.2	5.60 (1H, br s)
3″	161.6	
4″	32.9	2.14 (2H, m)
5″	11.7	1.00 (3H, t, J = 7.2)
6″	18.5	2.09 (3H, d, J = 0.8)
C14-OAc		
1‴	169.9	
2‴	21.0	2.00 (3H, s)

Figure 35. HSQC spectrum of compound No. 60

(in DMSO-d_6, 500 MHz)

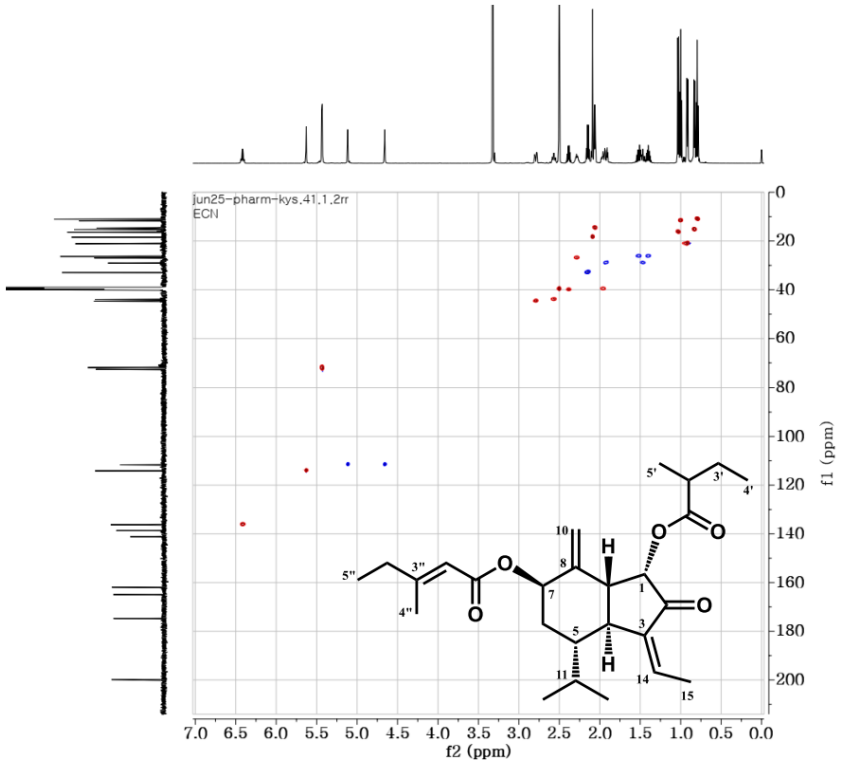

	^{13}C	^{1}H
1	71.9	5.43 (1H, d, J = 3.0)
2	199.8	
3	138.6	
4	44.0	2.57 (1H, m)
5	39.1	1.95 (1H, m)
6	29.1	1.47 (1H, m) 1.92 (1H, m)
7	72.6	5.43 (1H, m)
8	141.1	
9	44.7	2.79 (1H, m)
10	111.7	4.66 (1H, br s) 5.12 (1H, br s)
11	27.0	2.29 (1H, m)
12	21.1	0.92 (3H, d, J = 7.2)
13	15.3	0.83 (3H, d, J = 7.2)
14	136.2	6.42 (1H, qd, J = 7.2, 3.0)
15	14.7	2.06 (3H, dd, J = 7.2, 2.4)
C1-OMebu		
1′	174.8	
2′	39.7	2.39 (1H, m)
3′	26.3	1.40 (1H, m) 1.51 (1H, m)
4′	11.1	0.80 (3H, t, J = 7.2)
5′	16.4	1.03 (3H, d, 6.6)
C7-OMesen		
1″	164.9	
2″	114.1	5.63 (1H, br s)
3″	161.9	
4″	32.9	2.15 (2H, m)
5″	11.8	1.00 (3H, t, J = 7.2)
6″	18.4	2.09 (3H, d, J = 0.8)

Figure 36. HSQC spectrum of compound No. 68

(in DMSO-d_6, 500 MHz)

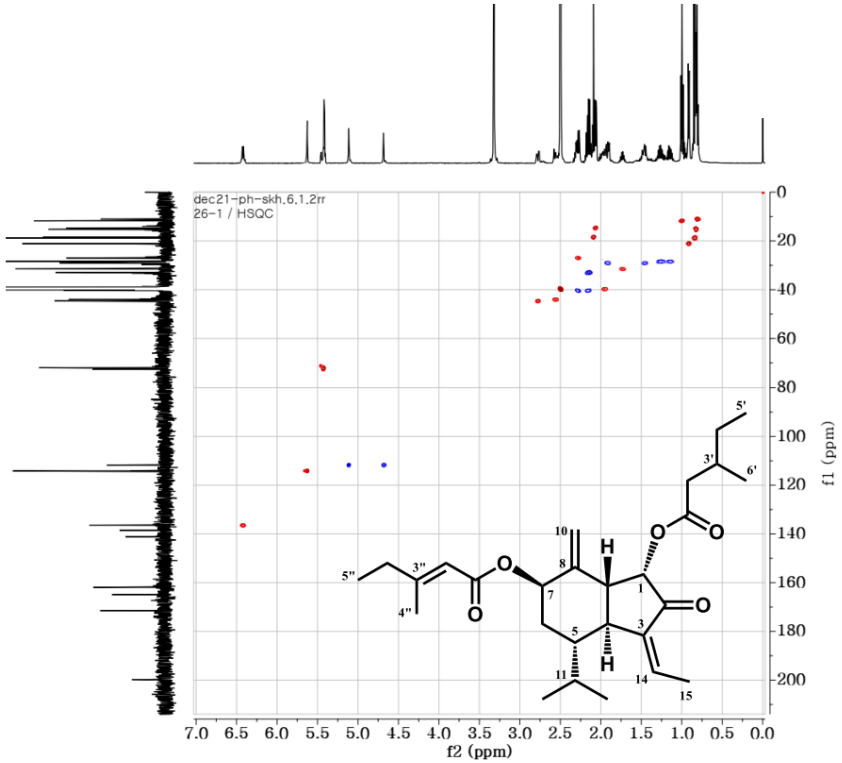

	^{13}C	^{1}H
1	72.6	5.43 (1H, d, J = 4.5)
2	199.8	
3	138.5	
4	44.0	2.56 (1H, m)
5	39.7	1.95 (1H, m)
6	29.1	1.46 (1H, m) 1.92 (1H, m)
7	72.0	5.46 (1H, m)
8	141.1	
9	44.6	2.78 (1H, m)
10	111.7	4.69 (1H, br s) 5.11 (1H, br s)
11	27.0	2.28 (1H, m)
12	21.1	0.91 (3H, d, J = 7.2)
13	15.3	0.83 (3H, d, J = 7.2)
14	136.4	6.42 (1H, qd, J = 7.2, 2.5)
15	14.7	2.06 (3H, dd, J = 7.2, 2.5)
C1-OMeval		
1′	171.4	
2′	40.3	2.15 (1H, m) 2.28 (1H, m)
3′	31.5	1.73 (1H, m)
4′	28.4	1.14 (1H, m) 1.28 (1H, m)
5′	11.0	0.81 (3H, t, J = 7.2)
6′	18.8	0.84 (3H, d, 7.2)
C7-OMesen		
1″	164.9	
2″	114.1	5.63 (1H, br s)
3″	161.9	
4″	32.9	2.15 (2H, m)
5″	11.8	1.00 (3H, t, J = 7.2)
6″	18.4	2.09 (3H, d, J = 0.8)

Figure 37. HSQC spectrum of compound No. 72

(in DMSO-d_6, 500 MHz)

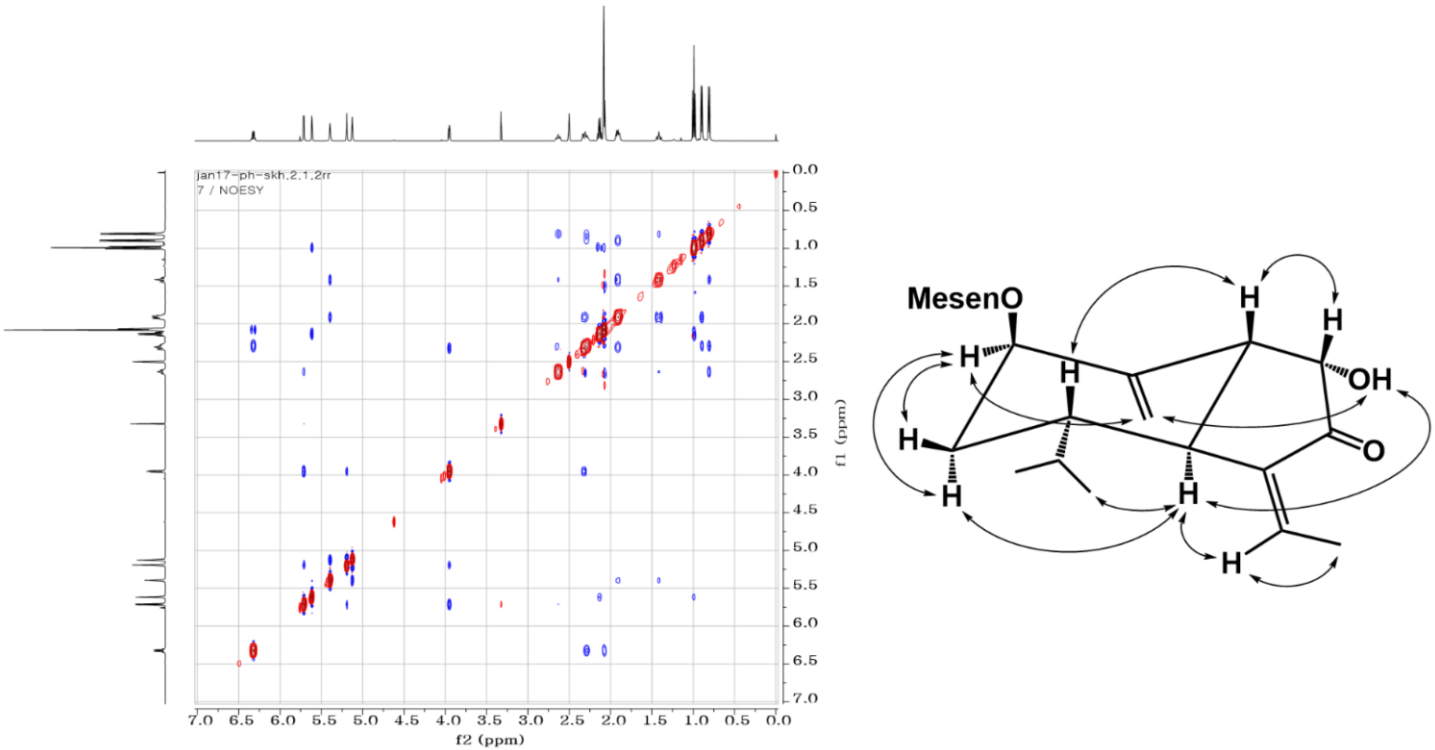

Figure 38. NOESY spectrum of compound No. 7

(in DMSO-d_6, 500 MHz)

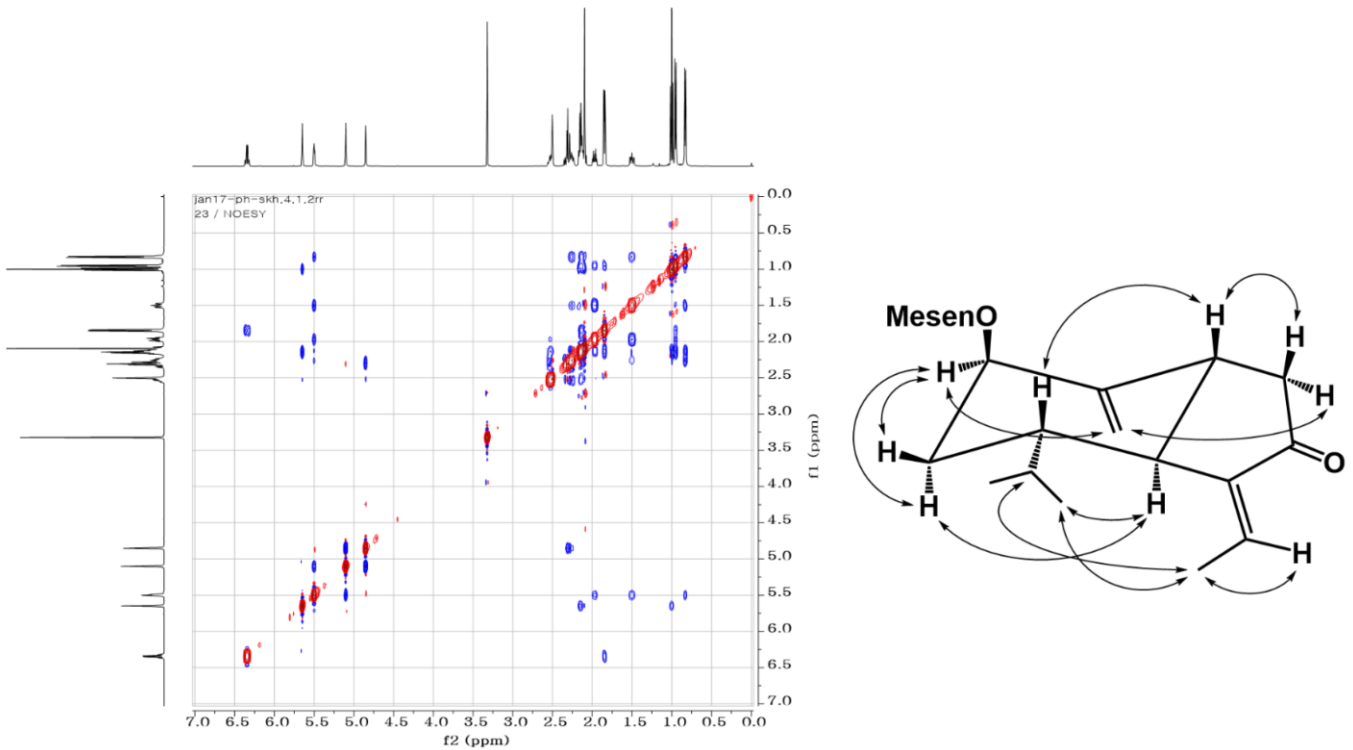

Figure 39. NOESY spectrum of compound No. 23

(in DMSO-d_6, 500 MHz)

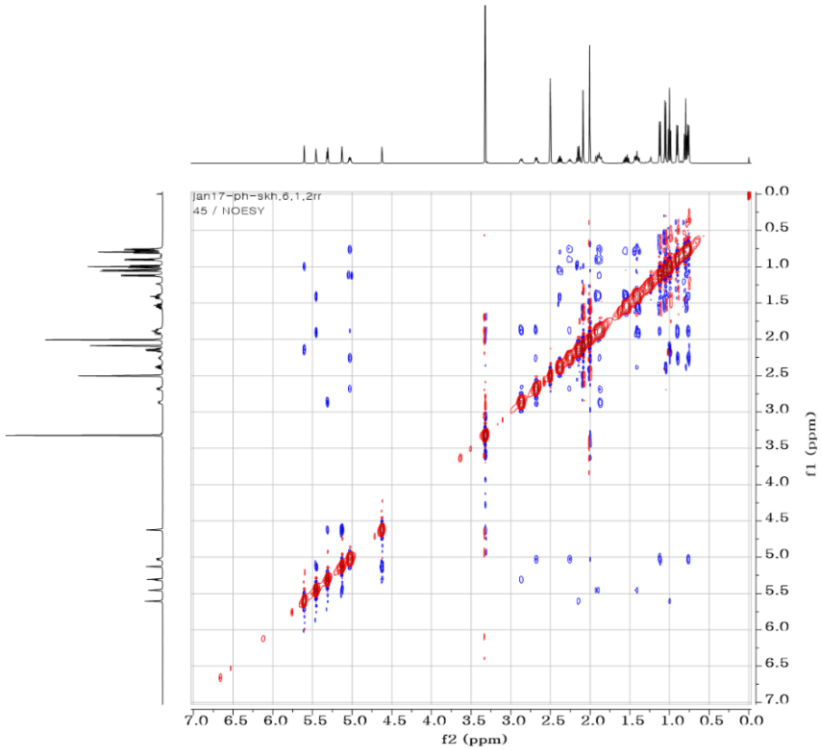

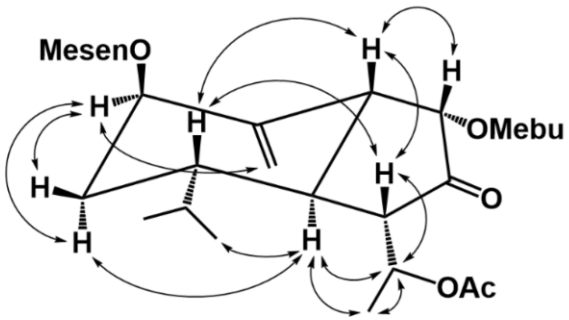

Figure 40. NOESY spectrum of compound No. 45

(in DMSO-d_6, 500 MHz)

2.4. CID-fragmentation behavior of sesquiterpenoids

CID trends of oplopane and bisabolane sesquiterpenoids by tandem mass spectrometry were investigated based on the product ion scan. Under the collision-induced dissociation (CID) in positive ion mode, the diagnostic ions were mainly produced by ester cleavages and double bond reduction corresponding to the loss of 60 Da for HOAc (acetic acid), 100 Da for HOAng (angelic acid) or HOSen (3-methylcrotonic acid), 102 Da for HOMebu (2-methylbutyric acid), and 114 Da for HOMesen (3-ethyl-*cis*-crotonic acid).

Taking compounds **45**, **12**, **14**, and **11** as examples of the four diagnostic ions, **Fig. 41** represented their fragmentation patterns in terms of the ester cleavages. Compound **45** generated the protonated ion $[M+H]^+$ at *m/z* 491.2989, and the product ions at *m/z* 431.2789, 377.2320, 317.2110, 233.1534, and 215.1429 corresponded to specific fragment ions of $[M+H–C_2H_4O_2]^+$, $[M+H–C_6H_{10}O_2]^+$, $[M+H–C_2H_4O_2–C_6H_{10}O_2]^+$, $[M+H–C_2H_4O_2–C_6H_{10}O_2–C_5H_{10}O_2+H_2O]^+$, and $[M+H–C_2H_4O_2–C_6H_{10}O_2–C_5H_{10}O_2]^+$, respectively **(Fig. 41A)**. Compound **12** generated the protonated ion $[M+H]^+$ at *m/z* 391.2472, and the product ions at *m/z* 331.2265, 277.1794, 235.1689, and 217.1587 corresponded to specific fragment ions of $[M+H–C_2H_4O_2]^+$, $[M+H–C_6H_{10}O_2]^+$, $[M+H–C_2H_4O_2–C_6H_{10}O_2–C_5H_{10}O_2+H_2O]^+$, and $[M+H–C_2H_4O_2–C_6H_{10}O_2–C_5H_{10}O_2]^+$, respectively **(Fig. 41B)**. The difference of **45** and **12** was the number of ester linkages and they were fragmented to *m/z* 215.1429 and 217.1587, respectively. Compound **14** generated the ammonium ion $[M+NH_4]^+$ at *m/z* 466.2433, and the product ions at *m/z* 449.2174, 349.1644,

289.1436, 247.1335, and 229.1225 corresponded to specific fragment ions of $[M+H]^+$, $[M+H–C_5H_8O_2]^+$, $[M+H–C_5H_8O_2–C_2H_4O_2]^+$, $[M+H–C_5H_8O_2–C_2H_4O_2–C_2H_4O_2]^+$, and $[M+H–C_5H_8O_2–C_2H_4O_2–C_2H_4O_2+H_2O]^+$, respectively **(Fig. 41C)**. Compound **11** generated the protonated ion $[M+ NH_4]^+$ at *m/z* 408.2380, and the product ions at *m/z* 391.2113, 291.1598, 249.1490, and 231.1384 corresponded to specific fragment ions of $[M+H]^+$, $[M+H–C_5H_8O_2]^+$, $[M+H–C_5H_8O_2–C_2H_4O_2+H_2O]^+$, $[M+H–C_5H_8O_2–C_2H_4O_2]^+$, respectively **(Fig. 41D)**. Likewise, **14** and **11** were fragmented to *m/z* 229.1225 and 231.1384, respectively.

In the case of compound **45**, a highly abundant sesquiterpenoid of the Farfarae Flos, its heteroisotopic molecular ion ($[(M+2)+H]^+$ at *m/z* 493) containing two deuteriums was more abundant than the monoisotopic molecular ion of **48** ($[M+H]^+$ at *m/z* 493). As shown in **Fig. 42**, the fragmentation pattern of the heteroisotopic species showed unusual isotopic ratios and these MS/MS data should be filtered for accurate identification.

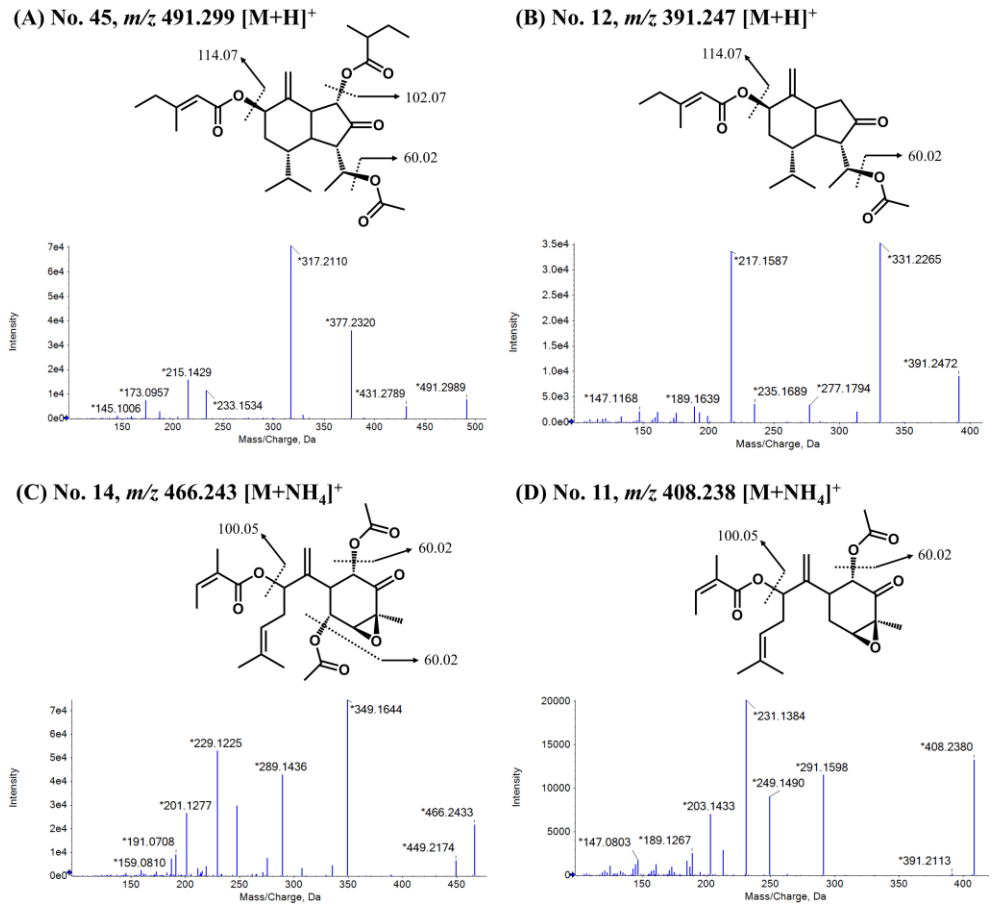

Figure 41. Representative MS/MS fragmentation behaviors

Representative MS/MS fragmentations behavior of oplopane and bisabolane sesquiterpenoids by product ion scan of Q-TOF MS/MS (collision energy 15 eV): (A) MS/MS of No. **45** for selected $[M+H]^+$ at *m/z* 491; (B) MS/MS of No. **12** for selected $[M+H]^+$ at *m/z* 391; (C) MS/MS of No. **14** for selected $[M+NH_4]^+$ at *m/z* 466; (D) MS/MS of No. **11** for selected $[M+NH_4]^+$ at *m/z* 408.

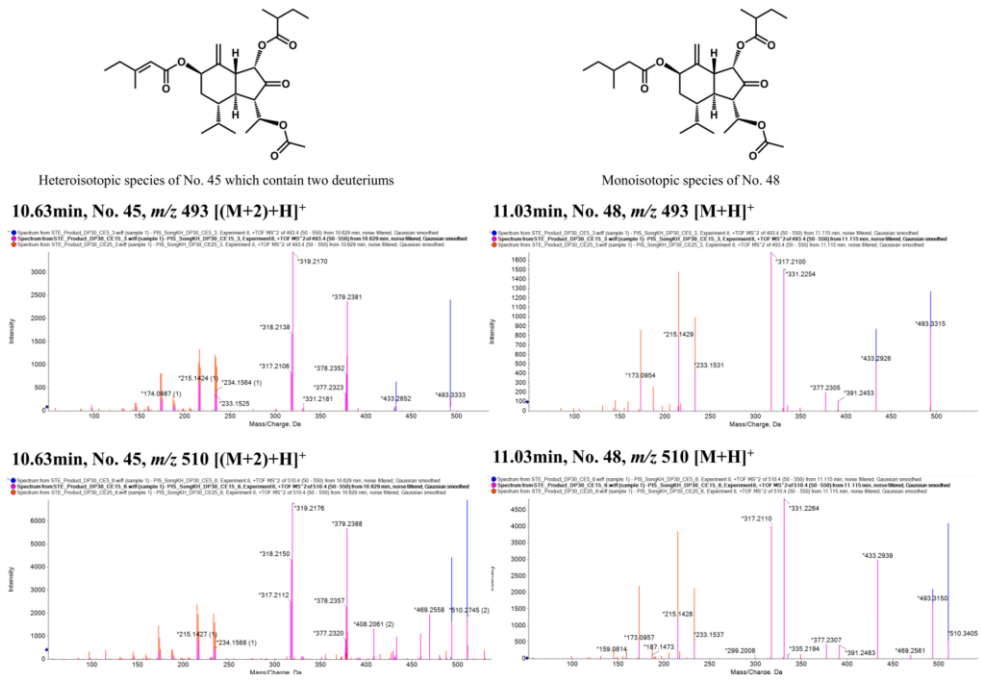

Figure 42. Fragmentation behaviors of mono- and hetero-isotopic ions

2.5. Quantification of sesquiterpenoids by MRM^{HR}

The diagnostic and precursor ions investigated in the present study were applied to the absolute quantification of the sesquiterpenoids in Farfarae Flos **(Fig. 43)**. A total of 8 isolated compounds **11**, **12**, **14**, **23**, **36**, **39**, **45**, and **68** were absolutely quantified based on their selectivity, linearity, LOD, LOQ, and precision by UHPLC-MRM^{HR}, and the validation parameters were described in **Table 6** and **Table 7**. As shown in **Fig. 44**, deconvolution of each target peak was performed based on the selection of precursor ions and the corresponding diagnostic ions of the sesquiterpenoids. Especially, the selection of *m/z* 408, 231.138 for compound **11** and *m/z* 391, 217.158 for compound **12** distinguished the highly overlapped compounds. Likewise, compound **36** (selected *m/z* 331, 217.158) was deconvoluted from compounds **35** (selected *m/z* 445, 215.143), **37** (selected *m/z* 431, 231.138), and **38** (selected *m/z* 479, 215.143) and absolutely quantified by the UHPLC-MRM^{HR} method. Under the optimized conditions, several kinds of *T. farfara* extracts were quantified. The yield of extraction and contents of 8 sesquiterpenoids were described in **Table 8** and **Table 9**. All the sesquiterpenoids were more abundant in buds than stems, and *n*-hexane was a preferable solvent to extract these classes of compounds compared to ethanol. The present study is the first report on the quantitative composition of oplopane and bisabolane sesquiterpenoids in *T. farfara* by UHPLC-MS/MS.

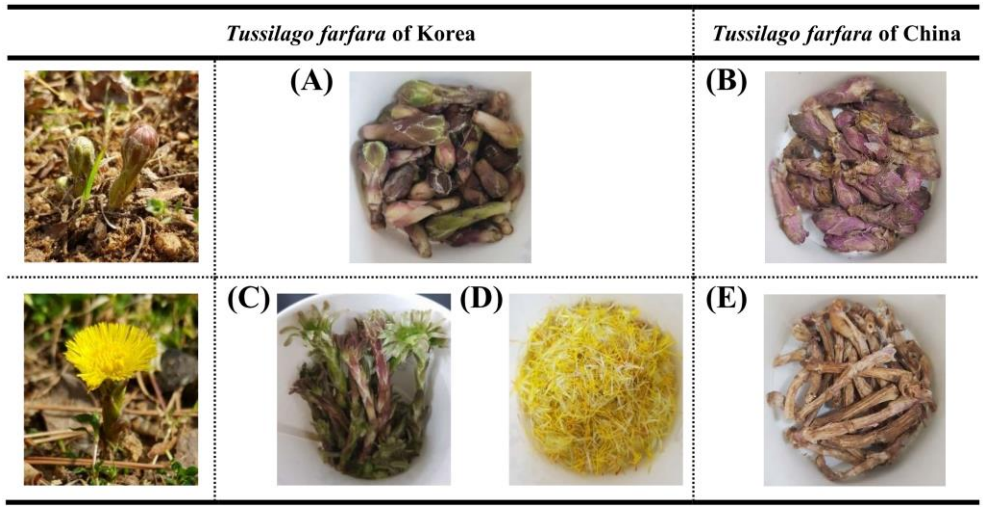

Figure 43. Herbal materials for quantification study

The dried buds (A, B), stems (C, E), and flowers (D) of *Tussilago farfara* L. Korean one was obtained from herbary of Seoul National University (A, C, and D), and Chinese one was purchased from domestic market (Omniherb, B and E).

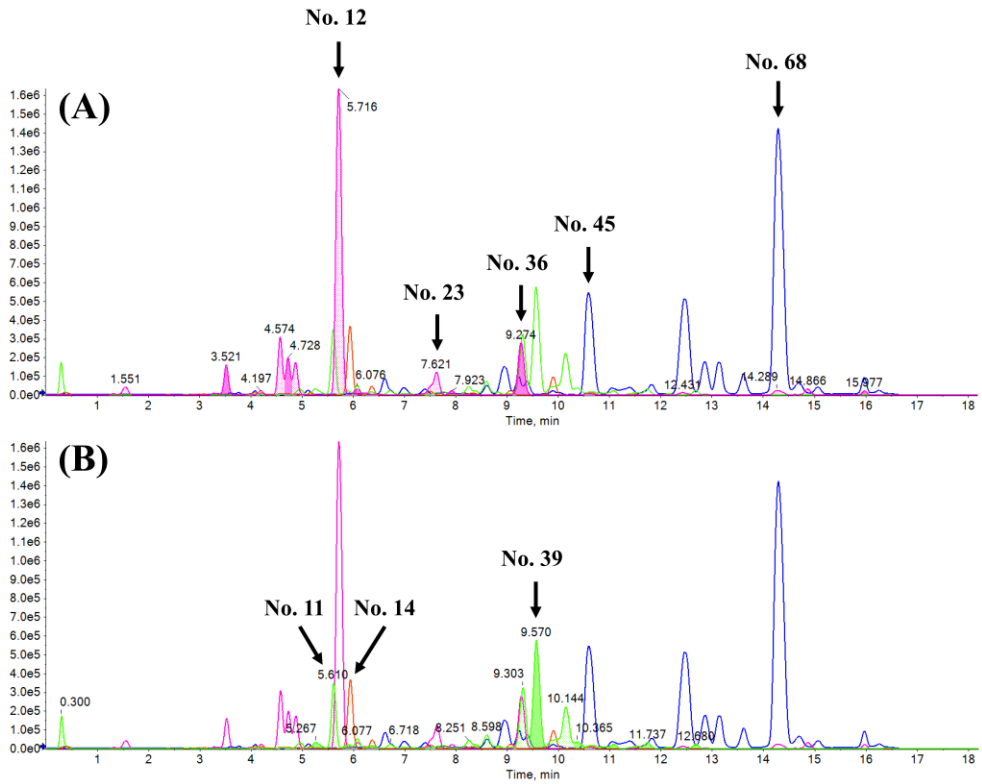

Figure 44. Dereplication of 8 sesquiterpenoids by UHPLC-MRM^{HR}

Diagnostic ions and the corresponding precursor ions were selected for the absolute quantification of (A) oplopane and (B) bisabolane sesquiterpenoids in Farfarae Flos.

Table 6. Quantitative parameters for sesquiterpenoids by UHPLC-MRM^{HR}

Analyte	Standard curve	Linear correalation (R^2)	Linear range (ppb)	LOD (pg)	LOQ (pg)
No. 11	y = 56.696x + 4.487	0.998	31.25 - 8000	7.4	24.7
No. 12	y = 6.440x + 37.898	0.997	31.25 - 8000	15.8	52.7
No. 14	y = 32.372x + 32.886	0.998	31.25 - 8000	8.0	26.7
No. 23	y = 11.504x + 34.499	0.998	31.25 - 8000	15.4	51.3
No. 36	y = 8.721x + 28.836	0.997	31.25 - 8000	14.6	48.7
No. 39	y = 16.860x + 1.054	0.997	31.25 - 8000	8.8	29.3
No. 45	y = 3.874x + 4.610	0.998	62.5 - 8000	28.6	95.3
No. 68	y = 1.658x + 2.804	0.998	62.5 - 8000	31.6	105.3

Table 7. Intra-day and inter-day precision of UHPLC-MRM^{HR}

Analyte	Rt	Intra-day variation (n = 5)		Inter-day variation (n = 3)	
		RSD for Rt (%)	RSD for P_A (%)	RSD for Rt (%)	RSD for P_A (%)
No. 11	5.64	0.08	2.16	0.06	1.11
No. 12	5.75	0.10	2.39	0.08	2.87
No. 14	5.97	0.07	2.03	0.10	3.64
No. 23	7.67	0.07	3.37	0.08	1.98
No. 36	9.33	0.08	2.96	0.07	2.23
No. 39	9.62	0.05	3.75	0.05	3.37
No. 45	10.67	0.07	3.85	0.06	4.16
No. 68	14.38	0.06	3.33	0.07	2.74

Table 8. Extraction yield of herbal materials

Sample	Bud_Korea		Flower_Korea		Stem_Korea		Bud_China		Stem_China	
Solvent	EtOH	*n*-Hex	EtOH	*n*-Hex	EtOH	*n*-Hex	EtOH	*n*-Hex	EtOH	*n*-Hex
Yield (%)	7.37	7.62	7.87	8.12	10.83	7.28	7.80	8.96	9.07	8.68

Table 9. Contents of 8 sesquiterpenoids in *Tussilago farfara* by UHPLC-MRM^{HR}

Sample		Content of analytes (mg/g)							
		No. 11	**No. 12**	**No. 14**	**No. 23**	**No. 36**	**No. 39**	**No. 45**	**No.68**
Bud_China	EtOH	**0.14** ± 0.01	**1.52** ± 0.03	**0.46** ± 0.02	**0.03** ± 0.005	**0.06** ± 0.007	**1.12** ± 0.03	**4.65** ± 0.08	**5.33** ± 0.09
	n-Hex	**0.24** ± 0.02	**1.94** ± 0.05	**0.60** ± 0.03	**0.04** ± 0.008	**0.11** ± 0.009	**1.51** ± 0.04	**5.52** ± 0.10	**6.88** ± 0.10
Stem_China	EtOH	**0.04** ± 0.01	**0.48** ± 0.01	**0.17** ± 0.01	**0.01** ± 0.005	**0.02** ± 0.004	**0.40** ± 0.01	**2.35** ± 0.05	**1.94** ± 0.05
	n-Hex	**0.05** ± 0.01	**0.69** ± 0.02	**0.22** ± 0.01	**0.02** ± 0.003	**0.05** ± 0.004	**0.50** ± 0.02	**2.69** ± 0.05	**2.66** ± 0.07
Bud_Korea	EtOH	ND	ND	**0.08** ± 0.01	ND	ND	**0.36** ± 0.01	**0.01** ± 0.003	ND
	n-Hex	ND	ND	**0.11** ± 0.02	ND	ND	**0.44** ± 0.04	**0.01** ± 0.002	ND
Flower_Korea	EtOH	ND	ND	ND	ND	ND	**0.01** ± 0.003	ND	ND
	n-Hex	ND	ND	ND	ND	ND	**0.01** ± 0.002	ND	ND
Stem_Korea	EtOH	ND	ND	**0.12** ± 0.01	ND	ND	**0.53** ± 0.02	**0.01** ± 0.004	ND
	n-Hex	ND	ND	**0.15** ± 0.03	ND	ND	**0.67** ± 0.02	**0.01** ± 0.004	ND

2.6. Discussion

This study was designed to develop LC-MS/MS dereplicative method for oplopane and bisabolane sesquiterpenoids in Farfarae Flos. In order to characterize the structurally diverse derivatives, i) four diagnostic ions were suggested and ii) precursor ion scanning was applied to investigate parent molecular ions and their MS/MS fragmentation behaviors.

Although the QTOF-MS/MS system has been applied to the non-targeted profiling of plant secondary metabolites [43], deconvolution of the sesquiterpenoids was difficult because the in-source fragmentation of these compounds disturbed the determination of the parent molecular ions. For example, as shown in **Table 1**, the precursor ion spectra of 17 compounds (No. **9**, **10**, **11**, **12**, **19**, **23**, **26**, **28**, **32**, **36**, **37**, **39**, **44**, **53**, **60**, **69**, and **72**) shared peak at *m/z* 331. While those of **23** and **36** indicated the value of parent molecular ions, the others were of the intermediate ions. Therefore, the combination of diagnostic filtering and precursor ion scan selectively identify these compounds, even though they were highly overlapped (No. **36** and **37)**. Furthermore, the QTOF-MS/MS system could also perform the precursor ion scan with highly resolved diagnostic *m/z*, the scan period for *m/z* 250–550 was too long (30 s cycle time for 0.1 s accumulation time) to collect reliable MS/MS data.

Therefore, Precursor ion scans (*m/z* 250–550) for the diagnostic ions were conducted using a QqQ-MS/MS system. The ionization energy (DP) was fixed at 30 V and three collision energies (5, 15, 25 eV) were selected to screen all the

intermediate and parent molecular ions. While the diagnostic and intermediate molecular ions were mainly protonated ions $[M+H]^+$, the parent molecular ions were both $[M+H]^+$ and $[M+NH_4]^+$ adducts. Although the source of the ammonia is hard to know, it is a common additive for LC-MS systems [47] and this ionization tendency made the parent ion annotation easier in the precursor ion scan.

Tussilagone (No. **12**) has been a chemical marker of the Farfarae Flos and the Chinese Pharmacopoeia set the regulation for the compound, which described that the tussilagone content in the Farfarae Flos must be greater than 0.07% (w/w) [26]. Although, HPLC-PDA quantification of the oplopane sesquiterpenoids (compounds **12** and **36**) was studied [10], as shown in **Fig. 44** and **Table 5**, the compounds **11** and **14** were overlapped with tussilagone even by the UHPLC separation. Likewise, compound **36** was highly overlapped with compounds **35**, **37**, and **38**. These chemical complexities and chromatographic behaviors made it difficult and unreliable to quantify the sesquiterpenoids using UV detection. Furthermore, MS1-based quantification would not be suitable for the sesquiterpenoids because the compounds were in-source fragmented and shared the same *m/z* values. Therefore, the MRM^{HR} method based on the diagnostic and precursor ions could eliminate untargeted metabolites allowing high sensitivity and low detection limits.

3. Activity based proteome profiling: Identification of target proteins of an oplopane sesquiterpenoid in breast cancer cells

3.1. Anti-proliferation activities of Farfarae Flos

Anti-proliferation activities of various samples from Chinese and Korean Farfarae Flos were investigated on MDA-MB-231 and MCF-7 breast cancer cells. Although some nonpolar fractions obtained from both herbal materials exhibit anti-proliferation activities, fraction 9 and 11 obtained from Chinese Farfarae Flos showed more potent acitivities **(Fig. 45)**. Considering the result of MS/MS chemical profiling of Farfarae Flos, these results indicate that oplopane sesquiterpenoids seemed to exhibit potent anti-proliferation activities because these compounds were not detected in Korean Farfarae Flos **(Table 9)**. Indeed, the nonpolar oplopane sesquiterpenoids **45** and **68** showed higher activities rather than bisabolane sesquiterpenoid **(Fig. 46A)**. Furthermore, the C-14-methoxy analogue of compound **7** and **68** showed substantially reduced anti-proliferation activities **(Fig. 46B)**. This result demonstrated that the α,β-unsaturated carbonyl moiety at five-membered ring of the oplopane sesquiterpenoid exerts as its pharmacophore. Therefore, the most cytotoxic compound **68** (**ECN**) was selected to further probe synthesis for activity-based proteome profiling.

(A)

Farfarae Flos (China)

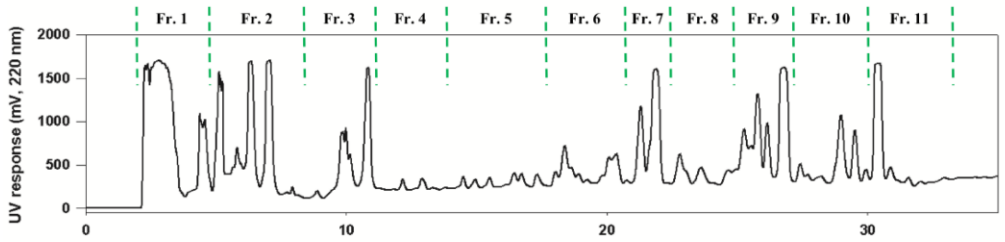

MTT assay

Sample		EtOH ext.	Fr. 1	Fr. 2	Fr. 3	Fr. 4	Fr. 5	Fr. 6	Fr. 7	Fr. 8	Fr. 9	Fr. 10	Fr. 11
MDA-MB-231	IC_{50}, μg/mL (95% CI)	**85.3** (82.1 – 88.5)	> 50	> 50	> 50	> 50	**45.5** (43.2 – 47.8)	> 50	> 50	**33.1** (30.7 – 35.5)	**9.7** (9.4 – 10.0)	**14.6** (4.3 – 5.3)	**4.8** (4.3 – 5.3)
MCF-7		**94.1** (90.2 – 98.0)	> 50	> 50	> 50	> 50	> 50	> 50	**41.4** (40.3 – 42.5)	**30.8** (29.4 – 32.2)	**9.1** (7.7 – 10.5)	**15.9** (4.3 – 5.3)	**6.5** (5.9 – 7.1)

(B)

Farfarae Flos (Korea)

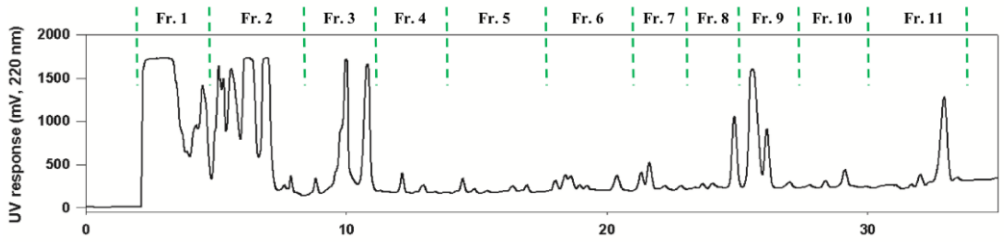

MTT assay

Sample		EtOH ext.	Fr. 1	Fr. 2	Fr. 3	Fr. 4	Fr. 5	Fr. 6	Fr. 7	Fr. 8	Fr. 9	Fr. 10	Fr. 11
MDA-MB-231	IC_{50}, μg/mL (95% CI)	**128.7** (122.0 – 135.4)	> 50	> 50	> 50	> 50	> 50	> 50	**41.7** (40.3 – 43.1)	> 50	**34.3** (33.5 – 35.1)	> 50	> 50
MCF-7		**122.8** (118.4 – 127.2)	> 50	> 50	> 50	> 50	> 50	> 50	**39.8** (38.3 – 41.3)	> 50	**36.1** (35.1 – 37.1)	> 50	> 50

Figure 45. Anti-proliferation activities of fractions from Farfarae Flos

Anti-proliferation activities of fraction from (A) Chinese and (B) Korean Farfarae Flos was measured by an MTT assay (n=3).

(A)

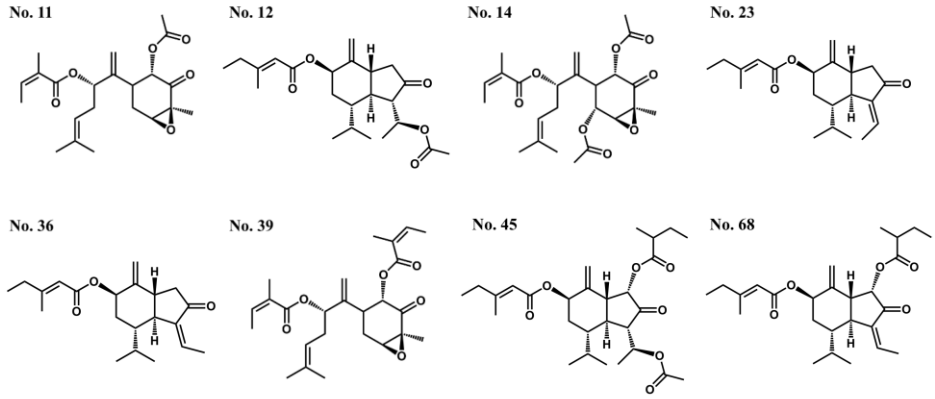

MTT assay

Sample		No. 11	No. 12	No. 14	No. 23	No. 36	No. 39	No. 45	No. 68
MDA-MB-231	IC_{50}, μM (95% CI)	**59.1** (58.0 – 60.2)	**45.8** (43.1 – 48.5)	**27.6** (26.4 – 28.8)	**34.9** (33.8 – 36.0)	**31.3** (29.3 – 33.3)	**28.7** (26.9 – 30.5)	**7.3** (6.7 – 7.9)	**7.1** (6.7 – 7.5)
MCF-7		**57.4** (54.5 – 60.3)	**44.5** (41.7 – 47.3)	**28.4** (26.6 – 30.2)	**39.7** (37.8 – 41.6)	**42.2** (41.0 – 43.4)	**26.5** (24.9 – 28.1)	**12.8** (12.1 – 13.5)	**11.9** (11.0 – 12.8)

(B)

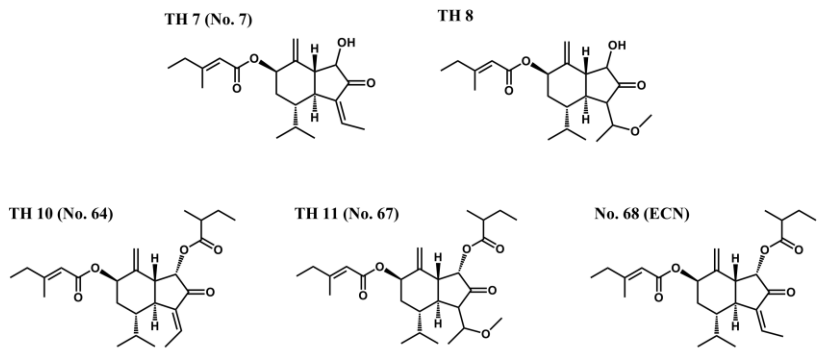

MTT assay

Sample		TH 7	TH 8	TH 10	TH 11	No. 68
MDA-MB-231	IC_{50}, μM (95% CI)	**11.3** (10.0 – 12.6)	**95.4** (93.8 – 97.0)	**13.8** (12.4 – 15.2)	**96.2** (93.8 – 98.6)	**7.5** (6.9 – 8.1)

Figure 46. Anti-proliferation activities of compounds from Farfarae Flos

Anti-proliferation activities of (A) compounds from Chinese Farfarae Flos and (B) their modified analogues was measured by an MTT assay (*n*=3).

3.2. Synthesis of ECN-based clickable probe

ECN-based clickable probe was synthesized for visualization and identification of ECN-binding proteins. ECN was designed to contain clickable azido group at the C10 position through two step reactions **(Fig. 47A)**: (1) epoxification of double bond at C8–C10 position by m-chloroperoxybenzoic acid (m-CPBA), and (2) necleophilic addition of azide to the epoxide group via $CeCl_3$-catalyzed reaction [96]. The two steps could be run on gram scales without loss of the α,β-unsaturated carbonyl moiety. The structural modification of probe was determined by comparing HSQC spectra of ECN, ECN-E, and ECN-N_3 **(Fig. 48–50)** and ^{15}N-HMBC spectrum of ECN-N3 **(Fig. 51)**. In addition, anti-proliferation activities of the synthetic products were evaluated in MDA-MB-231 and MCF-7 cells to investigate whether the chemical derivative would influence the anti-proliferative potency of ECN **(Fig. 47B)**. Upon 24-hour treatment of 8 concentrations, ECN-N_3 showed similar growth inhibitory effect with ECN, suggesting the retention of the biological activity.

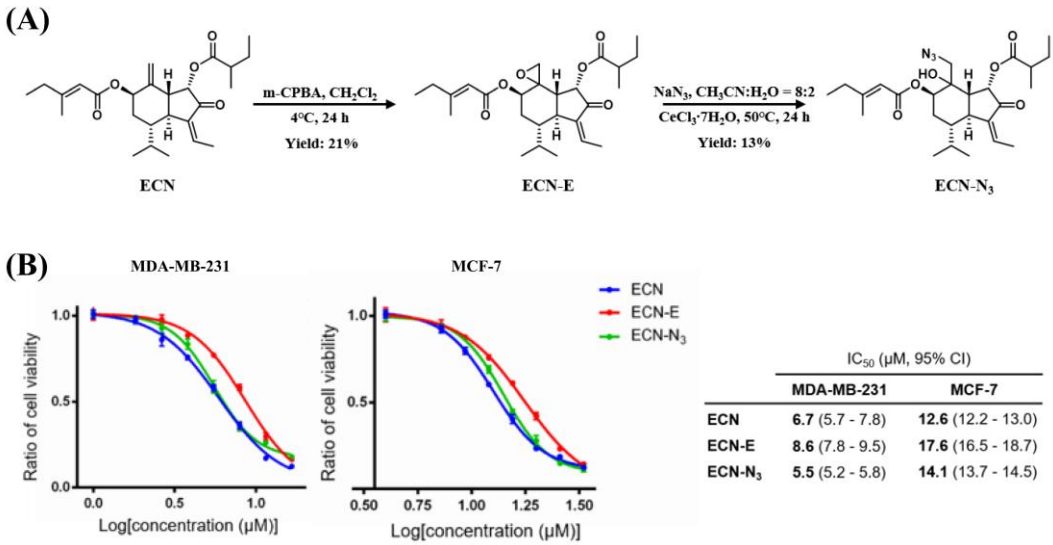

Figure 47. Synthesis of ECN-based clickable probe and anti-proliferation activity

(A) Schematic diagram of two step synthesis of ECN based clickable probe, ECN-N_3.
(B) Dose-dependent inhibition of MDA-MB-231 and MCF-7 cell proliferation by ECN, ECN-E, and ECN-N_3.

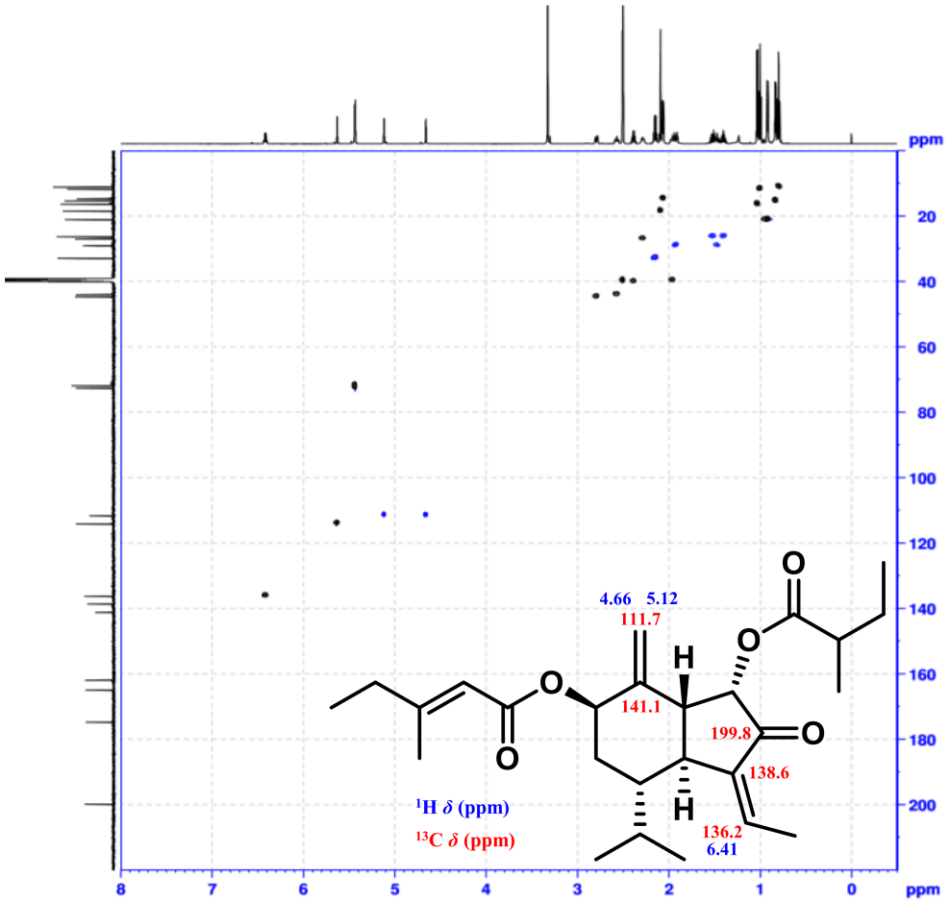

Figure 48. HSQC spectrum of ECN

(in DMSO-d_6, 500 MHz)

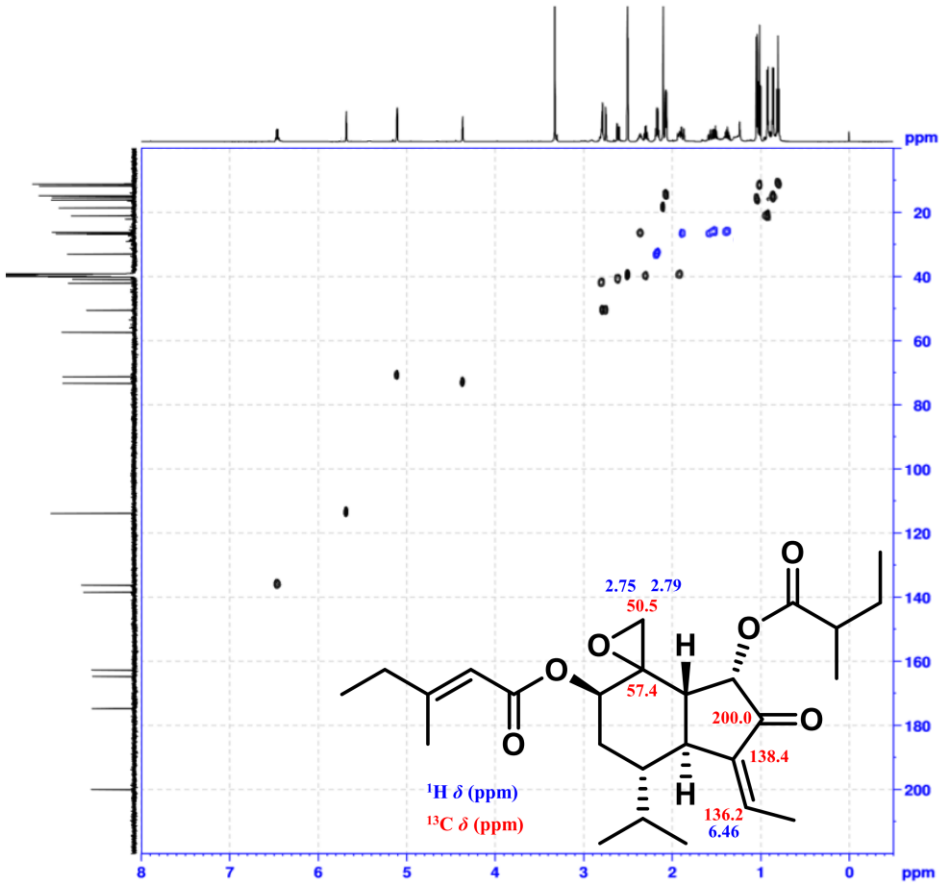

Figure 49. HSQC spectrum of ECN-E

(in DMSO-d_6, 500 MHz)

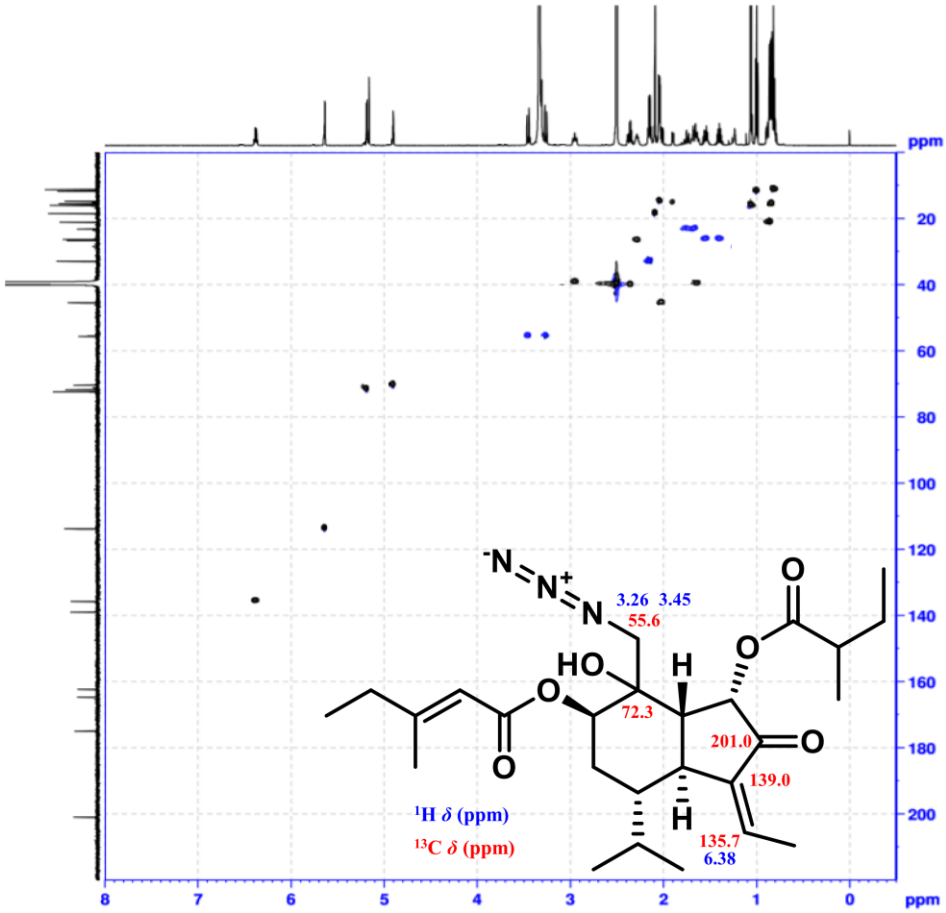

Figure 50. HSQC spectrum of ECN-N_3

(in DMSO-d_6, 500 MHz)

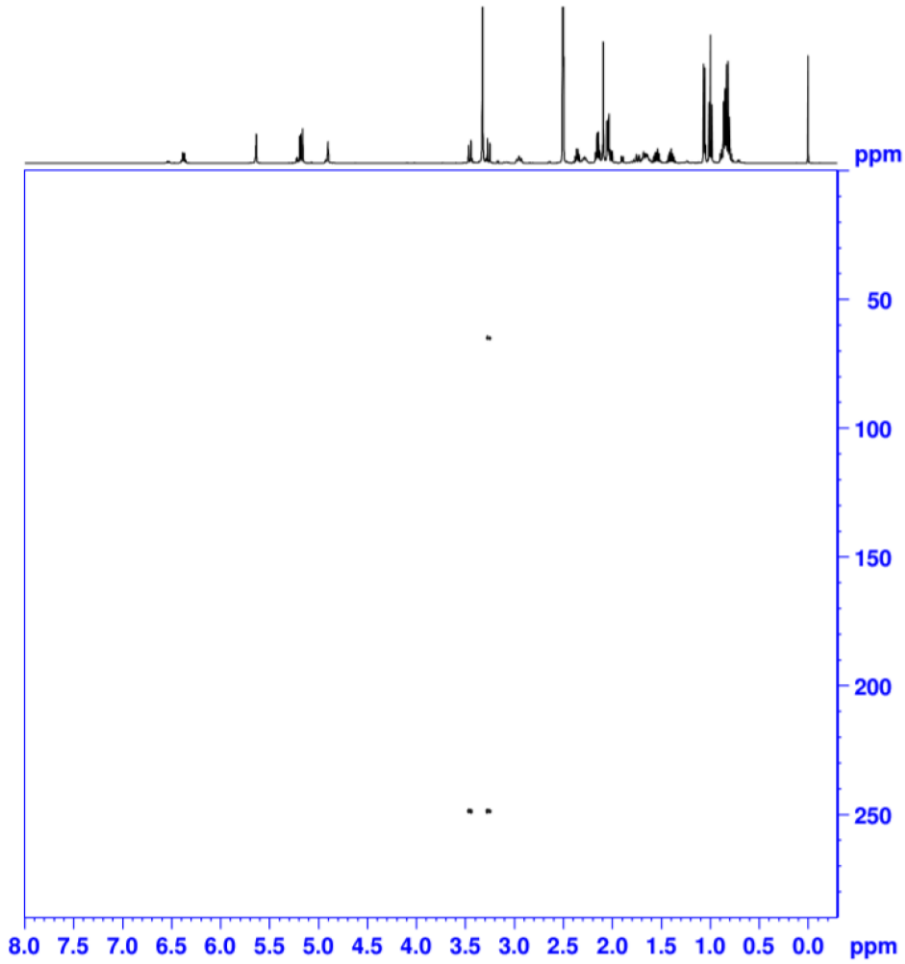

Figure 51. ^{15}N-HMBC spectrum of ECN-N_3

(in DMSO-d_6, 500 MHz)

3.3. Gel-based proteome profiling of clickable probe

Protein-interaction profile of the ECN-based probe by gel-based analysis were assessed *in situ* **(Fig. 52)**. The human breast cancer cell lines MDA-MB-231 and MCF-7 were treated with ECN-N_3 followed by cell lysis, coupling to cyanine3-alkyne via click reaction, SDS-PAGE, and visualization of probe-captured proteins by in-gel fluorescence scanning. The ECN-N_3 showed substantial concentration-dependent labeling of proteins in both cells, and treatment of excess ECN as competitive inhibitor blocked the labeling of target proteins in a concentration-dependent manner. These results indicated that the ECN-N_3 is suitable for quantitative MS-based proteomic experiments.

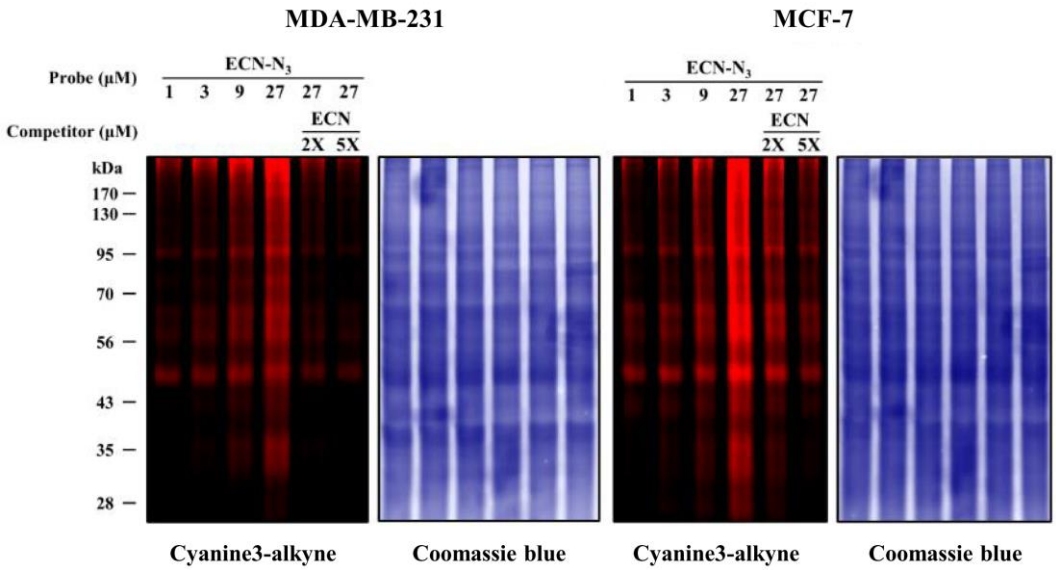

Figure 52. Gel-based profiling of ECN-N_3 labeled proteome *in situ*

Gel-based profiling of ECN-N3 labeled proteomes of MDA-MB-231 (left) and MCF-7 (right) cell lines in situ (living cells): fluorescence scanning (Cyanine 3, left) and coomassie blue staining (right), respectively.

3.4. MS-based profiling of target proteins of ECN

Potential cellular target proteins of ECN were identified using quantitative mass spectrometry (MS)-based analysis. Following the click reaction, biotin pull-down, TMT isobaric tagging, and LC-MS/MS procedures, more than 200 proteins were identified and quantified by the ECN-based probe in both MDA-MB-231 and MCF-7 cell line. A total of 26 and 32 identified proteins represented more than 3 enrichment ratio in MDA-MB-231 and MCF-7, respectively, and 17 proteins were shared across the two cell lines **(Table 10)**. Among those proteins, 14-3-3 protein zeta and peroxiredoxin-1 which showed highest positive/negative enrichment ratios were selected for the further verification studies.

Table 10. Identified target proteins of ECN in breast cancer cells

Protein	Gene	% Cov	Peptides	Ave ratio	Q-value
14-3-3 protein zeta	YWHAZ	42.0	7	5.56 ± 0.34	< 0.001
ATP synthase subunit beta	ATP5F1B	38.4	12	4.86 ± 0.26	< 0.001
Peroxiredoxin-1	PRDX1	45.2	7	4.63 ± 0.42	< 0.001
60 kDa heat shock protein	HSPD1	37.9	14	4.40 ± 0.19	< 0.001
Nucleophosmin	NPM1	32.8	6	4.12 ± 0.38	< 0.001
Profilin-1	PFN1	59.7	5	4.06 ± 0.33	< 0.001
40*S* ribosomal protein SA	RPSA	21.6	4	3.96 ± 0.41	< 0.001
Glyceraldehyde-3-phosphate dehydrogenase	GAPDH	43.8	9	3.93 ± 0.18	< 0.001
Nucleoside diphosphate kinase B	NME2	55.4	8	3.88 ± 0.33	< 0.001
Glucose-6-phosphate 1-dehydrogenase	G6PD	16.5	8	3.61 ± 0.39	< 0.001
Protein disulfide-isomerase A6	PDIA6	17.5	5	3.49 ± 0.27	< 0.001
Electron transfer flavoprotein subunit alpha, mitochondria	ETFA	19.0	4	3.35 ± 0.22	< 0.001
Cathepsin D	CTSD	44.4	6	3.30 ± 0.18	< 0.001
Actin, cytoplasmic 1	ACTB	48.9	12	3.17 ± 0.40	< 0.001
Heat shock cognate 71 kDa protein	HSPA8	21.4	10	3.10 ± 0.27	< 0.001
Peroxiredoxin-2	PRDX2	27.3	5	3.10 ± 0.34	< 0.001
ATP synthase subunit alpha	ATP5F1A	42.9	16	3.04 ± 0.23	< 0.001

Identified target proteins which is shared across in MDA-MB-231 and MCF-7 cells. The identification parameters (% coverage and number of identified peptides) and enrichment ratio were described those of MCF-7 cell line.

3.5. Thermodynamics and binding sites of ECN for target proteins

Among the identified target proteins, recombinant 14-3-3 protein zeta and peroxiredoxin-1 were further verified by isothermic calorimetry and their alkylation sites. The binding isotherms were analysed by fitting the data to a binding model to yield the binding constant (K_a), and the binding parameters, (n and ΔH). The results of the data are shown in **Fig. 53**. Furthermore, LC-MS/MS analyse of ECN-treated recombinant 14-3-3 protein zeta and peroxiredoxin-1 were conducted to determine the modification sites of ECN. Taking the interaction between α,β-unsaturated carbonyl moiety of ECN and cysteine residues of proteins into account, peptides containing Cys25, Cys94 of 14-3-3 protein zeta **(Fig. 54)** and Cys83 of peroxiredoxin-1 **(Fig. 55)** were significantly reduced by ECN in a concentration-dependent manner.

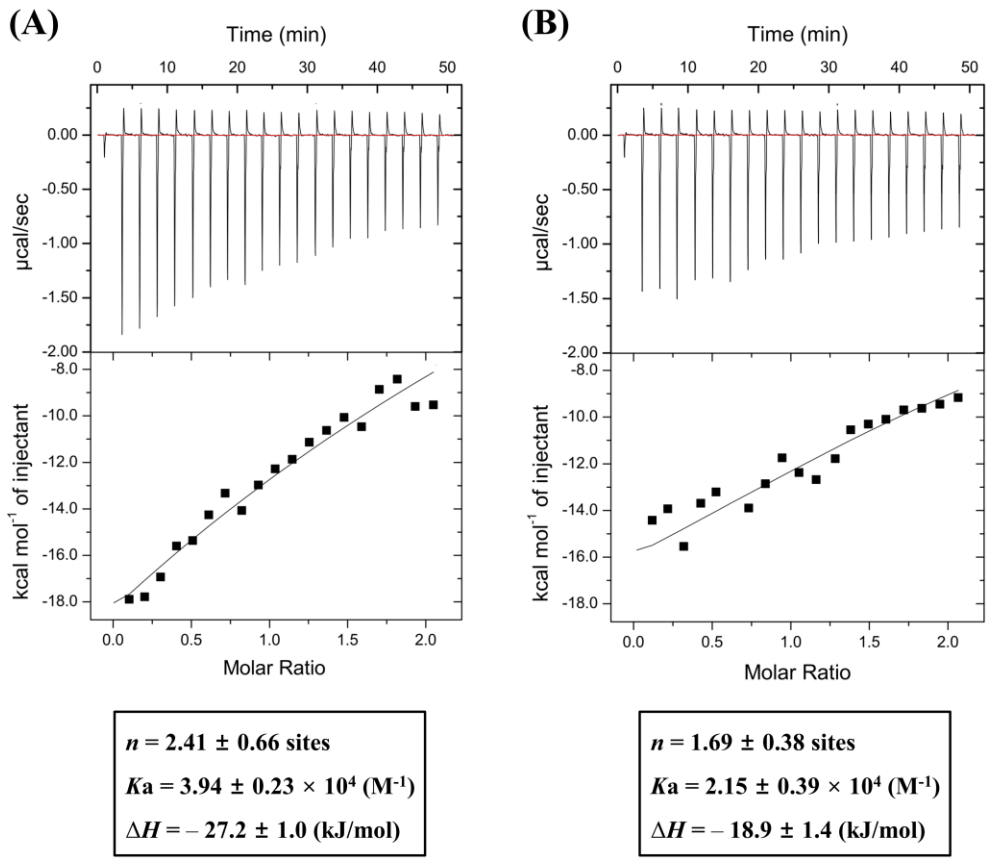

Figure 53. Thermograms and parameters for interaction of ECN with identified target proteins

Thermodynamics for the interaction of ECN with (A) 14-3-3 protein zeta and (B) peroxiredoxin-1 were investigated by isothermal titration calorimeter.

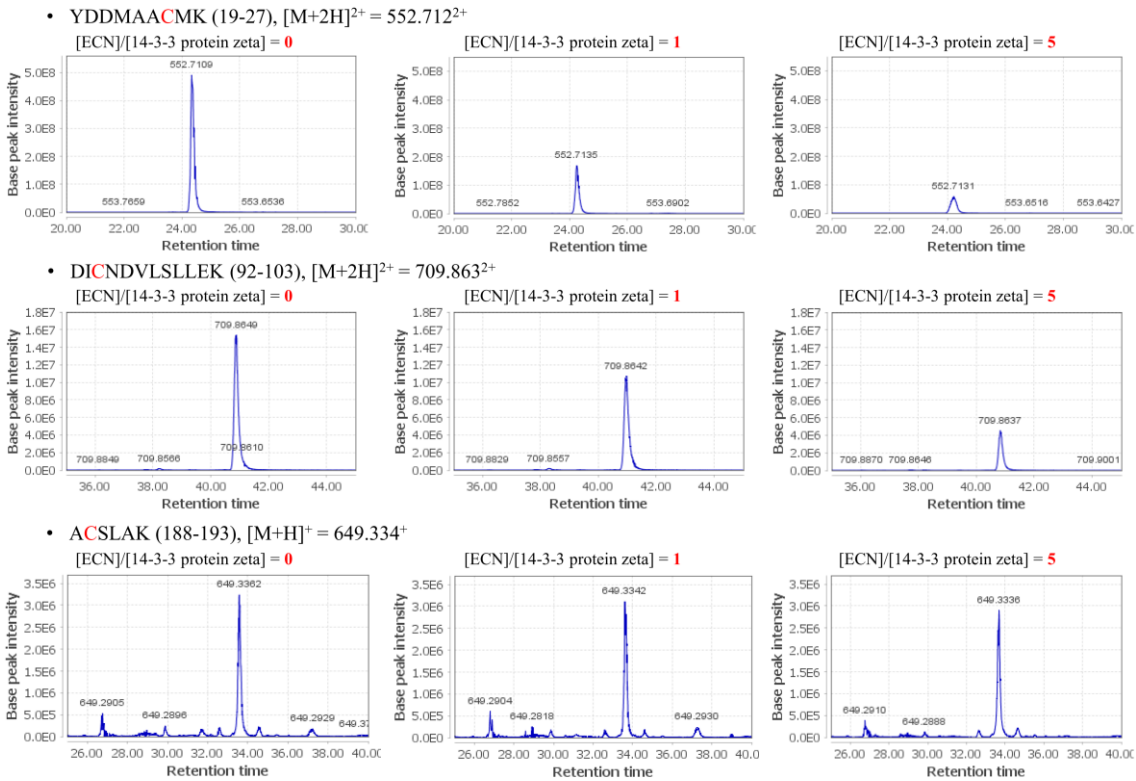

Figure 54. Alkylation of cysteine residues in 14-3-3 protein zeta by ECN

Identification of ECN binding sites in recombinant 14-3-3 protein zeta by LC-MS/MS. Extracted ion chromatogram at *m/z* 552.712 $[M+2H]^{2+}$, 709.863 $[M+2H]^{2+}$, 649.334 $[M+H]^{+}$, which correspond to the amino acid sequence of 14-3-3 protein zeta.

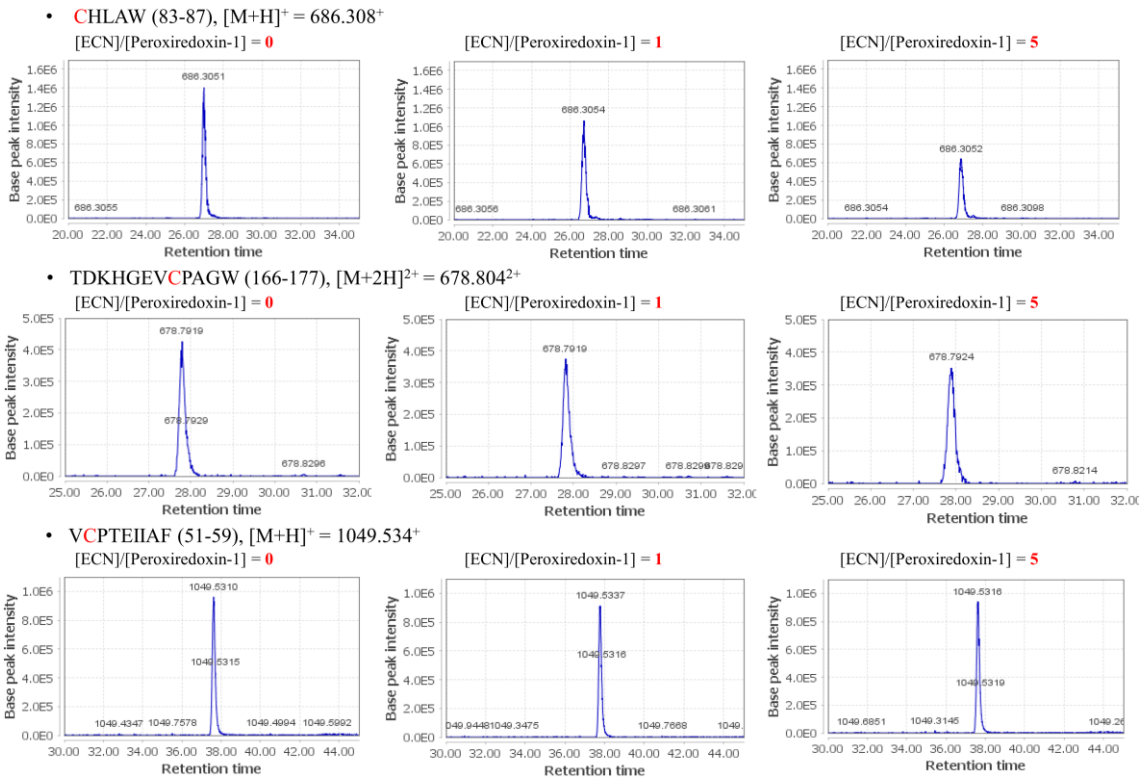

Figure 55. Alkylation of cysteine residues in peroxiredoxin-1 by ECN

Identification of ECN binding sites in recombinant peroxiredoxin-1 by LC-MS/MS. Extracted ion chromatogram at *m/z* 686.308 $[M+H]^+$, 678.804 $[M+2H]^{2+}$, 1049.534 $[M+H]^+$, which correspond to the amino acid sequence of peroxiredoxin-1.

3.6. Discussion

The present study was designed to identify target proteins of ECN, which showed anti-proliferation activity in human breast cancer cells, using a combination of activity-based profiling and isobaric labelling (TMT)-based quantitative mass spectrometry. One of the structural characteristics of ECN is presence of the α,β-unsaturated carbonyl moiety, which can act as a Michael reaction acceptor, modifying the cysteine thiols of protein [97, 98]. Indeed, the C-14-methoxy analogue of ECN showed reduced anti-proliferation activity **(Fig. 46)**. It has been suggested that the modification of cysteine thiols can largely affect the dimensional structure of many redox sensitive proteins and their functions [99–102].

In order to investigate the molecular interactions of ECN that might contribute to the anti-proliferation activity, ECN-based clickable probe containing azido groups was synthesized. Although the moderate potency (μM level) of ECN was not powerful in the pharmacological perspective, it emphasized an advantage of the chemical proteomic methods employing activity-based clickable probe which can capture even lower affinity interaction of small molecule−protein binding events *in situ*. Under the optimized click reaction and quantitative MS-based proteome profiling, more than 200 proteins were identified and quantified by the ECN-based probe in both MDA-MB-231 and MCF-7 cell lines. Among those identified target proteins, 14-3-3 protein zeta and peroxiredoxin-1 which showed highest positive/negative enrichment ratios were verified by isothermic calorimetry

and cysteine modification sites using their recombinant proteins. Many previous studies have established a strong relationship between 14-3-3 proteins and various cancer types [103–110], but cysteine modification-related functions were elusive. Peroxiredoxin-1 also plays an important role in cancer development and inflammation [111–114]. It is a dual functional protein which acts as both an antioxidant enzyme and a molecular chaperone. [115–116] Peroxiredoxin-1 have been reported to interact with essential siganlling molecules such as p53 [117], NF-kB [118], and TLR4 [119]. Recently, triptolide was reported as a possible inhibitor chaperone activity of peroxiredoxin-1 by binding to Cys83 and Cys173 residue [120–122]. Therefore, the interaction of ECN with Cys83 could be applied in the same manner.

Although these results could not confirm the role of ECN in breast cancer cells, it is possible that functional perturbation of multiple target proteins contributes to ECN-mediated anti-proliferation activity. Furthermore, the interaction with 14-3-3 protein zeta and peroxiredoxin-1 could suggest the molecular mechanism of ECN in anti-proliferative and anti-inflammatory effects, leading to further studies aimed at determining how these ECN-protein interactions may contribute to understand the biological activities. One of possible approaches is genetic knockout of individual proteins in various ECN-sensitive cell types to evaluate the role of the proteins in the biological activities of ECN.

IV. CONCLUSION

In the present study, preparative separation, chemical profiling, and activity-based proteome profiling of sesquiterpenoids from Farfarae Flos were performed.

Firstly, a novel fractionation and purification method of counter-current chromatography (CCC), called direct and continuous injection (DCI) mode, was developed to fractionate and preparatively separate sesquiterpenoids from Farfarae Flos. Since the extraction solution was used as a mobile phase in this method, solvent consumption could be greatly reduced. Moreover, the fractionation efficiency of CCC-DCI was much higher than those of conventional fractionations: solvent partitioning and open column chromatography. The developed method demonstrates that CCC is a useful technique for enriching target components from natural products.

Secondly, a liquid chromatography-electrospray ionization tandem mass spectrometry (LC-ESI-MS/MS)-based dereplicative method was developed to identify and quantify oplopane- and bisabolane-type sesquiterpenoids of the Farfarae Flos. Proposed diagnostic ions and two sequential MS/MS scan modes were successfully applied to characterize common skeletons, parent molecular ions, and their fragmentation patterns. Under the optimized UHPLC-MS/MS method, a total of 74 sesquiterpenoids were identified and relatively quantified. Consequently, the developed LC-MS/MS-based dereplicative method highlighted the chemical composition of the Farfarae Flos and could be applied to quality control of the herbal medicine.

Finally, target proteins of ECN in human breast cancer cells were identified by chemical proteomics methodology. ECN showed potent anti-proliferation activity in MDA-MB-231 and MCF-7 human breast cancer cells. The ECN-based clickable probe successfully capture the potential cellular target proteins, and a total of 17 proteins were proposed as direct target proteins of ECN. Furthermore, ECN interact with Cys25, Cys94 of 14-3-3 protein zeta and Cys83 of peroxiredoxin-1 based on its α,β-unsaturated carbonyl moiety. Although these results could not confirm the role of ECN in the breast cancer cells, the suggestion of multiple target proteins could contribute to understand the ECN-mediated anti-proliferative and anti-inflammatory effects.

REFERENCES

[1] Judzentiene, A; Budiene, J. Volatile Oils of Flowers and Stems of *Tussilago farfara* L. from Lithuania. *J Essent Oil Bear Pl* **14** (2011) 413–416.

[2] Barceloux, DG. Coltsfoot (*Tussilago farfara* L.). *Medical Toxicology of Natural Substances: Foods, Fungi, Medicinal Herbs, Plants, and Venomous Animals* (2008) 446–448.

[3] Kim, M-R; Lee, JY; Lee, H-H; Aryal, DK; Kim, YG; Kim, SK; Woo, E-R; Kang, KW. Antioxidative effects of quercetin-glycosides isolated from the flower buds of *Tussilago farfara* L. *Food Chem Toxicol* **44** (2006) 1299-1307.

[4] Gao, H; Huang, YN; Gao, B; Xu, PY; Inagaki, C; Kawabata, J. α-Glucosidase inhibitory effect by the flower buds of *Tussilago farfara* L. *Food Chem* **106** (2008) 1195–1201.

[5] Zhao, J; Evangelopoulos, D; Bhakta, S; Gray, Al; Seidel, V. Antitubercular activity of *Arctium lappa* and *Tussilago farfara* extracts and constituents. *J Ethnopharmacol* **155** (2014) 796–800.

[6] Li, Z-Y; Zhi, H-J; Xue, S-Y; Sun, H-F; Zhang, F-S; Jia, J-P; Xing, J; Zhang, L-Z; Qin, X-M. Metabolomic profiling of the flower bud and rachis of *Tussilago farfara* with antitussive and expectorant effects on mice. *J Ethnopharmacol* **140** (2012) 83-90.

[7] Li, Z-Y; Zhi, H-J; Zhang, F-S; Sun, H-F; Zhang, L-Z; Jia, J-P; Xing, J; Qin, X-M. Metabolomic profiling of the antitussive and expectorant plant *Tussilago farfara* L. by nuclear magnetic resonance spectroscopy and multivariate data

analysis. *J Pharm Biomed Anal* **75** (2013) 158–164.

[8] Wang, D; Fang, L; Wang, X; Qiu, J; Huang, L. Preparative separation and purification of sesquiterpenoids from *Tussilago farfara* L. by high-speed counter-current chromatography. *Quim. Nova* **34** (2011) 804-807.

[9] Jiang, Z; Liu, F; Goh, JJL; Yu, L; Li, SFY; Ong, ES; Ong, CN. Determination of senkirkine and senecionine in *Tussilago farfara* using microwave-assisted extraction and pressurized hot water extraction with liquid chromatography tandem mass spectrometry, *Talanta* **79** (2009) 539–546.

[10] Seo, UM; Zhao BT; Kim WI; Seo EK; Lee JH; Min BS; Shin BS; Son JK; Woo MH. Quality evaluation and pattern recognition analyses of bioactive marker compounds from Farfarae Flos using HPLC/PDA. *Chem Pharm Bull* **63** (2015) 546–553.

[11] Uysal, S; Senkardes, I; Mollica, A; Zengin, G; Bulut, G; Dogan, A; Glamoclija, J; Sokovic, M; Lobine, D; Mahomoodally, FM. Biologically active compounds from two members of the Asteraceae family: Tragopogon dubius Scop. and *Tussilago farfara* L. *J Biomol Struct Dyn* (2018) 1–13.

[12] Hwangbo, C; Lee, HS; Park, J; Choe, J; Lee, JH. The anti-inflammatory effect of tussilagone, from *Tussilago farfara*, is mediated by the induction of heme oxygenase-1 in murine macrophages. *Int Immunopharmacol* **9** (2009) 1578–1584.

[13] Lee, J; Kang, U; Seo, EK; Kim, YS. Heme oxygenase-1-mediated anti-inflammatory effects of tussilagonone on macrophages and 12-*O*-tetradecanoyl phorbol-13-acetate-induced skin inflammation in mice. *Int Immunopharmacol* **34** (2016) 155–164.

[14] Li, H; Lee, HJ; Ahn, YH; Kwon, HJ; Jang, C-Y; Kim, W-Y; Ryu, J-H. Tussilagone suppresse colon cancer cell proliferation by promoting the degradation of β-catenin. *Biochem Biophys Res Commun* **443** (2014) 132–137.

[15] Lim, HJ; Dong, GZ; Lee, HJ; Ryu, JH. In vitro neuroprotective activity of sesquiterpenoids from the flower buds of *Tussilago farfara*. *J Enzyme Inhib Med Chem* **30** (2015) 852-856.

[16] Lee, J; Song, K; Huh, E; Oh, MS; Kim, YS. Neuroprotection against 6-OHDA toxicity in PC12 cells and mice through the Nrf2 pathway by a sesquiterpenoid from *Tussilago farfara*. *Redox Biol* **18** (2018) 6–15.

[17] Kikuchi, M; Suzuki, N. Studies on the constituents of *Tussilago farfara* L. II. Structure of new sesquiterpenoids isolated from the flower buds. *Chem Pharm Bull* **40**(10) (1992) 2753–2755.

[18] Ryu, J-H; Jeong, YS; Sohn, DH. A new bisabolane epoxide from *Tussilago farfara*, and inhibition of nitric oxide synthesis in LPS-activated macrophages, *J Nat Prod* **62** (1999) 1437–1438.

[19] Yaoita, Y; Kamazawa, H; Kikuchi, M. Structure of new oplopane-type sesquiterpenoids from the flower buds of *Tussilago farfara* L. *Chem Pharm Bull* **47**(5) (1999) 705–707.

[20] Yaoita, Y; Suzuki, N; Kikuchi, M. Structures of new sesquiterpenoids from Farfarae Flos. *Chem Pharm Bull* **49**(5) (2001) 645–648.

[21] Park, HR; Yoo, MY; Seo, JH; Kim, IS; Kim, NY; Kang, JY; Cui, L; Lee, C-S; Lee, C-H; Lee, HS. Sesquiterpenoids isolated from the flower buds of *Tussilago*

farfara L. inhibit diacylglycerol acyltransferase. *J Agric Food Chem* **56** (2008) 10493–10497.

[22] Liu, L-L; Yang, J-L; Shi, Y-P. Sesquiterpenoids and other constituents from the flower buds of *Tussilago farfara*. *J Asian Nat Prod Res* **13**(10) (2011) 920–929.

[23] Li, W; Huang, X; Yang, X-W. New sesquiterpenoids from the dired flower buds of *Tussilago farfara* and their inhibition on NO production in LPS-induced RAW264.7 cells. *Fitoterapia* **83** (2012) 318–322.

[24] Jang, H; Lee, JW; Lee, C; Jin, Q; Choi, JY; Lee, D; Han, SB; Kim, Y; Hong, JT; Lee, MK; Hwang, BY. Sesquiterpenoids from *Tussilago farfara* inhibit LPS-induced nitric oxide production in macrophage RAW264.7 cells. *Arch Pharm Res* **39** (2016) 127–132.

[25] Xu, J; Sun, X; Kang, J; Liu, F; Wang, P; Ma, J; Zhou, H; Jin, D-Q; Ohizumi, Y; Lee, D; Bartlam, M; Guo, Y. Chemical and biological profiles of Tussilago farfara: Structures, nitric oxide inhibitory activities, and interaction with iNOS protein. *J Funct Foods* **32** (2017) 37–45.

[26] Committee for the Pharmacopoeia of People's Republic of China, 2010. Pharmacopoeia of People's Republic of China, Part 1. *Chemical Industry Publishing House* (2010) pp. 312.

[27] Ito, Y. Golden rules and pitfalls in selecting optimum conditions for high-speed counter-current chromatography. *J. Chromatogr. A* **1065** (2005) 145–168.

[28] Ito, Y; Bowman, RL. Countercurrent chromatography: Liquid-liquid partition chromatography without solid support. *J Chromatogr Sci* **8** (1970) 315-323.

[29] Pauli, GF; Pro, SM; Friesen, JB. Countercurrent separation of natural products. *J Nat Prod* **71** (2008) 1489–1508.

[30] McAlpine, JB; Friesen, JB; Pauli, GF. Separation of natural products by countercurrent chromatography. *Methods Mol Biol* **864** (2012) 221-254.

[31] Berthod, A; Maryutina T; Spivakov, B; Shpigun, O; Sutherland IA. Countercurrent chromatography in analytical chemistry (IUPAC technical report). *Pure Appl Chem* **81** (2009) 355-387.

[32] Liu, M; Tao, L; Chau, SL; Wu, R; Zhang, H; Yang, Y; Yang, D; Bian, Z; Lu, A; Han, Q; Xu, H. Folding fan mode counter-current chromatography offers fast blind screening for drug discovery. Case study: Finding anti-enterovirus 71 agents from *Anemarrhena asphodeloides*. *J Chromatogr A* **1368** (2014) 116–124.

[33] Lee, KJ; Xu, M-Y; Shehzad, O; Seo, EK; Kim, YS. Separation of triterpenoid saponins from the root of *Bupleurum falcatum* by counter current chromatography: The relationship between the partition coefficients and solvent system composition. *J Sep Sci* **37** (2014) 3587-3594.

[34] Lin J-M; Liu L-B; Liu Y. Determination of pesticide residues in fruits and vegetables by using GC/MS and LC/MS. *Handbook of Pesticides, CRC Press* (2009) pp. 497-523.

[35] Wolfender, J-L; Marti, G; Thomas, A; Bertrand, S. Current approaches and challenges for the metabolite profiling of complex natural extracts. *J Chromatogr A* **1382** (2015) 136–164.

[36] Cai, T; Guo, Z-Q; Xu, X-Y; Wu, Z-J. Recent (2000-2015) developments in the

analysis of minor unknown natural products based on characteristic fragment information using LC-MS. *Mass Spectrom Rev* **37** (2018) 202–216.

[37] Kind, T; Tsugawa, H; Cajka, T; Ma, Y; Lai, Z; Mehta, SS; Wohlgemuth, G; Barupal, DK; Showalter, MR; Arita, M; Fiehn, O. Identification of small molecules using accurate mass MS/MS search. *Mass Spectrom Rev* **37** (2018) 513–532.

[38] Domon, B; Aebersold R. Mass spectrometry and protein analysis. Science **312** (2006) 212-217.

[39] Lv, C; Chen, L; Fu, P; Yang, N; Liu, Q; Xu, Y; Sun, Q; Li, R; Zhan, C; Zhang, W; Liu, R. Simultaneous quantification of 11 active constituents in Shexiang Baoxin Pill by ultraperformance convergence chromatography combined with tandem mass spectrometry. *J Chromatogr B* **1052** (2017) 135–141.

[40] Nothias-Scaglia, L-F; Schmitz-Afonso, I; Renucci, F; Roussi, F; Touboul, D; Costa, J; Litaudon, M; Paolini, J. Insights on profiling of phorbol, deoxyphorbol, ingenol and jatrophane diterpene esters by high performance liquid chromatography coupled to multiple stage mass spectrometry. *J Chromatogr A* **1422** (2015) 128–139.

[41] Porfirio, S; Gomes da Silva, MDR; Peixe, A; Cabrita, MJ; Azadi, P. Current analytical methods for plant auxin quantification – A review. *Anal Chim Acta* **902** (2016) 8–21.

[42] Hoffmann, T; Krug, D; Huttel, S; Muller, R. Improving natural products identification through targeted LC-MS/MS in an untargeted secondary metabolomics workflow. *Anal Chem* **86** (2014) 10780–10788.

[43] Heiling, S; Khanal, S; Barsch, A; Zurek, G; Baldwin, IT; Gaquerel, E. Using the knowns to discover the unknowns: MS-based dereplication uncovers structural diversity in 17-hydroxygeranyllinalool diterpene glycoside production in the Solanaceae. *Plant J* **85** (2016) 561–577.

[44] Shi, X-J; Yang W-Z; Qiu, S; Yao, C-L; Shen, Y; Pan, H-Q; Bi, Q-R; Yang, M; Wu, W-Y; Guo, D-A. An in-source multiple collision-neutral loss filtering based nontargeted metabolomics approach for the comprehensive analysis of malonyl-ginsenosides from *Panax ginseng*, *P. quinquefolius*, and *P. notoginseng*. *Anal Chim Acta* **952** (2017) 59–70.

[45] Armah, FA; Amponsah, IK; Mensah, AY; Dickson, RA; Steenkamp, PA; Madala, NE; Adokoh, CK. Leishmanicidal activity of the root bark of *Erythrophleum Ivorense* (Fabaceae) and identification of some of its compounds by ultra-performance liquid chromatography quadrupole time of flight mass spectrometry (UPLC-QTOF-MS/MS). *J Ethnopharmacol* **211** (2018) 207–216.

[46] Evans, AM; Dehaven, CD; Barrett, T; Mitchell, M; Milgram, E. Integrated, nontargeted ultrahigh performance liquid chromatography/electrospray ionization tandem mass spectrometry platform for the identification and relative quantification of the small-molecule complement of biological systems. *Anal Chem* **81** (2009) 6656–6667.

[47] Weissberg, A; Dagan, S. Interpretation of ESI(+)-MS-MS spectra-Towards the identification of “unknowns”. *Int J Mass Spectrom* **299** (2011) 158–168.

[48] Zhang, H; Zheng, D; Li, H-H; Wang, H; Tan, H-S; Xu, H-X. Diagnostic filtering to screen polycyclic polyprenylated acylphloroglucinols from *Garcinia*

oblongifolia by ultrahigh performance liquid chromatography coupled with ion mobility quadrupole time-of-flight mass spectrometry. *Anal Chim Acta* **912** (2016) 85–96.

[49] Allard, P-M; Peresse, T; Bisson, J; Gindro, K; Marcourt, L; Pham, VC; Roussi, F; Litaudon, M; Wolfender, J-L. Integration of molecular networking and *in-silico* MS/MS fragmentation for natural products dereplication. *Anal Chem* **88** (2016) 3317–3323.

[50] Newman, DJ; Cragg, GM. Natural products as sources of new drugs over the 30 years from 1981 to 2010. *J Nat Prod* **75** (2012) 311–335.

[51] Rix, U; Superti-Furga, G. Target profiling of small molecules by chemical proteomics. *Nat Chem Biol* **5**(9) (2009) 616–624.

[52] Wright, MH; Tao, Y; Drechsel, J; Krysiak, J; Chamni, S; Weigert-Munoz, A; Harvey, NL; Romo, D; Sieber, SA. Quantitative chemoproteomic profiling reveals multiple target interactions of spongiolactone derivatives in leukemia cells. *Chem Commun* **53** (2017) 12818–12821.

[53] Ctortecka, C; Palve, V; Kuenzi, BM; Fang, B; Sumi, NJ; Izumi, V; Novakova, S; Kinose, F; Rix, LLR; Haura, EB; Koomen, JM; Rix, U. Functional proteomics and deep network interrogation reveal a complex mechanism of action of midostaurin in lung cancer cells. *Mol Cell Proteom* **17** (2018) 2434–2447.

[54] Shi, H; Zhang, C-J; Chen, GYJ; Yao, SQ. Cell-based proteome profiling of potential dasatinib targets by use of affinity-based probes. *J Am Chem Soc* **134** (2012) 3001–3014.

[55] Parker, CG; Kuttruff, CA; Galmozzi, A; Jørgensen, L; Yeh, C-H; Hermanson, DJ; Wang, Y; Artola, M; McKerrall, SJ; Josyln, CM; Nørremark, B; Dünstl, G; Felding, J; Saez, E; Baran, PS; Cravatt, BF. Chemical proteomics identifies SLC25A20 as a functional target of the ingenol class of actinic keratosis drugs. *ACS Cent Sci* **3** (2017) 1276–1285.

[56] Zhou, Y; Di, Z; Li, X; Shan, Y; Li, W; Zhang, H; Xiao, Y. Chemical proteomics reveal CD147 as a functional target of pseudolaric acid B in human cancer cells. *Chem Commun* **53** (2017) 8671–8674.

[57] Leitner, A. A review of the role of chemical modification methods in contemporary mass spectrometry-based proteomics research. *Anal Chim Acta* **1000** (2018) 2–19.

[58] Sletten, EM; Bertozzi, CR. Bioorthogonal chemistry: Fishing for selectivity in a sea of functionality. *Angew Chem Int Ed* **48** (2009) 6974–6998.

[59] Zhang, J; Wang, J; Ng, S; Lin, Q; Shen, H-M. Development of a novel method for quantification of autophagic protein degradation by AHA labeling. *Autophagy* **10**(5) (2014) 901–912.

[60] Ovaa, H; Swieten, PF; Kessler, BM; Leeuwenburgh, MA; Fiebiger, E; Nieuwendijk, Adrianus MCH; Galardy, PJ; Marel, GA; Ploegh, HL; Overkleeft, HS. Chemistry in living cells: Detection of active proteasomes by a two-step labeling strategy. *Angew Chem* **115** (2003) 3754–3757.

[61] Evans, MJ; Cravatt, BF. Mechanism-based profiling of enzyme families. *Chem Rev* **106** (2006) 3279–3301.

[62] Speers, AE; Adam, GC; Cravatt, BF. Activity-based protein profiling *in vivo* using a copper(I)-catalyzed azide-alkyne [3 + 2] cycloaddition. *J Am Chem Soc* **125** (2003) 4686–4687.

[63] Paulick, MG; Bogyo, Matthew. Application of activity-based probes to the study of enzymes involved in cancer progression. *Curr Opin Genet Dev* **18** (2008) 97–106.

[64] Griffin, NM; Yu, J; Long, F; Oh, P; Shore, S; Li, Y; Koziol, JA; Schnitzer, JE. Label-free, normalized quantification of complex mass spectrometry data for proteomic analysis. *Nat Biotechnol* **28**(1) (2010) 83–91.

[65] Tyanova, S; Temu, T; Cox, J. The MaxQuant computational platform for mass spectrometry-based shotgun proteomics. *Nat Protoc* **11**(12) (2016) 2301–2319.

[66] Wang, J; Gao, L; Lee, YM; Kalesh, KA; Ong, YS; Lim, J; Jee, J-E; Sun, H; Lee, SS; Hua, Z-C; Lin, Q. Target identification of natural and traditional medicines with quantitative chemical proteomics approaches. *Pharmacol Therapeut* **162** (2016) 10–22.

[67] Wang, J; Tan, XF; Nguyen, VS; Yang, P; Zhou, J; Gao, M; Li, Z; Lim, TK; He, Y; Ong, CS; Lay, Y; Zhang, J; Zhu, G; Lai, S-L; Ghosh, D; Mok, YK; Shen, H-M; Lin, Q. A quantitative chemical proteomics approach to profile the specific cellular targets of andrographolide, a promising anticancer agent that suppresses tumor metastasis. *Mol Cell Proteom* **13**(3) (2014) 876–886.

[68] Wang, J; Zhang, C-J; Chia, WN; Loh, CCY; Li, Z; Lee, YM; He, Y; Yuan, L-X; Lim, TK; Liu, M; Liew, CX; Lee, YQ; Zhang, J; Lu, N; Lim, CT; Hua, Z-C; Liu, B; Shen, H-M; Tan, KSW; Lin, Q. Haem-activated promiscuous targeting of

artemisinin in *Plasmodium falciparum*. *Nat Commun* **6**(10111) (2015).

[69] Zhou, Y; Li, W; Zhang, X; Zhang, H; Xiao, Y. Global profiling of cellular targets of gambogic acid by quantitative chemical proteomics. *Chem Commun* **52** (2016) 14035–14038.

[70] Whitby, LR; Obach, RS; Simon, GM; Hayward, MM; Cravatt, BF. Quantitative chemical proteomic profiling of the *in vivo* targets of reactive drug metabolites. *ACS Chem Biol* **12** (2017) 2040–2050.

[71] Médard, G; Pachl, F; Ruprecht, B; Klaeger, S; Heinzlmeir, S; Helm, D; Qiao, H; Ku, X; Wilhelm, M; Kuehne, T; Wu, Z; Dittmann, A; Hopf, C; Kramer, K; Kuster, B. Optimized chemical proteomics assay for kinase inhibitor profiling. *J Proteome Res* **14** (2015) 1574–1586.

[72] Navarro, P; Kuharev, J; Gillet, LC; Bernhardt, OM; MacLean, B; Rost, HL; Tate, SA; Tsou, C-C; Reiter, L; Distler, U; Rosenberger, G; Perez-Riverol, Y; Nesvizhskii, AI; Aebersold, R; Tenzer, S. A multicenter study benchmarks software tools for label-free proteome quantification. *Nat Biotechnol* **34**(11) (2016) 1130–1140.

[73] Rooden, EJ; Florea, BI; Deng, H; Baggelaar, MP; Esbroeck, ACM; Zhou, J; Overkleeft, HS; Stelt, M. Mapping *in vivo* target interaction profiles of covalent inhibitors using chemical proteomics with label-free quantification. *Nat Protoc* **13**(4) (2018) 752–767.

[74] Rauniyar, N; Yates, JR. Isobaric labeling-based relative quantification in shotgun proteomics. *J Proteom Res* **13** (2014) 5293–5309.

[75] Ha, IJ; Kang, M; Na, YC; Park, Y; Kim, YS. Preparative separation of minor saponins from *Platycodi Radix* by high-speed counter-current chromatography. *J Sep Sci* **34** (2011) 2559-2565.

[76] Park, SB; Kim, YS. Simultaneous separation of three isomeric sennosides from senna leaf (*Cassia acutifolia*) using counter-current chromatography. *J Sep Sci* **38** (2015) 3502-3507.

[77] Lee, KJ; Song, KH; Choi, W; Kim, YS. A strategy for the separation of diterpenoid isomers from the root of *Aralia continentalis* by countercurrent chromatography: The distribution ratio as a substitute for the partition coefficient and a three-phase solvent system. *J Sep Sci* **1406** (2015) 224-230.

[78] Sutherland, IA. Recent progress on the industrial scale-up of counter-current chromatography. *J Chromatogr A* **1151** (2007) 6-13.

[79] Chen, L; Zhang, Q; Yang, G; Fan, L; Tang, J; Garrard, I; Ignatova, S; Fisher, D; Sutherland, IA. Rapid purification and scale-up of honokiol and magnolol using high-capacity high-speed counter-current chromatography. *J Chromatogr A* **1142** (2007) 115-122.

[80] Du, Q; Jiang, H; Yin, J; Xu, Y; Du, W; Li, B; Du, Q. Scaling up of high-speed countercurrent chromatographic apparatus with three columns connected in series for rapid preparation of (-)-epicatechin. *J Chromatogr A* **1271** (2013) 62-66.

[81] Guan, YH; Hewitson, P; Heuvel, RN; Zhao, Y; Siebers, RP; Zhuang, Y-P; Sutherland, I. Scale-up protein separation on stainless steel wide bore toroidal columns in the type-J counter-current chromatography. *J Chromatogr A* **1424** (2015) 102-110.

[82] Vieira, MN; Costa, FN; Leitao, GG; Garrard, I; Hewitson, P; Ignatova, S; Winterhalter, P; Jerz, G. *Schinus terebintifolius* scale-up countercurrent chromatography (Part I): High performance countercurrent chromatography fractionation of triterpene acids with off-line detection using atmospheric pressure chemical ionization mass spectrometry. *J Chromatogr A* **1389** (2015) 39-48.

[83] Costa, FN; Vieira, MN; Garrard, I; Hewitson, P; Jerz, G; Leitao, GG; Ignatova, S. *Schinus terebintifolius* scale-up countercurrent chromatography (Part II): Intra-apparatus scale-up and inter-apparatus method transfer. *J Chromatogr A* **1466** (2016) 76-83.

[84] Li, Z-Y; Zhi, H-J; Xue, S-Y; Sun, H-F; Zhang, F-S; Jia, J-P; Xing, J; Zhang, L-Z; Qin, X-M. Metabolomic profiling of the flower bud and rachis of *Tussilago farfara* with antitussive and expectorant effects on mice. *J Ethnopharmacol* **140** (2012) 83–90.

[85] Zhang, X-S; Ren, W; Bian, B-L; Zhao, H-Y; Wang, S. Comparative metabolism of tussilagone in rat and human liver microsomes using ultra-high-performance liquid chromatography coupled with high-resolution LTQ-Orbitrap mass spectrometry. *Mass Spectrom* **29** (2015) 1641–1650.

[86] Zhi, H-J; Qin, X-M; Sun, H-F; Zhang, L-Z; Guo, X-Q; Li, Z-Y. Metabolic fingerprinting of *Tussilago farfara* L. using ^{1}H-NMR spectroscopy and multivariate data analysis. *Phytochem Anal* **23** (2012) 492-501.

[87] Cao, K; Xu, Y; Mu, X; Zhang, Q; Wang, R; Lv, J. Sensitive determination of pyrrolizidine alkaloids in *Tussilago farfara* L. by field-amplified, sample-stacking, sweeping micellar electrokinetic chromatography. *J Sep Sci* **39** (2016) 4243–4250.

[88] Smyrska-Wieleba, N; Wojtanowski, KK; Mroczek, T. Comparative HILIC/ESI-QTOF-MS and HPTLC studies of pyrrolizidine alkaloids in flowers of *Tussilago farfara* and roots of *Arnebia euchroma*, *Phytochem Lett* **20** (2017) 339–349.

[89] Lee, M-R; Cha, M-R; Jo, K-J; Yoon, M-Y; Park, H-R. Cytotoxic and apoptotic activities of *Tussilago farfara* extract in HT-29 human colon cancer cells. *Food Sci Biotechnol* **17**(2) (2008) 308–312.

[90] Ravipati, AS; Zhang, L; Koyyalamudi, SR; Jeong, SC; Reddy, N; Bartlett, J; Smith, PT; Pedro, N; Melguizo, A; Cantizani, J; Asensio, F; Vicente, F. Anti-proliferative activities of selected Chinese medicinal herbs against human cancer cell lines. *Phytopharmacol* **4**(2) (2013) 206–219.

[91] Lee, H-J; Cho, H-S; Jun, SY; Lee, J-J; Yoon J-Y; Lee, J-H; Song, H-H; Choi, SH; Kim, S-Y; Saloura, V; Park, CG; Kim, N-S. *Tussilago farfara* L. augments TRAIL-induced apoptosis through MKK7/JNK activation by inhibition of MKK7-TIPRL in human hepatocellular carcinoma cells. *Oncol Rep* **32** (2014) 1117–1123.

[92] Li, H; Lee, HJ; Ahn, YH; Kwon, HJ; Jang, C-Y; Kim, W-Y; Ryu, J-H. Tussilagone suppresses colon cancer cell proliferation by promoting the degradation of β-catenin. *Biochem Biophys Res Commun* **443** (2014) 132–137.

[93] Wang, Q; Chen, T-H; Bastow, KF; Morris-Natschke, SL; Lee, K-H; Chen, D-F. Songaricalarins A−E, cytotoxic oplopane sesquiterpenes from *Ligularia songarica*. *J Nat Prod* **76** (2013) 305–310.

[94] Folter, JD; Sutherland, IA. Universal counter-current chromatography modelling based on counter-current distribution. *J Chromatogr A* **1216** (2009)

4218–4224.

[95] Wang, Q; Chen, T-H; Bastow, KF; Lee, K-H; Chen, D-F. Altaicalarins A–D, cytotoxic bisabolane sesquiterpenes from *Ligularia altaica*. *J Nat Prod* **73** (2010) 139–142.

[96] Sabitha, G; Babu, RS; Rajkumar, M; Yadav, JS. Cerium(III) chloride promoted highly regioselective ring opening of epoxides and aziridines using NaN_3 in acetonitrile: A facile synthesis of 1,2-azidoalcohols and 1,2-azidoamines. *Org Lett* **4**(3) (2002) 343–345.

[97] Dinkova-Kostova, AT; Holtzclaw, WD; Cole, RN; Itoh, K; Wakabayashi, N; Katoh, Y; Yamamoto, M; Talalay, P. Direct evidence that sulfhydryl groups of Keap1 are the sensors regulating induction of phase 2 enzymes that protect against carcinogens and oxidants. *Proc Natl Acad Sci U S A* **99** (2002) 11908-11913.

[98] Dinkova-Kostova, AT; Massiah, MA; Bozak, RE; Hicks, RJ; Talalay, P. Potency of Michael reaction acceptors as inducers of enzymes that protect against carcinogenesis depends on their reactivity with sulfhydryl groups. *Proc Natl Acad Sci U S A* **98** (2001) 3404-3409.

[99] LoPachin, RM; Barber, DS; Gavin, T. Molecular mechanisms of the conjugated α,β-unsaturated carbonyl derivatives: Relevance to neurotoxicity and neurodegenerative diseases. *Toxicol Sci* **104**(2) (2008) 235–249.

[100] Yang, H; Lundback, P; Ottosson, L; Erlandsson-Harris, H; Venereau, E; Bianchi, ME; Al-Abed, Y; Andersson, U; Tracey, KJ; Antoine, DJ. Redox modification of cysteine residues regulates the cytokine activity of high mobility group box-1 (HMGB1). *Mol Med* **18** (2012) 250–259.

[101] Hahn, Y-I; Kim, S-J; Choi, B-Y; Cho, K-C; Bandu, R; Kim, KP; Kim, D-H; Kim, W; Park, JS; Han, BW; Lee, J; Na, H-K; Cha, Y-N; Surh, Y-J. Curcumin interacts directly with the cysteine 259 residue of STAT3 and induces apoptosis in H-Ras transformed human mammary epithelial cells. *Sci Rep* **8**(6409) (2018).

[102] Hong, WG; Kim, JY; Cho, JH; Hwang, S-G; Song, J-Y; Lee, E; Chang, T-S; Um, H-D; Park, JK. AMRI-59 functions as a radiosensitizer via peroxiredoxin I-targeted ROS accumulation and apoptotic cell death induction. *Oncotarget* **8**(69) (2017) 114050–114064.

[103] Rose, R; Erdmann, S; Bovens, S; Wolf, A; Rose, M; Hennig, S; Waldmann, H; Ottmann, C. Identification and structure of small-molecule stabilizers of 14–3–3 protein–protein interactions. *Angew Chem Int Ed* **49** (2010) 4129–4132.

[104] Yoshida, K; Yamaguchi, T; Natsume, T; Kufe, D; Miki, Y. JNK phosphorylation of 14-3-3 proteins regulates nuclear targeting of c-Abl in the apoptotic response to DNA damage. *Nat Cell Biol* **7**(3) (2005) 278–285.

[105] Li, Y; Zou, L; Li, Q; Haibe-Kains, B; Tian, R; Li, Y; Desmedt, C; Sotiriou, C; Szallasi, Z; Iglehart, JD; Richardson, AL; Wang, ZC. Amplification of LAPTM4B and YWHAZ contributes to chemotherapy resistance and recurrence of breast cancer. *Nat Med* **16**(2) (2010) 214–219.

[106] Zhao, J; Du, Y; Horton, JR; Upadhyay, AK; Lou, B; Bai, Y; Zhang, X; Du, L; Li, M; Wang, B; Zhang, L; Barbieri, JT; Khuri, FR; Cheng, X; Fu, H. Discovery and structural characterization of a small molecule 14-3-3 protein-protein interaction inhibitor. *PNAS* **108**(39) (2011) 16212–16216.

[107] Zhao, J; Meyerkord, CL; Du, Y; Khuri, FR; Fu, Haian. 14-3-3 proteins as

potential therapeutic targets. *Semin Cell Dev Biol* **22** (2011) 705–712.

[108] Ottmann, C. Small-molecule modulators of 14-3-3 protein–protein interactions. *Bioorg Med Chem* **21** (2013) 4058–4062.

[109] Xu, J; Acharya, S; Sahin, O; Zhang, Q; Saito, Y; Yao, J; Wang, H; Li, P; Zhang, L; Lowery, FJ; Kuo, W-L; Xiao, Y; Ensor, J; Sahin, AA; Zhang, XH-F; Hung, M-C; Zhang, JD; Yu, D. 14-3-3ζ turns TGF-β's function from tumor suppressor to metastasis promoter in breast cancer by contextual changes of Smad partners from p53 to Gli2. *Cancer Cell* **27** (2015) 177–192.

[110] Hong, L; Chen, W; Xing, A; Wu, D; Wang, S. Inhibition of tyrosine 3-monooxygenase/ tryptophan 5-monooxygenase activation protein zeta (YWHAZ) overcomes drug resistance and tumorigenicity in ovarian cancer. *Cell Physiol Biochem* **49** (2018) 53–64.

[111] Kang, SW; Chae, HZ; Seo, MS; Kim, K; Baines, IC; Rhee, SG. Mammalian peroxiredoxin isoforms can reduce hydrogen peroxide generated in response to growth factors and tumor necrosis factor-*α*. *J Biol Chem* **273**(11) (1998) 6297–6302.

[112] Wagner, E; Luche, S; Penna, L; Chevallet, M; Dorsselaer, AV; Leize-Wagner, E; Rabilloud, T. A method for detection of over oxidation of cysteines: peroxiredoxins are oxidized in vivo at the active-site cysteine during oxidative stress. *Biochem J* **366** (2002) 777–785.

[113] Yang, K-S; Kang, SW; Woo, HA; Hwang, SC; Chae, HZ; Kim, K; Rhee, SG. Inactivation of human peroxiredoxin I during catalysis as the result of the oxidation of the catalytic site cysteine to cysteine-sulfinic acid. *J Biol Chem* **277**(41) (2002)

38029–38036.

[114] Neumann, CA; Cao, J; Manevich, Y. Peroxiredoxin 1 and its role in cell signaling. *Cell Cycle* **8**(24) (2009) 4072–4078.

[115] Rhee, SG; Kil, IS. Multiple functions and regulation of mammalian peroxiredoxins. *Annu Rev Biochem* **86** (2017) 749–775.

[116] Teixeira, F; Tse, E; Castro, H; Makepeace, KAT; Meinen, BA; Borchers, CH; Poole, LB; Bardwell, JC; Tomás, AM; Southworth, DR; Jakob, U. Chaperone activation and client binding of a 2-cysteine peroxiredoxin. *Nat Commun* **10**(659) (2019).

[117] Morinaka, A; Funato, Y; Uesugi, K; Miki, H. Oligomeric peroxiredoxin-I is an essential intermediate for p53 to activate MST1 kinase and apoptosis. *Oncogene* **30** (2011) 4208–4218.

[118] Wang, X; He, S; Sun, J-M; Delcuve, GP; Davie, JR. Selective association of peroxiredoxin 1 with genomic DNA and COX-2 upstream promoter elements in estrogen receptor negative breast cancer cells. *Mol Biol Cell* **21** (2010) 2987–2995.

[119] Riddell, JR; Wang, X-Y; Minderman, H; Gollnick, SO. Peroxiredoxin 1 stimulates secretion of proinflammatory cytokines by binding to TLR4. *J Immunol* **184** (2010) 1022–1030.

[120] Zhao, Q; Ding Y; Deng, Z; Lee, O-Y; Gao, P; Chen, P; Rose, RJ; Zhao, H; Zhang, Z; Tao, X-P; Heck, AJR; Kaod, R; Yang, D. Natural products triptolide, celastrol, and withaferin A inhibit the chaperone activity of peroxiredoxin. *Chem Sci* **6** (2015) 4124–4130.

[121] Lee, WS; Choi, K-S; Riddell, J; Ip, C; Ghosh, D; Park, J-H; Park, Y-M. Human peroxiredoxin 1 and 2 are not duplicate proteins: The unique presence of Cys83 in Prx1 underscores the structural and functional differences between Prx1 and Prx2. *J Biol Chem* **282**(30) (2007) 22011–22022.

[122] Cho, KJ; Park, Y; Khan, T; Lee, J-H; Kim, S; Seok, JH; Chung, YB; Cho, AE; Choi, Y; Chang, T-S; Kim, KH. Crystal structure of dimeric human peroxiredoxin-1 C83S mutant. *Bull Korean Chem Soc* **36** (2015) 1543–1545.

ABSTRACT IN KOREAN

관동(*Tussilago farfara* L.)은 국화과의 다년생 약초로서 관동의 말린 꽃봉오리(관동화, Farfarae Flos)는 전통 의학에서 기침, 기관지염 및 천식과 같은 호흡기 질환을 치료하기 위해 사용되었다. 주요 생리활성성분으로는 플라보노이드, 테르페노이드, 퀸산유도체 등이 보고되었으며, 특히 세스퀴테르펜 화합물군이 항염증, 세포증식억제, 뇌신경보호 등에서 높은 효능을 나타내었다. 따라서 본 연구에서는 관동화 유래 세스퀴테르펜 화합물에 대한 1) 대량 분리법, 2) LC-MS 기반의 성분 프로파일링, 3) 유방암 세포주에서의 표적단백질 규명을 수행하였다.

항류크로마토그래피를 이용하여 관동화 유래 세스퀴테르펜 화합물의 대량분획법(직접연속주입법, Direct and Continuous Injection mode)을 고안하였다. 추출액 자체를 이동상으로 사용함으로써 유기용매의 사용량을 크게 줄였으며, 관동화 1 kg의 추출물 315.9 g으로부터 6.8 g의 세스퀴테르펜 강화분획을 한 번에 획득하였다. 기존의 항류크로마토그래피 분리방법은 1~5 g의 추출물을 주입하기 때문에 직접연속주입법을 통해 분리 시간과 비용을 절감할 수 있었다. 또한, 주요 세스퀴테르펜 단일화합물의 정량분석을 수행하였고 용매분획법이나 컬럼크로마토그래피를 이용해 얻어진 분획물에 비해 높은 함량을 확인하였다.

UPLC-MS/MS 기법을 이용하여 관동화의 oplopane 및

bisabolane 계열의 세스퀴테르펜에 대한 성분프로파일을 제시하였다. 해당 화합물군은 질량분석기의 ESI 이온화과정에서 쉽게 In-source fragmentation (IS-CID) 되는 화합물로서 모분자 질량값을 얻기 위해 QqQ-MS의 Precursor ion scan을 적용하였다. 구조적 특성을 기반으로 네 가지의 특이적 이온(diagnostic ions, $[M+H]^+$ 215, 217, 229, 231)을 선정하여 총 74종의 화합물에 대한 모분자 질량값을 확인하였고, Q-TOF MS의 Product ion scan을 이용하여 각 모분자 이온의 특징적인 쪼개짐 양상(fragmentation pattern)을 고분해능 수준에서 확인하였다. 또한 11종의 화합물을 분리 및 구조동정하여 고안된 동시분석법을 검증하였고, MRM^{HR} 분석법을 이용하여 관동화 추출물에 함유된 주요 세스퀴테르펜 화합물의 함량을 확인하였다.

유방암 세포주 MDA-MB-231과 MCF-7에 대한 ECN (7β-(3′-ethyl *cis*-crotonoyloxy)-1α-(2′-methyl butyryloxy)-3,14-dehydro-*Z*-notonipetranone)의 높은 세포증식억제능을 확인하였고, Chemical Proteomics 기법을 이용하여 표적단백질을 제시하였다. *In vitro* 스크리닝 결과, 관동화 유래 세스퀴테르펜 화합물군은 항염증효능 뿐만 아니라 세포증식억제능을 보였으며 그 중 ECN이 가장 높은 효능을 나타냈다. ECN 기반의 clickable probe를 합성하여 세포 내에서의 click 반응으로 표적 단백질을 분획하였고, 가수분해된 펩타이드 혼합물의 TMT isobaric label 및 Orbitrap MS/MS 분석을 통

하여 음성대조군 대비 3배 이상의 선택성을 갖는 17종의 표적단백질을 규명하였다. 또한, 높은 선택성을 갖는 두 종의 표적단백질 14-3-3 protein zeta, peroxiredoxin-1에 대한 ECN의 작용 위치(binding site)와 결합친화도(ITC)를 확인하였다.

본 연구 결과들을 종합하여 볼 때, 관동화 유래 세스퀴테르펜 화합물군에 대한 LC-MS/MS 성분프로파일은 관동화를 포함하는 생약제제의 품질관리에 적용될 수 있으며, oplopane 골격의 세스퀴테르펜에 대한 표적단백질을 규명함으로써 세포증식억제능에 한하여 유효성분과 약효의 상관관계를 확인하는데 기초가 되는 연구로 사료된다.

주 요 어: 관동화, 세스퀴테르펜, 향류크로마토그래피, 직접연속주입법, 질량분석기반 성분프로파일, 세포증식억제, 생리활성기반 표적단백체

학 번: 2013-23461